International Earth Rotation and Reference Systems Service (IERS)
Service International de la Rotation Terrestre et des Systèmes de Référence

IERS Technical Note No. 38

Analysis and results of ITRF2014

Z. Altamimi, P. Rebischung, L. Métivier, X. Collilieux

Verlag des Bundesamts für Kartographie und Geodäsie
Frankfurt am Main 2017

Analysis and results of ITRF2014

Z. Altamimi, P. Rebischung, L. Métivier, X. Collilieux

(IERS Technical Note ; No. 38)

International Earth Rotation and Reference Systems Service
Central Bureau
Bundesamt für Kartographie und Geodäsie
Richard-Strauss-Allee 11
60598 Frankfurt am Main
Germany
phone: ++49-69-6333-273/261/250
fax: ++49-69-6333-425
e-mail: central_bureau@iers.org
URL: www.iers.org

ISSN: 1019-4568 (print version)
ISBN: 978-3-86482-088-5 (print version)

An online version of this document is available at:
http://www.iers.org/TN38

Print: MegaDruck.de Produktions- und Vertriebs GmbH, Westerstede, Germany

Table of Contents

1 Summary

The ITRF2014 is an improved realization of the International Terrestrial Reference System (ITRS) and is demonstrated to be of higher quality than the past ITRF versions. It involves two main innovations dealing with the modeling of station non-linear motions, namely seasonal (annual and semi-annual) signals present in the time series of station positions and post-seismic deformations for 124 sites that were subject to major earthquakes. It is achieved through a two-step procedure: (1) stacking the time series of station positions and Earth Orientation Parameters (EOPs) provided by the four IERS Technique Centers (TC); (2) combining the long-term solutions as obtained in step 1, together with local ties in co-location sites. The two-step procedure makes use of full variance-covariance information provided in SINEX format. The TC solutions incorporated in the ITRF2014 combination are free from any external constraints, thus preserving the actual space geodesy estimates of station positions and EOPs. The ITRF2014 origin is defined in such a way that it has zero translations and translation rates with respect to the mean Earth center of mass, as defined by the SLR station positions time series. Its scale is defined by zero scale factor and zero scale rate with respect to the mean of VLBI and SLR long-term solutions as obtained by stacking their respective time series. The ITRF2014 orientation (at epoch 2010.0) and its rate are aligned to the ITRF2008 using 127 stations of high geodetic quality.

The ITRF2014 includes the positions and velocities of 1499 stations located at 975 sites. Figure 1 shows the coverage of these sites, underlying the co-located space geodesy techniques.

This technical note describes the main ITRF2014 products: station positions and velocities, the post fit residuals of the least squares adjustment as well as the transformation parameters between ITRF2014 and ITRF2008. The main technical procedure used to generate the ITRF2014, a thorough discussion of its quality as well as most important geodetic and geophysical results were published in Altamimi et al. [2016], appended to this Technical Note.

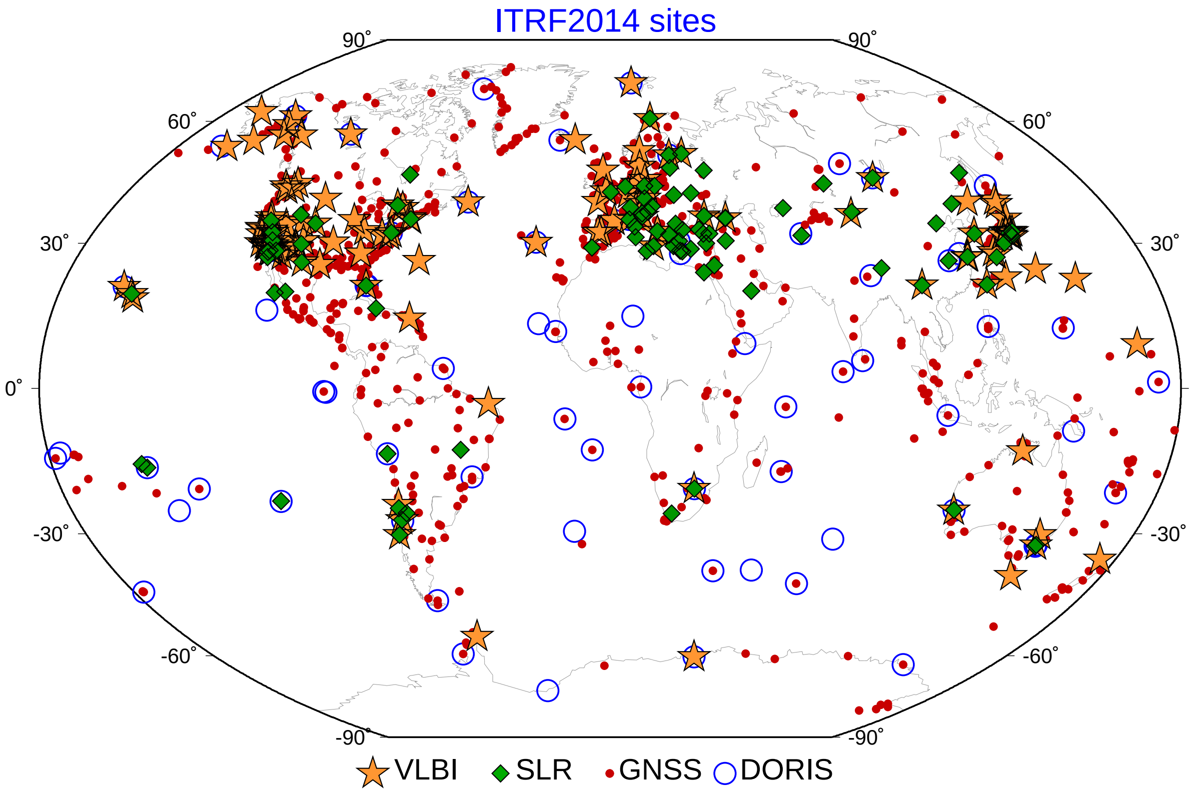

Fig. 1: ITRF2014 network

2 ITRF2014 input data

As for any ITRF solution, the ITRF2014 relies not only on space geodesy solutions (stations positions time series and EOPs), but also on local ties at co-location sites. In the following two sub-sections we describe the two sets of data used in the ITRF2014 construction.

2.1 Space geodesy solutions

We recall that the ITRF input time series solutions are provided on a daily basis for GNSS, session-wise for VLBI, weekly for DORIS and fortnightly and weekly for SLR, by the International Association of Geodesy (IAG) International Services of satellite techniques: International GNSS Service (IGS), International Laser Ranging Service (ILRS), and International DORIS Service (IDS) and on a daily (VLBI session-wise) basis by the International VLBI Service (IVS). Each per-technique time series is already a combination of the individual Analysis Center (AC) solutions of that technique. A typical solution includes notably the positions of a network of stations, EOPs as well as the associated variance-covariance matrix. Table 1 summarizes the submitted solutions by the IAG services, specifying the time span, solution type and the constraints applied by the TCs as well as the estimated Earth Orientation Parameters (EOPs).

The VLBI contribution to the ITRF2014 involves 5789 session-wise solutions [Bachmann et al., 2016], [Nothnagel et al., 2015], with 407 sessions involving 2 stations only which were discarded from the ITRF2014 processing since they are not designed for the TRF determination. The majority (86%) of the VLBI sessions includes a small number of stations, ranging between 3 to 9. 391 sessions involve 10-19 stations, 8 sessions with 20 stations, while two sessions exceptionally include 21 and 32 stations, respectively (see Appendix 6).

The ILRS solution comprises 244 fortnightly solutions, with polar motion and Length of Day (LOD) estimated each three days for the period 1983.0-1993.0, using LAGEOS I satellite data, and 1147 weekly solutions with daily polar motion and LOD estimates afterwards, using data acquired on LAGEOS I and II and ETALON I and II satellites [Luceri and Pavlis, 2016], (see Appendix 5).

The IGS submitted time series comprise 7714 daily solutions, resulting from the second reprocessed campaign, and cover the time period 1994.0 - 2015.1 [Rebischung et al., 2016]. Two IGS Analysis Centers have used available and exploitable GLONASS data in addition to GPS, namely Center for Orbit Determination in Europe (CODE) and European Space Operations Center (ESA). The starting dates of GLONASS ob-

Table 1: Summary of Submitted Solutions to ITRF2014

TC	Data-Span	Sampling	Solution Type	Constraints	EOPs
IVS	1980.0 – 2015.0	Daily	Normal Eq.	None	PM, PMr, LOD[a], UT1–UTC
ILRS	1983.0 – 1993.0	Fortnightly	Var-Cov	Loose	PM, LOD
	1993.0 – 2015.0	Weekly	Var-Cov	Loose	PM, LOD
IGS	1994.0 – 2015.1	Daily	Var-Cov	Minimum	PM, PMr, LOD
IDS	1993.0 – 2015.0	Weekly	Var-Cov	Minimum	PM

[a] PM: Polar Motion, PMr: Polar Motion rate, LOD: Length of Day

servations are 2002 for CODE and 2009 for ESA when the constellation became almost complete (see Appendix 4).

The DORIS contribution is a combined time series involving six ACs, using data from all available satellites with onboard DORIS receiver, and comprises 1140 weekly solutions, spanning the period 1993. – 2015.0 [Moreaux et al., 2016] (see Appendix 3).

More detailed descriptions of the submitted solutions are available in the appendix of this technical note.

Figure 1 illustrates the full ITRF2014 network, comprising 1499 stations located in 975 sites, where about 10% of them are co-located with 2, 3, or 4 distinct space geodetic instruments. Over the entire ITRF2014 observation history, we used local ties available for 91 co-location sites with two or more technique instruments which were or are currently operating. The GNSS network is playing a major role connecting the three other techniques, since 33 SLR, 40 VLBI and 46 DORIS stations were or are currently co-located with GNSS.

2.2 Local ties in co-location sites

The ITRF combination fundamentally depends on the availability of co-location sites where (1) two or more geodetic instruments of different techniques are operated and (2) local surveys between instrument measuring points are available. Local surveys are usually conducted using terrestrial measurements (direction angles, distances, and spirit leveling) or the GPS technique. Least Squares adjustments of local surveys are performed by national agencies operating ITRF co-location sites to provide differential coordinates (local ties) connecting the instrument reference points.

The local ties (mainly old ones) which are not available in SINEX format were converted into a complete set of positions for each site, provided in SINEX format. This has been achieved by solving for the following system of observation equations (1):

$$\begin{pmatrix} \Delta x_s^{i,j} \\ \Delta y_s^{i,j} \\ \Delta z_s^{i,j} \end{pmatrix} = \begin{pmatrix} x^j - x^i \\ y^j - y^i \\ z^j - z^i \end{pmatrix} \tag{1}$$

Where ($\Delta x_s^{i,j}$, $\Delta y_s^{i,j}$, $\Delta z_s^{i,j}$) are the geocentric components of the tie vector linking two points i and j, of a given data set s. The standard deviations (SD) ($\sigma\Delta x_s^{i,j}$, $\sigma\Delta y_s^{i,j}$, $\sigma\Delta z_s^{i,j}$) for each local tie vector are used to compute a diagonal variance matrix. If these SD are not available, they are computed by :

$$\sigma_{computed} = \sqrt{\sigma_1^2 + \sigma_2^2} \tag{2}$$

where,

σ_1 = 3 mm and $\sigma_2 = 10^{-6} \times \sqrt{(\Delta x_s^{i,j})^2 + (\Delta y_s^{i,j})^2 + (\Delta z_s^{i,j})^2}$

The equation system (1) needs of course initial coordinates for one point per tie vector set s, which are taken from existing ITRF solutions with 1 meter as standard deviation.

In addition to the local ties used in the ITRF2008 computation, a certain number of local ties used in the ITRF2014 computations are new, either resulting from new co-location sites, or from new surveys. 36 new surveys were conducted since the release of ITRF2008 and their determined local tie SINEX files, together with the old ones, were used in the ITRF2014 computation. In total, 139 local tie SINEX files were used in the ITRF2014, versus 104 for ITRF2008. Over the entire ITRF2014 observation history, we used local ties available for 91 co-location sites with two or more technique instruments which were or are currently operating.

The agencies that provided new local tie SINEX files are: Geoscience Australia, Istituto Nazionale di Astrofisica, Bologna, Italy, USA National Geodetic Survey, Onsala Space Observatory, Sweden, Geodetic Observatory Wettzell/Bundesamts für Kartographie und Geodäsie, Germany, Geographical Survey Institute (GSI), Japan. All the DORIS co-location sites were re-adjusted by the IGN survey department in order to generate full SINEX files, including the most recent surveys operated at these sites. All the local tie SINEX files used in the ITRF2014 combination are available at http://itrf.ign.fr/local_surveys.php.

Similar to past ITRF solutions, the local ties used in the ITRF2014 combination are provided in SINEX (Solution INdependent EXchange) format with known measurement epochs (with the exception of a few old ties), and 80% of them are available with full variance-covariance information.

Counting the number of co-locations between VLBI, SLR and DORIS, taken by pairs, we find 11 VLBI-SLR, 12 VLBI-DORIS and 11 SLR-DORIS. These are very small numbers of co-locations to allow a reliable combination of these three techniques alone. Therefore, the GNSS network is playing a major role in the ITRF combination, by linking together the three other techniques. We count in total 212 tie vectors between GNSS and the three other technique reference points: 62 for VLBI, 50 for SLR and 67 for DORIS. Additional 14 ties were also used between old and current DORIS beacon reference points in DORIS-only sites.

3 ITRF2014 data analysis

The general strategy adopted for the ITRF formation involves two-step procedure and described in [Altamimi et al., 2002, 2007, 2011]: (1) stacking the individual time series to estimate a long-term solution per technique comprising station positions at a reference epoch, station velocities and daily EOPs; and (2) combining the resulting long-term solutions of the four techniques together with the local ties at co-location sites.

For the first time in the International Terrestrial Reference Frame (ITRF) history, the ITRF2014 is generated with an enhanced modeling of non-linear station motions, including seasonal (annual and semi-annual) signals of station positions and Post-Seismic deformation (PSD) for sites that were subject to major earthquakes.

The seasonal signals were modeled using a sinusoidal function as described below, while the PSDs were accounted for, before the stacking, by applying parametric models that were first fitted to IGS daily station position time series.

3.1 Combination model

The CATREF combination model used for the ITRF combination is extensively described in previous publications, e.g. [Altamimi et al., 2002], [Altamimi et al., 2007]. For the ITRF2014 generation, we followed the same analysis strategy used for the ITRF2008 combination, but enhanced by modeling the nonlinear station motions.

The main two equations of the combination model are given below for completeness. They involve a 14-parameter similarity transformation, station positions and velocities and EOPs and are written as:

$$\left\{\begin{array}{lcl} X_s^i & = & X_c^i + (t_s^i - t_0)\dot{X}_c^i \\ & + & T_k + D_k X_c^i + R_k X_c^i \\ & + & (t_s^i - t_k)\left[\dot{T}_k + \dot{D}_k X_c^i + \dot{R}_k X_c^i\right] \\ & & \\ \dot{X}_s^i & = & \dot{X}_c^i + \dot{T}_k + \dot{D}_k X_c^i + \dot{R}_k X_c^i \end{array}\right. \quad (3)$$

$$\begin{cases} x_s^p &= x_c^p + R2_k \\ y_s^p &= y_c^p + R1_k \\ UT_s &= UT_c - \frac{1}{f} R3_k \\ \dot{x}_s^p &= \dot{x}_c^p \\ \dot{y}_s^p &= \dot{y}_c^p \\ LOD_s &= LOD_c \end{cases} \tag{4}$$

where for each point i, X_s^i (at epoch t_s^i) and $\dot{X}_s^i$ are positions and velocities of technique solution s and X_c^i (at epoch t_0) and $\dot{X}_c^i$ are those of the combined solution c. For each individual frame k, as implicitly defined by solution s, D_k is the scale factor, T_k the translation vector and R_k the rotation matrix. The dotted parameters designate their derivatives with respect to time. The translation vector T_k is composed of three origin components, namely T_x, T_y, T_z, and the rotation matrix of three small rotation angles: R_x, R_y, R_z, following the three axes, respectively X, Y, Z. t_k is a conventionally selected epoch of the 7 transformation parameters. In addition to Eq. (3) involving station positions (and velocities), the EOPs are added by Eq. (4), making use of pole coordinates x_s^p, y_s^p and universal time UT_s as well as their daily rates $\dot{x}_s^p$, $\dot{y}_s^p$ and LOD_s. The link between the combined frame and the EOPs is ensured via the three rotation parameters appearing in the first three lines of Eq. (4).

The first line of Equation (3) and the entire equation (4) are used to estimate long-term solutions for each technique, by accumulating (rigorously stacking) the individual technique time series of station positions and EOPs. In this process, the second line of equation (3) and the rates of the translation, scale and rotation parameters are not included, because station velocities are not available at the weekly (daily) basis. Moreover, a precise definition of the reference frame associated with the resulting long-term solution (comprising station positions at a reference epoch, station velocities and EOPs) has to be clearly specified. As transformation parameters are estimated between each weekly (or session-wise) frame and the long-term frame, it becomes necessary to define the long-term frame origin, scale, orientation and their time evolution, and therefore to complete the rank deficiency of the constructed normal equation. It is essential that the long-term solutions be representative of the mean origin and mean scale information of the space geodesy techniques. The particular type of minimal constraints introduced in Altamimi et al. [2007] have been designed for such purpose and are consequently used here to preserve the long-term solution origin (for SLR and DORIS) and scale (for VLBI, SLR and DORIS).

In addition to station positions and EOPs, described by equations 3 and 4, the combination model includes also the periodic terms modeled as a sinusoidal function. The general equation used for the estimation of the periodic signals embedded in the time series of station positions is written as:

$$\Delta X_f = \sum_{i=1}^{n_f} \mathbf{a}^i \cos(\omega_i t) + \mathbf{b}^i \sin(\omega_i t) \tag{5}$$

where ΔX_f is the total sum of the contributions of all the frequencies considered, n_f is the number of frequencies, $\omega_i = \frac{2\pi}{\tau_i}$, where τ_i is the period of the i^{th} frequency, e.g. annual, semi-annual, etc.

Each frequency adds six parameters per station, i.e $(a_x^i, a_y^i, a_z^i, b_x^i, b_y^i, b_z^i)^T$, in addition to the six position and velocity parameters.

For more details, the reader may refer to the full ITRF2014 article [Altamimi et al., 2016] appended to this technical note.

3.2 ITRF2014 frame definition

The second step of the ITRF2014 analysis consists in combining the long-term solutions of the four technique solutions together with local ties at co-location sites. The ITRF2014 is specified by the following frame parameters:

1. Origin: The ITRF2014 origin is defined in such a way that there are zero translation parameters at epoch 2010.0 and zero translation rates with respect to the mean origin of the ILRS SLR time series;
2. Scale: The scale of the ITRF2014 is defined in such a way that there is zero scale factor at epoch 2010.0 and zero scale rate with respect to the average of the implicit scales and scale rates of VLBI and SLR time series.
3. Orientation: The ITRF2014 orientation is defined in such a way that there are zero rotation parameters at epoch 2010.0 and zero rotation rates between ITRF2014 and ITRF2008. These two conditions were applied over a set of 127 reference stations located at 125 sites as illustrated by Figure 2.

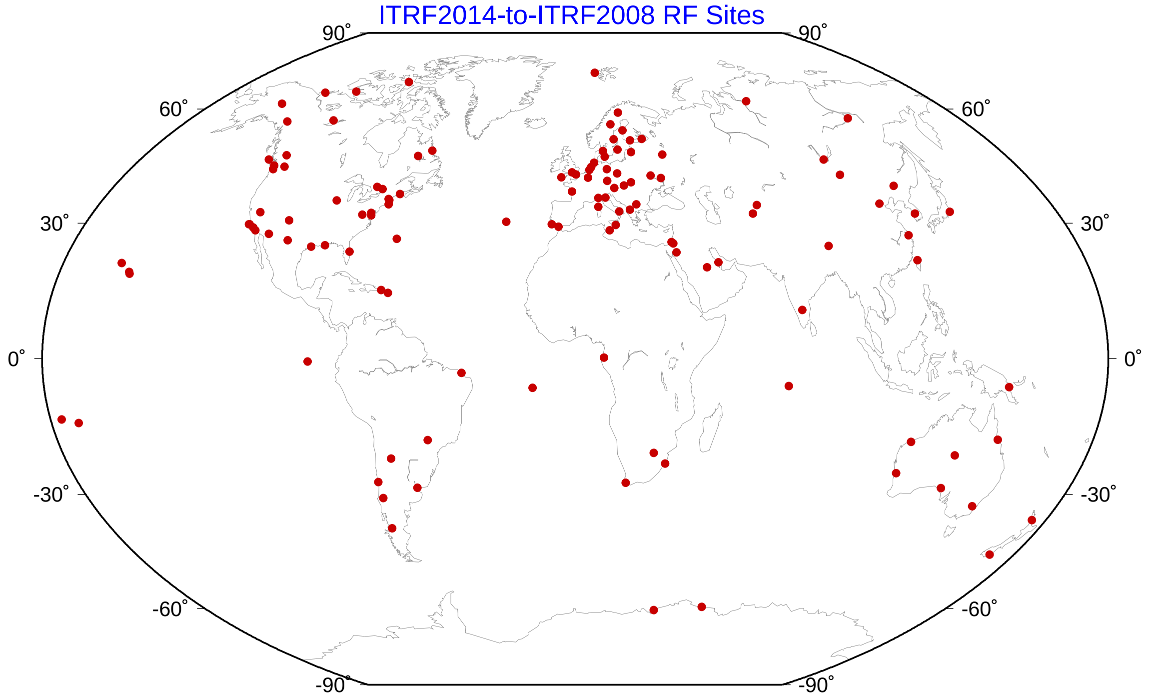

Fig. 2: Location of the reference frame sites used in the estimation of the 14 transformation parameters between ITRF2014 and ITRF2008 and their orientation alignment

4 ITRF2014 results

4.1 ITRF2014 origin and scale

The submitted ILRS SLR solution was used to define the ITRF2014 origin, by fixing to zero (and consequently eliminating from the normal equation) the 6 parameters (translations and rates) of its corresponding long-term cumulative solution. The long-term intrinsic origin of the latter is preserved via the usage of internal constraints [Altamimi et al., 2007], over the time span 1993.0-2015.0.

An estimate of the translation components between ITRF2014 and ITRF2008 showed small translation components at epoch 2010.0, namely 1.6, 1.9 and 2.4 mm, along the three axes X,Y,Z, respectively. The translation rates are statistically zero over the three components. These results are an indication of the level of the ITRF origin stability achievable today using SLR data, dominated by LAGEOS I and II observations [Luceri and Pavlis, 2016].

The ITRF2014 scale is specified by the average of VLBI and SLR scales, i.e. ITRF2014 scale is defined to be in the middle of the scales of VLBI and SLR long-term solutions. This choice is justified by the fact that we do not have any means to discriminate between the two technique solutions and therefore their simple average is a fair choice that minimizes the scale impact for these two techniques when using the ITRF2014 products. The result of the final ITRF2014 combination showed then a scale factor between VLBI and SLR solutions of 1.37 (± 0.10) ppb at epoch 2010.0 and a scale rate of 0.02 (± 0.02) ppb/yr. The ITRF2014 results regarding the level of the scale agreement between SLR and VLBI confirm the ITRF2008 finding and are an indication of the persistent scale offset between the two technique solutions.

4.2 ITRF2014 products

The ITRF2014 main products are:

- Station positions at epoch 2010.0 and velocities. These values are split into four tables corresponding to the four techniques: VLBI, SLR, GPS and DORIS. They are also provided in SINEX files with full variance covariance information. All the corresponding files are available through the ITRF2014 web and ftp sites. See next Chapter for access to these files.

- The Post-Seismic Deformation parametric models which are an integral part of the ITRF2014 products. The users should then

be aware that they must compute the model corrections, using the equations supplied in Appendix C of Altamimi et al. [2016], see Appendix 2, to be then added to the ITRF2014 coordinates if the needed position epoch occurs during the post-seismic relaxation period. Failing to do so would introduce position errors at the decimeter level for many stations impacted by PSDs. More information and some useful subroutines in Fortran are provided at the ITRF2014 web site:
http://itrf.ign.fr/ITRF_solutions/2014/.

- Earth orientation parameters. Consistent series of polar motion and its daily rates, universal time (UT1–UTC) and Length of Day (LOD), with the latter being determined by VLBI uniquely. The reason for using LOD values from VLBI only is to avoid contaminating the VLBI estimates by biased determinations from satellite techniques. The EOP series are also available through the ITRF2014 web and ftp sites (see below).

4.3 Transformation parameters between ITRF2014 and ITRF2008

For many applications and in order to ensure the link between ITRF2014 and ITRF2008, it is essential to assess consistently the transformation parameters between the two frames. The same 127 stations displayed in Figure 2 that were used to ensure the alignment of the ITRF2014 orientation and rate parameters to the ITRF2008, were also used to estimate the transformation parameters between the two frames. The main criterion for the selection of these 127 stations were (1) to have the best possible site distribution; (2) to involve as many as possible VLBI, SLR, GNSS and DORIS stations and (3) to have the best agreement between the two frames in terms of post-fit residuals of the 14-parameter transformation. Regarding this third criteria, the WRMS values of the 14-parameter similarity transformation fit are 1.8, 1.6 and 2.4 mm in position (at epoch 2010.0) and 0.2, 0.2, 0.3 mm/yr in velocity, in East, North and Vertical components, respectively. Table 2 lists the transformation parameters from ITRF2014 to ITRF2008, to be used with the transformation formula given by equation (6).

$$\left\{ \begin{array}{l} \begin{pmatrix} x \\ y \\ z \end{pmatrix}_{i08} = \begin{pmatrix} x \\ y \\ z \end{pmatrix}_{i14} + T + D \begin{pmatrix} x \\ y \\ z \end{pmatrix}_{i14} + R \begin{pmatrix} x \\ y \\ z \end{pmatrix}_{i14} \\ \begin{pmatrix} \dot{x} \\ \dot{y} \\ \dot{z} \end{pmatrix}_{i08} = \begin{pmatrix} \dot{x} \\ \dot{y} \\ \dot{z} \end{pmatrix}_{i14} + \dot{T} + \dot{D} \begin{pmatrix} x \\ y \\ z \end{pmatrix}_{i14} + \dot{R} \begin{pmatrix} x \\ y \\ z \end{pmatrix}_{i14} \end{array} \right. \tag{6}$$

where $i08$ designates ITRF2008 and $i14$ ITRF2014, T is the translation vector, $T = (T_x, T_y, T_z)^T$, D is the scale factor and R is the matrix containing the rotation angles, given by

$$R = \begin{pmatrix} 0 & -R_z & R_y \\ R_z & 0 & -R_x \\ -R_y & R_x & 0 \end{pmatrix}$$

The dotted parameters designate their time derivatives. The values of the 14 parameters are those listed in Table 2. Note that the inverse transformation from ITRF2008 to ITRF2014 follows by interchanging (i14) with (i08) and changing the sign of the transformation parameters.

Table 2: Transformation Parameters at epoch 2010.0 and their rates from ITRF2014 to ITRF2008, to be used with equation (6)

	Tx mm $\dot{T}x$ mm/y	Ty mm $\dot{T}y$ mm/y	Tz mm $\dot{T}z$ mm/y	D ppb $\dot{D}$ ppb/y	Rx mas $\dot{R}x$ mas/y	Ry mas $\dot{R}y$ mas/y	Rz mas $\dot{R}z$ mas/y
	1.6	1.9	2.4	-0.02	0.00	0.00	0.00
±	0.2	0.1	0.1	0.02	0.06	0.06	0.06
	0.0	0.0	-0.1	0.03	0.00	0.00	0.00
±	0.2	0.1	0.1	0.02	0.06	0.06	0.06

4.4 Consistency between local ties and space geodesy estimates

One of the most important by-products of the ITRF2014 combination is the assessment of the level of agreement between local ties and space geodesy estimates, through the availability of the post-fit residuals at co-location sites. In case of large discrepancies, discriminating between local ties and space geodesy estimates is a very delicate exercise, because the reasons for these discrepancies could be due to errors in local ties, in space geodesy estimates or in both. However quantifying the level of agreement between the two ensembles is very critical for further investigation and hopefully for identifying the error sources. At co-location sites, not only station position residuals are computed, but also velocity residuals. Therefore in order to take into account velocity disagreements between the technique solutions, it is more effective to compute the tie discrepancies at their measurement epochs.

The complete list of the residuals (or tie discrepancies) is available in Appendix 1. If we count the percentage of sites where the tie discrepancy is less than 5 mm, we find approximately: 42%, 29% and 23% for GNSS-VLBI, GNSS-SLR and GNSS-DORIS, respectively.

5 Access to the ITRF2014 files

All the ITRF2014 related files are available at the ITRF2014 web site

http://itrf.ign.fr/ITRF_solutions/2014/.

5.1 ITRF2014 SINEX files

The ITRF2014 SINEX files are available via anonymous ftp:

ftp itrf.ign.fr

username: anonymous
password: e-mail address
move to the itrf2014 directory (cd pub/itrf/itrf2014)

- compressed full ITRF2014 SINEX file (ITRF2014.SNX.gz, available on request)
- ITRF2014-TRF.SNX.gz ITRF2014 Station positions and velocities
- ITRF2014-EOP-IVS.SNX.gz VLBI Station positions, velocities and EOPs starting from 1980.0
- ITRF2014-TRF-IVS.SNX.gz VLBI Station positions and velocities
- ITRF2014-EOP-ILRS.SNX.gz SLR Station positions, velocities and EOPs starting from 1983.0
- ITRF2014-TRF-ILRS.SNX.gz SLR Station positions and velocities
- ITRF2014-EOP-IGS.SNX.gz GPS Station positions, velocities and EOPs starting from 1994.0
- ITRF2014-TRF-IGS.SNX.gz GPS Station positions and velocities
- ITRF2014-EOP-IDS.SNX.gz DORIS Station positions, velocities and EOPs starting from 1993.0
- ITRF2014-TRF-IDS.gz DORIS Station positions and velocities

For alternative access, see https://www.iers.org/ITRF.

5.2 ITRF2014 other files

- ITRF2014_EOP-F1.DAT. Complete EOP list file: one line per day (MJD) listing all parameter of that day.

- ITRF2014_EOP-F2.DAT. Complete EOP list file: one parameter per line.
- ITRF2014-RESIDUALS.DAT. Station position, velocity and local tie residuals of the ITRF2014 combination

Discontinuity files: 4 files (one per technique) of station position discontinuities, in SINEX format

- ITRF2014-soln-vlbi.snx
- ITRF2014-soln-slr.snx
- ITRF2014-soln-gnss.snx
- ITRF2014-soln-doris.snx

Post-Seismic Deformation files: 4 files (one per technique) of post-seismic deformation model parameters, in SINEX format

- ITRF2014-psd-vlbi.snx
- ITRF2014-psd-slr.snx
- ITRF2014-psd-gnss.snx
- ITRF2014-psd-doris.snx

and in CATREF intenal format:

- ITRF2014-psd-vlbi.dat
- ITRF2014-psd-slr.dat
- ITRF2014-psd-gnss.dat
- ITRF2014-psd-doris.dat

5.3 Post-seismic deformations

Equations for post-seismic deformation models and their variance propagation are available in the following pdf file: ITRF2014-PSD-model-eqs-IGN.pdf, but also in Appendix C of Altamimi et al. [2016] appended to this Technical Note at Appendix 2.
Subroutines in Fortran for PSD computations are also available:

- parametric.f: Compute the post-seismic deformation correction "d" using CATREF internal files ITRF2014-psd*.dat

- psd-example.f: EXAMPLE of user subroutine to add "d" by calling parametric.f to X Y Z at epoch t, using CATREF internal files ITRF2014-psd*.dat
- psdmatc.f : Compute the two terms of the matrix C (see pdf file ITRF2014-psd-model-eqs-IGN.pdf) of the parametric model LOG or EXP, necessary for the variance computation.

Notes on the post-seismic deformation (PSD) models.

The full equations of the parametric models used in the ITRF2014 generation are supplied in the pdf file "ITRF2014-psd-model-eqs-IGN.pdf". The full PSD estimated parameters and their variances are provided in SINEX format, files: ITRF2014-psd-vlbi.snx, ITRF2014-psd-slr.snx, ITRF2014-psd-gnss.snx, ITRF2014-psd-doris.snx

ITRF2014 solution provides the usual/classical estimates: station positions at a given epoch (2010.0, for ITRF2014), station velocities and EOPs. A user who wants to compute the position of a station affected by post-seismic deformations at a an epoch during the relaxation (non-linear) period should compute first the $\delta X(t)_{PSD}$ which is the total sum of the PSD corrections. The user should read the model parameters (EQ epoch, model type, LOG or/and EXP, amplitude and relaxation time) in one of the following two files:

- SINEX file (ITRF2014-psd*.snx). These SNX files provided per technique contain the full information of the parametric models used in the ITRF2014 generation, including the variance-covariance information. It is strongly recommended to use these SNX files, especially if the user needs to compute the variance of the estimated corrections. Please refer to the equations in the pdf file "ITRF2014-PSD-model-eqs-IGN.pdf". A Fortran subroutine called "psdmatc.f" is provided which allows to compute the terms of the matrix used in the variance-covariance propagation equations.
- CATREF internal file (ITRF2014-psd*.dat). In this case a subroutine called "parametric.f" is provided that allows computing $\delta X(t)_{PSD}$. An example of a subroutine called "psd-example.f" is provided as an example of use of that routine. Please read the commentary lines in the provided Fortran files. Note that using CATREF internal files does not allow computing the variance-covariance matrix of $\delta X(t)_{PSD}$.

References

Altamimi Z, Sillard P, Boucher C (2002) ITRF2000: A New Release of the International Terrestrial Reference Frame for Earth Science Applications, J Geophys Res 107(B10):2214, doi:10.1029/2001JB000561.

Altamimi Z, Collilieux X, Legrand J, Garayt B, Boucher C (2007) ITRF2005: A New Release of the International Terrestrial Reference Frame based on time series of station positions and Earth Orientation Parameters, 2007, J Geophys Res 112 (B09401), doi:10.1029/2007JB004949.

Altamimi Z, Collilieux X, Métivier L (2011) ITRF2008: an improved solution of the international terrestrial reference frame, Journal of Geodesy, 85 (8) (457-473), DOI: 10.1007/s00190-011-0444-4, DOI: 10.1007/s00190-011-0444-4.

Altamimi, Z., P. Rebischung, L. Métivier, and X. Collilieux (2016), ITRF2014: A new release of the International Terrestrial Reference Frame modeling nonlinear station motions, J. Geophys. Res. Solid Earth, 121, doi:10.1002/2016JB013098.

Bachmann, S., D. Thaller, O. Roggenbuck, M. Lösler, and L. Messerschmitt (2016), IVS contribution to ITRF2014. Journal of Geodesy, 90: 631-654, doi: 10.1007/s00190-016-0899-4.

Luceri, V., and E. Pavlis (2016), The ILRS contribution to ITRF2014, Available at Appendix 5.

Moreaux, G., F. G. Lemoine, H. Capdeville, S. Kuzin, M. Otten, P. Stepanek, P. Willis, P. Ferrage (2016), Contribution of the International DORIS Service to the 2014 realization of the International Terrestrial Reference Frame, Advances in Space Research, doi:10.1016/j.asr.2015.12.021.

Nothnagel, A.; International VLBI Service for Geodesy and Astrometry (IVS); (2015): The IVS data input to ITRF2014. International VLBI Service for Geodesy and Astrometry, GFZ Data Services. http://doi.org/10.5880/GFZ.1.1.2015.002

Rebischung, P., Z. Altamimi, J. Ray, and B. Garayt (2016), The IGS contribution to ITRF2014, J. Geod., doi: 10.1007/s00190-016-0897-6.

Appendices

Appendix 1 ITRF2014 terrestrial tie and space geodesy discrepancies

ITRF2014 tie discrepancies at tie epochs in (E)ast, (N)orth and (U)p.
Tie Discrepancies = Space Geodesy - Terrestrial Tie (in mm)
Each tie vector component is flagged by '-' if the residual is less
than 5 mm and by '*' otherwise.

GPS GPS Tie Discrepancies

Id	DOMES	Soln	Id	DOMES	Soln	East mm	North mm	Up mm	Tie Epoch	Flg	Technique Epochs Start	Technique Epochs End	Technique Epochs Start	Technique Epochs End	Spans	Spans
METS	10503S011	1	METZ	10503M005	1	-0.2	-0.5	-2.8	0:299	---	94:002	10:195	98:290	12:130	16.53	13.56
WTZR	14201M010	1	WTZA	14201M013	1	5.8	0.9	8.3	12:153	*-*	95:038	10:182	97:329	15:045	15.39	17.22
WTZR	14201M010	1	WTZZ	14201M014	2	0.5	1.4	-1.3	12:153	---	95:038	10:182	03:161	11:035	15.39	7.66
HRAO	30302M004	2	HARB	30302M009	1	2.5	2.1	2.3	3:214	---	98:026	04:323	00:224	11:334	6.81	11.30
STJO	40101M001	6	STJ2	40101M004	1	0.2	3.0	7.7	13:190	--*	00:148	13:031	10:137	15:045	12.68	4.75
YAR2	50107M004	3	YARR	50107M006	1	-0.7	0.4	-6.9	3:305	--*	02:137	12:099	98:298	07:157	9.90	8.61
YAR2	50107M004	3	YARR	50107M006	1	-0.6	-0.5	-8.9	10:201	--*	02:137	12:099	98:298	07:157	9.90	8.61
YAR2	50107M004	3	YAR3	50107M008	3	-0.6	1.9	10.9	10:201	--*	02:137	12:099	08:340	12:103	9.90	3.35

GPS VLBI Tie Discrepancies

Id	DOMES	Soln	Id	DOMES	Soln	East mm	North mm	Up mm	Tie Epoch	Flg	Technique Epochs Start	Technique Epochs End	Technique Epochs Start	Technique Epochs End	Spans	Spans
GRAS	10002M006	4	7605	10002M003	1	-1.9	-1.6	-0.7	9:238	---	04:295	15:046	89:255	89:258	10.32	0.01
NYA1	10317M003	2	7331	10317S003	1	2.8	-3.4	-1.4	3:228	---	99:154	15:046	94:277	14:364	15.70	20.24
ONSA	10402M004	2	7213	10402S002	1	5.8	-0.2	-5.5	2:193	*-*	99:033	15:046	80:208	14:357	16.04	34.41
ONSA	10402M004	2	7213	10402S002	1	1.5	-1.4	4.4	14:173	---	99:033	15:046	80:208	14:357	16.04	34.41
METS	10503S011	1	7601	10503M002	1	1.4	-1.6	-5.9	0:299	--*	94:002	10:195	89:186	89:193	16.53	0.02
METS	10503S011	1	7601	10503M002	1	0.2	0.2	-30.7	12:184	--*	94:002	10:195	89:186	89:193	16.53	0.02
SVTL	12350M001	4	7380	12350S001	1	-5.8	-5.7	-30.9	5: 1	***	08:298	15:045	03:065	14:346	6.31	11.77
ZECK	12351M001	3	7381	12351S001	1	-22.3	-0.9	18.6	5: 1	*-*	06:211	11:201	05:356	07:124	4.97	1.36
MEDI	12711M003	3	7230	12711S001	2	0.0	-0.6	2.3	7:241	---	01:093	15:045	96:340	14:093	13.87	17.32
MEDI	12711M003	3	7230	12711S001	2	0.3	-3.9	1.5	13:165	---	01:093	15:045	96:340	14:093	13.87	17.32
NOT1	12717M004	1	7547	12717S001	1	-4.0	-2.2	2.6	5:264	---	00:252	15:046	89:154	14:191	14.44	25.10
NOT1	12717M004	1	7547	12717S001	1	0.0	1.8	-5.2	13:193	--*	00:252	15:046	89:154	14:191	14.44	25.10
MATE	12734M008	4	7243	12734S005	1	-2.9	-5.4	-5.0	4:300	-**	99:169	08:329	90:277	14:364	9.44	24.24

MADR	13407S012	10	1565	13407S010	1	-2.6	8.5	5.9	99: 1	-**	03:316	11:018	88:244	96:341	7.18	8.27
YEBE	13420M001	1	7333	13420S001	1	0.8	0.8	-19.9	99:322	--*	00:273	15:045	96:308	03:197	14.38	6.70
WTZR	14201M010	1	7224	14201S004	1	-2.4	-4.1	1.8	12:153	---	95:038	10:182	83:355	14:364	15.39	31.02
SHAO	21605M002	1	7227	21605S009	1	-1.3	-10.2	-3.5	3:332	-*-	95:009	02:172	88:100	11:053	7.45	22.87
TSKB	21730S005	5	7345	21730S007	4	-3.0	0.9	1.6	8: 16	---	05:293	08:129	05:297	08:109	2.55	2.49
TSKB	21730S005	9	7345	21730S007	6	-3.0	3.1	-4.5	11:192	---	11:243	15:046	11:094	14:364	3.46	3.74
HRAO	30302M004	2	7232	30302S001	1	1.1	1.5	-0.8	3:214	---	98:026	04:323	86:009	14:329	6.81	28.88
HRAO	30302M004	2	7378	30302S009	1	-2.8	-6.7	16.0	14: 58	-**	98:026	04:323	12:285	14:357	6.81	2.20
HRAO	30302M004	2	7232	30302S001	1	2.3	-12.2	16.2	14: 58	-**	98:026	04:323	86:009	14:329	6.81	28.88
PDEL	31906M004	1	7609	31906M001	1	3.6	-1.4	2.5	14:268	---	00:108	06:348	92:150	92:156	6.66	0.02
STJO	40101M001	6	7625	40101M003	1	3.5	1.6	4.0	99:269	---	00:148	13:031	02:317	05:279	12.68	2.90
STJO	40101M001	6	7625	40101M003	1	2.1	0.8	-1.2	13:190	---	00:148	13:031	02:317	05:279	12.68	2.90
ALGO	40104M002	4	7282	40104S001	1	-1.4	-2.4	9.9	99: 1	--*	97:016	12:344	84:237	06:216	15.90	21.94
DRAO	40105M002	2	7283	40105M001	1	0.2	-1.4	-0.7	89:234	---	94:042	12:298	84:237	01:158	18.70	16.78
YELL	40127M003	3	7296	40127M004	1	-1.9	-5.2	-10.8	1:285	-**	96:235	13:199	91:181	06:215	16.90	15.09
YELL	40127M003	3	7285	40127M001	1	-2.0	-3.4	-0.7	1:285	---	96:235	13:199	84:237	85:249	16.90	1.03
FAIR	40408M001	2	7225	40408S002	1	-0.3	-6.4	1.8	1:274	-*-	96:108	02:308	84:189	02:304	6.55	18.31
VNDP	40420M007	4	7223	40420M002	1	4.0	-0.3	0.0	91:335	---	95:313	03:357	83:239	91:210	8.12	7.92
KOKB	40424M004	4	1311	40424S001	1	-0.1	1.0	8.0	2:319	--*	04:148	15:046	84:189	94:074	10.72	9.69
KOKB	40424M004	4	7298	40424S007	1	1.3	0.7	10.1	2:319	--*	04:148	15:046	93:159	14:353	10.72	21.53
KOKB	40424M004	4	7298	40424S007	1	3.9	0.8	12.2	14: 81	--*	04:148	15:046	93:159	14:353	10.72	21.53
WES2	40440S020	12	7205	40440S002	1	19.3	3.9	7.7	96:278	*-*	01:208	14:176	79:215	92:182	12.91	12.91
WES2	40440S020	12	7209	40440S003	1	11.8	-0.2	15.6	96:278	*-*	01:208	14:176	81:133	14:247	12.91	33.31
MDO1	40442M012	1	7613	40442S017	1	1.2	-6.7	9.7	93: 76	-**	94:002	04:337	92:013	14:338	10.92	22.89
MDO1	40442M012	1	7613	40442S017	1	1.7	3.8	-11.5	13: 54	--*	94:002	04:337	92:013	14:338	10.92	22.89
PIE1	40456M001	1	7234	40456S001	1	2.6	-3.2	-4.8	92:336	---	94:002	99:152	88:252	97:240	5.41	8.97
NLIB	40465M001	1	7612	40465S001	1	-1.3	-0.7	-2.5	93: 64	---	94:002	09:320	92:241	14:338	15.87	22.27
BREW	40473M001	1	7614	40473S001	1	0.7	-1.3	2.0	11:209	---	01:320	15:045	93:111	14:338	13.25	21.62
MKEA	40477M001	1	7617	40477S001	1	-1.7	2.3	1.0	96:221	---	96:234	06:289	93:200	06:193	10.15	12.98
BRFT	41602M002	3	7297	41602S001	1	-0.2	-4.4	8.9	6: 78	--*	07:177	11:005	93:111	14:364	3.53	21.69
FORT	41602M001	2	7297	41602S001	1	0.8	0.0	9.0	93:264	--*	00:081	06:059	93:111	14:364	5.94	21.69
SANT	41705M003	2	1404	41705S006	1	16.5	5.5	-9.1	92:192	***	96:199	10:058	91:324	96:331	13.61	5.02

CONZ	41719M002	3	7640	41719S001	1	4.5	-1.9	6.9	3: 80	--*	05:138	10:058	02:133	10:057	4.78	7.79
CONZ	41719M002	7	7640	41719S001	4	-0.2	-2.5	13.5	12:337	--*	11:201	15:046	11:045	14:150	3.58	3.29
CRO1	43201M001	8	7615	43201S001	1	-4.4	2.6	1.6	94: 16	---	06:055	10:143	93:176	14:338	4.24	21.44
TIDB	50103M108	3	1545	50103S010	1	0.7	3.5	-0.4	95:263	---	04:353	15:046	88:144	10:224	10.16	22.22
TIDB	50103M108	3	1545	50103S010	1	-1.7	0.4	-15.0	7:254	--*	04:353	15:046	88:144	10:224	10.16	22.22
YAR2	50107M004	3	7376	50107S012	1	-8.1	-1.5	-27.6	10:201	*-*	02:137	12:099	11:146	14:353	9.90	3.57
HOB2	50116M004	5	7242	50116S002	1	3.5	-2.1	-4.5	2: 81	---	04:359	15:046	89:269	14:234	10.14	24.90
HOB2	50116M004	5	7242	50116S002	1	3.0	-2.6	-3.5	9:330	---	04:359	15:046	89:269	14:234	10.14	24.90
HOB2	50116M004	5	7374	50116S007	1	6.8	0.6	-3.0	9:330	*--	04:359	15:046	10:280	14:353	10.14	4.20
WARK	50243M001	1	7377	50243S001	1	-0.3	-3.9	14.7	12:338	--*	09:039	13:362	11:059	14:353	4.88	3.80
KAT1	59968M001	1	7375	59968S001	1	-1.7	-2.3	3.9	11:153	---	10:072	15:045	11:167	14:353	4.93	3.51
SYOG	66006S002	2	7342	66006S004	1	0.2	5.3	33.2	0: 1	-**	99:299	07:026	99:312	13:325	7.25	14.04
OHI2	66008M005	2	7245	66008S001	1	-3.0	4.5	-3.5	2: 43	---	03:054	09:030	93:025	10:034	5.93	17.02
OHI2	66008M005	2	7245	66008S001	1	1.4	7.1	3.1	13: 41	-*-	03:054	09:030	93:025	10:034	5.93	17.02
MKEA	40477M001	2	7617	40477S001	2	1.0	-1.0	3.7	15:193	---	06:289	14:291	06:242	14:338	8.01	8.26

GPS SLR Tie Discrepancies

Id	DOMES	Soln	Id	DOMES	Soln	East mm	North mm	Up mm	Tie Epoch	Flg	Technique Epochs Start	End	Start	End	Spans	
GRAS	10002M006	4	7835	10002S001	2	-1.4	-10.7	-9.2	99:284	-**	04:295	15:046	90:079	99:337	10.32	9.71
GRAS	10002M006	4	7845	10002S002	1	-5.7	-5.4	-4.4	99:284	**-	04:295	15:046	97:327	14:358	10.32	17.08
GRAS	10002M006	4	7845	10002S002	1	-3.4	-3.0	-4.5	9:238	---	04:295	15:046	97:327	14:358	10.32	17.08
AJAC	10077M005	1	7848	10077M002	1	-7.5	-6.0	18.5	0: 1	***	00:022	08:222	02:042	05:300	8.55	3.71
METS	10503S011	1	7806	10503S014	1	-2.4	-8.7	-11.3	0:299	-**	94:002	10:195	98:064	04:338	16.53	6.75
GRAZ	11001M002	2	7839	11001S002	3	3.4	0.0	-8.8	92:319	--*	96:178	01:119	99:326	15:002	4.84	15.11
SOFI	11101M002	2	7505	11101M001	1	-0.7	0.6	3.1	95:266	---	99:232	10:094	95:273	95:294	10.62	0.06
BOR1	12205M002	2	7811	12205S001	1	-1.4	0.4	1.0	94: 10	---	99:152	15:046	93:206	02:208	15.71	9.01
CAGL	12725M003	2	7545	12725M002	1	1.1	1.3	3.1	95:161	---	01:192	13:263	85:311	94:070	12.19	8.34
MATE	12734M008	4	7541	12734M004	1	-1.7	-3.6	-5.4	4:300	--*	99:169	08:329	86:010	94:168	9.44	8.43
MATE	12734M008	4	7941	12734S008	1	-0.1	-0.4	-3.1	4:300	---	99:169	08:329	01:184	14:361	9.44	13.48
HERT	13212M010	2	7840	13212S001	1	-1.2	1.7	0.6	8:177	---	07:339	15:045	83:104	15:002	7.20	31.72
SFER	13402M004	7	7824	13402S007	1	6.3	-3.8	-14.7	9:192	*-*	05:199	14:030	99:102	14:361	8.54	15.71
KOSG	13504M003	1	8833	13504M002	1	1.1	-1.7	0.3	93:104	---	94:002	03:076	84:116	95:203	9.20	11.24
ZIMM	14001M004	2	7810	14001S001	1	3.9	2.5	-2.3	96: 95	---	98:311	15:046	84:171	95:119	16.27	10.86
ZIMM	14001M004	2	7810	14001S007	1	-1.4	3.0	-3.8	96: 95	---	98:311	15:046	97:362	14:308	16.27	16.85

POTS	14106M003	3	7836	14106S009	1	4.3	0.3	5.8	94:221	--*	95:276	09:106	93:004	04:164	13.53	11.44
POTS	14106M003	3	7841	14106S011	1	-18.3	0.6	-4.4	94:221	*--	95:276	09:106	04:050	14:362	13.53	10.85
WTZR	14201M010	1	8834	14201S018	1	1.3	3.0	18.4	12:153	--*	95:038	10:182	91:014	00:343	15.39	9.90
SOLA	20101M001	2	7832	20101S001	1	1.3	-7.4	-3.2	12: 35	-*-	04:140	15:046	01:017	11:318	10.74	10.82
BJFS	21601M001	1	7249	21601S004	1	0.0	6.8	1.5	3:171	-*-	99:293	11:071	99:231	11:031	11.39	11.45
WUHN	21602M001	6	7231	21602S004	1	-13.6	-31.3	-8.1	3:342	***	04:361	11:071	00:117	04:345	6.21	4.62
SHAO	21605M002	1	7837	21605S001	2	2.6	-4.1	-11.0	3:332	--*	95:009	02:172	95:304	05:104	7.45	9.45
URUM	21612M001	2	7355	21612M002	1	7.2	2.7	4.9	99: 1	*--	99:267	05:151	03:127	03:301	5.68	0.48
HRAO	30302M004	2	7501	30302M003	1	0.2	4.8	5.8	3:214	--*	98:026	04:323	93:180	12:098	6.81	18.78
HRAO	30302M004	2	7501	30302M003	1	3.7	-4.0	23.2	14: 58	--*	98:026	04:323	93:180	12:098	6.81	18.78
QUIN	40433M004	2	7109	40433M002	1	-4.6	12.6	32.0	85:247	-**	98:092	10:158	82:363	97:130	12.18	14.36
MDO1	40442M012	1	7080	40442M006	1	5.0	-7.3	21.3	93: 76	***	94:002	04:337	88:043	14:359	10.92	26.87
MDO1	40442M012	1	7080	40442M006	1	-4.0	1.5	-27.7	13: 54	--*	94:002	04:337	88:043	14:359	10.92	26.87
MAUI	40445S008	1	7119	40445M004	1	3.6	2.5	-12.6	6:260	--*	99:001	15:046	06:311	14:354	16.12	8.12
MAUI	40445S008	1	7210	40445M001	3	-0.3	2.4	-1.8	6:260	---	99:001	15:046	94:026	99:216	16.12	5.52
GODE	40451M123	1	7105	40451M105	1	0.0	2.8	-1.9	8: 1	---	94:002	12:220	82:364	15:003	18.60	32.01
GODE	40451M123	1	7105	40451M105	1	0.6	-1.4	-1.5	12:196	---	94:002	12:220	82:364	15:003	18.60	32.01
MONP	40497M004	4	7110	40497M001	1	2.3	-6.4	4.7	99:280	-*-	00:083	10:095	83:057	99:289	10.03	16.64
EISL	41703M003	1	7097	41703M002	1	3.9	-36.4	-3.9	1: 46	-*-	94:026	03:027	87:329	95:090	9.00	7.35
CONZ	41719M002	3	7405	41719M001	1	4.2	-3.2	7.5	3: 80	--*	05:138	10:058	02:107	10:058	4.78	7.87
CONZ	41719M002	7	7405	41719M001	4	11.1	-20.1	13.1	12:337	***	11:201	15:046	11:072	14:084	3.58	3.03
AREQ	42202M005	3	7403	42202M003	1	0.5	-4.1	4.3	95: 1	---	94:365	96:318	90:184	94:161	1.87	3.94
AREQ	42202M005	7	7403	42202M003	7	-1.2	-11.0	4.0	13: 12	-*-	07:227	14:092	14:101	14:345	6.63	0.67
AREQ	42202M005	6	7403	42202M003	5	2.2	8.1	-6.0	7:123	-**	01:189	07:228	01:190	07:230	6.11	6.11
YAR2	50107M004	3	7090	50107M001	1	-1.8	1.9	10.9	3:305	--*	02:137	12:099	83:011	15:003	9.90	31.98
YAR2	50107M004	3	7090	50107M001	1	-3.4	2.1	8.6	10:201	--*	02:137	12:099	83:011	15:003	9.90	31.98
STR1	50119M002	6	7825	50119S003	1	-3.4	-2.9	-11.0	9:317	--*	03:311	15:045	04:220	15:003	11.27	10.41
STR1	50119M002	6	7849	50119S001	1	-2.8	-1.4	-17.3	1:209	--*	03:311	15:045	98:190	03:016	11.27	4.52
STR1	50119M002	6	7825	50119S003	1	-0.6	-3.5	-11.8	1:209	--*	03:311	15:045	04:220	15:003	11.27	10.41
THTI	92201M009	3	7124	92201M007	2	-3.7	-4.6	8.8	7:278	--*	04:013	15:046	01:305	14:345	11.09	13.11
THTI	92201M009	3	7822	92201M017	1	-8.6	-10.6	13.0	11:128	***	04:013	15:046	11:176	11:272	11.09	0.26
SVTL	12350M001	3	1888	12350S002	1	1.5	1.2	-0.2	96: 74	---	04:337	08:297	12:036	14:361	3.89	2.89
SMST	21726M001	1	7838	21726S001	1	15.3	-0.9	-0.6	7: 1	*--	07:001	11:071	82:361	04:247	4.19	21.69

GPS DORIS Tie Discrepancies

Id	DOMES	Soln	Id	DOMES	Soln	East	North	Up	Tie		-----Technique	Epochs-----	----	----	----Spans	-----
						mm	mm	mm	Epoch	Flg	Start	End	Start	End		
GRAS	10002M006	4	GR3B	10002S018	1	3.1	-7.2	0.5	9:238	-*-	04:295	15:046	08:300	13:209	10.32	4.75
TLSE	10003M009	1	TLHA	10003S003	1	4.1	-1.5	-11.5	4: 34	--*	01:005	10:055	97:236	07:189	9.14	9.87
TLSE	10003M009	1	TLSA	10003S001	1	4.0	5.9	-1.9	4: 34	-*-	01:005	10:055	93:010	97:229	9.14	4.60
TLSE	10003M009	1	TLSB	10003S005	1	-1.6	-17.1	-8.4	14: 43	-**	01:005	10:055	07:182	12:302	9.14	5.33
REYK	10202M001	4	REYA	10202S001	1	-5.6	-8.0	1.5	4:248	**-	03:165	07:263	93:003	98:242	4.27	5.65
REYK	10202M001	4	REYB	10202S002	3	-2.4	-1.1	-1.6	4:248	---	03:165	07:263	00:177	04:249	4.27	4.20
REYK	10202M001	4	REZB	10202S003	1	-0.1	-2.6	-1.1	4:248	---	03:165	07:263	04:256	05:079	4.27	0.52
NYA1	10317M003	2	SPIA	10317S002	1	1.4	-3.5	-9.9	3:228	--*	99:154	15:046	93:003	99:080	15.70	6.21
NYA1	10317M003	2	SPIB	10317S004	1	-0.5	1.4	-3.6	3:228	---	99:154	15:046	99:213	03:229	15.70	4.04
NYA1	10317M003	2	SPJB	10317S005	1	-1.2	-2.7	-4.7	3:228	---	99:154	15:046	03:228	14:362	15.70	11.37
METS	10503S011	1	META	10503S013	1	-0.7	-0.5	-10.3	0:299	--*	94:002	10:195	93:003	00:303	16.53	7.82
METS	10503S011	1	METB	10503S015	1	0.8	2.1	-8.0	0:299	--*	94:002	10:195	00:317	12:183	16.53	11.63
METS	10503S011	1	MEUB	10503S016	1	1.2	-1.0	-29.3	12:184	--*	94:002	10:195	12:183	14:362	16.53	2.49
METS	10503S011	1	METB	10503S015	1	-3.5	-0.4	-29.8	12:184	--*	94:002	10:195	00:317	12:183	16.53	11.63
YSSK	12329M003	3	SAKA	12329S001	4	-1.8	0.6	0.8	4:231	---	03:269	06:320	04:025	04:235	3.14	0.57
YSSK	12329M003	3	SAKB	12329S002	1	-1.7	0.9	2.9	4:231	---	03:269	06:320	04:241	05:324	3.14	1.23
KIT3	12334M001	1	KITA	12334S004	1	-23.2	7.5	-4.3	1:115	**-	94:238	12:291	93:003	96:147	18.15	3.39
KIT3	12334M001	1	KITB	12334S005	1	-10.5	9.7	2.7	1:115	**-	94:238	12:291	96:147	01:119	18.15	4.92
KIT3	12334M001	1	KIUB	12334S006	1	6.7	6.9	-1.2	1:115	**-	94:238	12:291	01:147	13:153	18.15	12.02
DYNG	12602M006	1	DIOB	12602S012	1	-2.4	-3.1	-5.6	11:131	--*	11:133	14:339	06:161	14:362	3.56	8.55
WUHN	21602M001	6	JIUB	21602S005	1	-10.1	-17.1	-15.5	3:342	***	04:361	11:071	05:065	12:288	6.21	7.61
WUHN	21602M001	8	JIUB	21602S005	1	-4.5	-10.7	-31.8	12:285	-**	11:082	13:311	05:065	12:288	2.63	7.61
WUHN	21602M001	8	JIVB	21602S006	1	-0.5	5.6	-29.3	12:285	-**	11:082	13:311	13:153	14:362	2.63	1.57
PTAG	22006M005	3	MANB	22006S002	4	-2.5	3.3	2.0	14:339	---	12:244	15:042	12:169	14:362	2.45	2.53
BAKO	23101M002	8	CICB	23101S002	2	-0.8	-1.1	2.9	0:350	---	02:252	06:199	02:293	06:204	3.85	3.76
HRAO	30302M004	2	HBKB	30302S006	1	4.0	4.8	0.4	3:214	---	98:026	04:323	00:226	06:267	6.81	6.11
HRAO	30302M004	2	HBKA	30302S202	1	2.5	-3.6	-2.5	3:214	---	98:026	04:323	93:003	97:145	6.81	4.39
HRAO	30302M004	2	HBLA	30302S005	1	-2.7	1.2	-15.2	3:214	--*	98:026	04:323	97:159	00:226	6.81	3.18
HARB	30302M009	1	HBMB	30302S008	1	0.9	2.2	1.9	14: 58	---	00:224	11:334	07:063	14:362	11.30	7.82
PDEL	31906M004	1	PDLB	31906S001	1	12.2	6.1	2.5	1: 79	**-	00:108	06:348	99:010	01:231	6.66	2.61
PDEL	31906M004	1	PDMB	31906S002	1	12.5	4.5	2.5	1: 79	*--	00:108	06:348	01:287	07:280	6.66	5.98
PDEL	31906M004	1	PDMB	31906S002	2	6.7	-10.2	6.5	14:268	***	00:108	06:348	08:160	14:271	6.66	6.30
NKLG	32809M002	1	LIBA	32809S002	1	14.5	2.0	13.9	99: 36	*-*	00:089	10:123	93:010	99:038	10.09	6.08
NKLG	32809M002	1	LIBB	32809S003	1	8.0	4.1	5.0	99: 36	*--	00:089	10:123	99:087	05:338	10.09	6.69
NKLG	32809M002	1	LICB	32809S004	1	-1.7	2.6	1.9	10:125	---	00:089	10:123	05:338	08:216	10.09	2.67
SEY1	39801M001	5	MAHB	39801S005	1	-4.0	-1.8	-12.8	12:168	--*	07:180	11:012	01:189	09:074	3.54	7.69
SEY1	39801M001	5	MAIB	39801S006	1	-7.9	1.3	12.4	12:168	*-*	07:180	11:012	13:055	14:362	3.54	1.84

STJO	40101M001	6	STJB	40101S002	1	0.3	10.6	1.1	99:269	-*-	00:148	13:031	99:276	13:118	12.68	13.57
STJO	40101M001	6	STJB	40101S002	1	-1.0	4.2	1.4	13:190	---	00:148	13:031	99:276	13:118	12.68	13.57
STJO	40101M001	6	STKB	40101S003	1	-4.7	9.5	-1.9	13:190	-*-	00:148	13:031	13:265	14:362	12.68	1.27
YELL	40127M003	3	YELB	40127S008	1	3.6	-4.5	-2.6	1:285	---	96:235	13:199	01:301	07:140	16.90	5.56
YELL	40127M003	3	YEMB	40127S009	1	2.7	-2.7	-0.1	1:285	---	96:235	13:199	07:202	14:362	16.90	7.44
YELL	40127M003	3	YEMB	40127S009	1	-1.0	-0.6	1.1	13:198	---	96:235	13:199	07:202	14:362	16.90	7.44
FAIR	40408M001	2	FAIB	40408S005	1	10.2	-4.4	-14.3	1:274	*-*	96:108	02:308	00:009	02:314	6.55	2.84
KOKB	40424M004	4	KOLB	40424S009	1	-14.1	-28.7	-0.2	2:319	**-	04:148	15:046	02:342	14:362	10.72	12.05
KOKB	40424M004	4	KOKA	40424S008	1	-10.9	-29.3	7.3	2:319	***	04:148	15:046	93:003	02:321	10.72	9.87
KOKB	40424M004	4	KOLB	40424S009	1	3.7	-2.4	5.3	14: 81	--*	04:148	15:046	02:342	14:362	10.72	12.05
GODE	40451M123	1	GREB	40451S176	1	5.4	-5.8	-10.8	8: 1	***	94:002	12:220	00:191	12:134	18.60	11.84
GODE	40451M123	1	GRFB	40451S178	1	1.7	-3.6	-5.3	12:196	--*	94:002	12:220	12:148	14:362	18.60	2.59
MONP	40497M004	4	MONB	40497S008	1	2.5	6.5	4.0	5:335	-*-	00:083	10:095	05:344	07:350	10.03	2.02
MONP	40497M004	4	MOOB	40497S009	1	1.8	7.1	4.6	5:335	-*-	00:083	10:095	07:357	10:038	10.03	2.13
RIOG	41507M004	3	RIOA	41507S003	1	-8.5	3.5	-3.5	1: 15	*--	99:338	07:033	93:003	95:022	7.16	2.05
RIOG	41507M004	3	RIOB	41507S004	2	-4.0	13.4	-10.0	1: 15	-**	99:338	07:033	98:081	01:014	7.16	2.82
RIOG	41507M004	3	RIPB	41507S005	1	0.8	-4.4	3.8	1: 15	---	99:338	07:033	01:070	08:111	7.16	7.11
RIO2	41507M006	2	RIRB	41507S007	1	-5.3	17.5	-1.1	14:142	**-	12:284	15:046	12:106	14:362	2.35	2.70
EISL	41703M003	1	EASB	41703S009	1	5.9	2.4	-3.9	1: 46	*--	94:026	03:027	01:238	08:202	9.00	6.90
EISL	41703M003	1	EASA	41703S008	1	-2.6	13.8	-22.3	1: 46	-**	94:026	03:027	93:003	01:014	9.00	8.03
SANT	41705M003	2	SAOB	41705S008	1	0.8	0.7	1.5	96:339	---	96:199	10:058	97:012	00:338	13.61	3.89
SANT	41705M003	2	SANB	41705S009	1	0.0	1.5	1.6	96:339	---	96:199	10:058	01:189	06:008	13.61	4.50
GLPS	42005M002	1	SCRB	42005S001	1	-0.2	1.6	3.1	5: 92	---	03:006	08:057	05:092	09:158	5.14	4.18
AREQ	42202M005	7	ARFB	42202S007	2	15.4	12.2	33.8	13: 12	***	07:227	14:092	07:230	14:096	6.63	6.63
AREQ	42202M005	6	ARFB	42202S007	1	0.1	14.2	-1.8	7:123	-*-	01:189	07:228	06:232	07:231	6.11	1.00
YAR2	50107M004	3	YARB	50107S010	1	2.7	15.0	13.7	3:305	-**	02:137	12:099	99:311	03:334	9.90	4.06
YAR2	50107M004	3	YASB	50107S011	1	-4.2	11.4	16.3	3:305	-**	02:137	12:099	03:334	14:362	9.90	11.08
YAR2	50107M004	3	YASB	50107S011	1	-2.0	9.5	12.4	10:201	-**	02:137	12:099	03:334	14:362	9.90	11.08
STR1	50119M002	6	MSPB	50119S004	1	-4.4	6.6	-4.8	9:317	-*-	03:311	15:045	04:102	14:362	11.27	10.71
STR1	50119M002	6	MSOB	50119S002	1	-6.7	7.9	-8.1	1:209	***	03:311	15:045	99:066	03:019	11.27	3.87
STR1	50119M002	6	MSPB	50119S004	1	-9.0	5.3	-9.1	1:209	***	03:311	15:045	04:102	14:362	11.27	10.71
CHAT	50207M001	2	CHAB	50207S001	1	-4.4	-1.0	3.6	99: 56	---	01:333	12:066	99:066	06:218	10.27	7.42
GUAM	50501M002	1	GUAB	50501S001	1	6.2	0.0	23.6	93:346	*-*	95:019	02:116	94:163	00:226	7.27	6.17
SYOG	66006S002	2	SYOB	66006S001	1	-5.9	7.0	-39.6	0: 1	***	99:299	07:026	93:115	98:116	7.25	5.00
SYOG	66006S002	2	SYPB	66006S003	1	5.0	8.1	-6.0	0: 1	***	99:299	07:026	99:101	08:195	7.25	9.26
ROTH	66007M003	1	ROTB	66007S002	1	6.3	10.2	-34.1	11: 33	***	10:037	15:045	05:085	07:189	5.02	2.28
ROTH	66007M003	1	ROUB	66007S003	1	3.4	9.3	-27.3	11: 33	-**	10:037	15:045	07:315	11:038	5.02	3.24
ROTH	66007M003	1	ROVB	66007S004	1	2.3	4.8	-4.9	11: 33	---	10:037	15:045	11:100	14:341	5.02	3.66

```
KERG 91201M002  2 KERB 91201S003  1   -5.9  -4.3  -5.2  7:101 *-* 99:092 08:211 94:324 01:084  9.33   6.34
KERG 91201M002  2 KESB 91201S004  1    4.7   1.0   6.9  7:101 --* 99:092 08:211 01:119 04:039  9.33   2.78
KERG 91201M002  2 KETB 91201S005  1    5.5  12.7   8.3  7:101 *** 99:092 08:211 07:112 14:348  9.33   7.65
KERG 91201M002  2 KETB 91201S005  1    6.4  -6.9   4.0 12: 89 **- 99:092 08:211 07:112 14:348  9.33   7.65

DUM1 91501M001  4 ADEA 91501S001  1   -6.6  -6.9   5.4  8: 39 *** 98:084 15:046 93:003 98:088 16.90   5.23
DUM1 91501M001  4 ADEB 91501S002  1   -6.0   0.9   6.8  8: 39 *-* 98:084 15:046 04:081 08:041 16.90   3.89
DUM1 91501M001  4 ADFB 91501S003  1   -2.7  -2.9   9.0  8: 39 --* 98:084 15:046 08:055 10:248 16.90   2.53

THTI 92201M009  3 PAPB 92201S007  1   -2.9 -12.7   9.7  7:278 -** 04:013 15:046 95:218 98:102 11.09   2.68
THTI 92201M009  3 PAQB 92201S008  1   -3.5   1.6  15.8  7:278 --* 04:013 15:046 98:270 07:280 11.09   9.03
THTI 92201M009  3 PATB 92201S010  1   -2.7  -6.5  20.3  7:278 -** 04:013 15:046 07:301 14:362 11.09   7.17
THTI 92201M009  3 PATB 92201S010  1   -1.9  -0.9  19.8 11:128 --* 04:013 15:046 07:301 14:362 11.09   7.17

GAMB 92301M003  1 RILB 92301S003  1   -3.5   8.2  32.2 11:218 -** 00:099 10:276 09:088 11:100 10.48   2.03
GAMB 92301M003  1 RIMB 92301S004  1   -2.3   7.5  32.4 11:218 -** 00:099 10:276 11:233 14:362 10.48   3.35

NOUM 92701M003  4 NOUB 92701S002  1    1.6   9.8   5.5  5:236 -** 03:361 07:080 02:083 02:286  3.23   0.56
NOUM 92701M003  4 NOWB 92701S003  1    0.6  24.7  28.8  5:236 -** 03:361 07:080 05:247 11:121  3.23   5.66
NOUM 92701M003  4 NOUA 92701S001  1    1.9  17.2   2.3  5:236 -*- 03:361 07:080 93:010 00:191  3.23   7.50

FTNA 92902S002  1 FUUB 92902S003  1   17.2 -14.8   4.1 12:139 **- 98:268 05:346 12:253 14:285  7.21   2.09
FTNA 92902S002  1 FUTB 92902S001  1   -1.8   1.0  12.8 12:139 --* 98:268 05:346 01:028 08:356  7.21   7.90

KOUG 97301M402  2 KRWB 97301S006  1   -4.6 -20.1  23.1 11: 56 -** 13:099 15:045 11:142 14:362  1.85   3.60
KOUG 97301M402  2 KRUB 97301S004  1   -3.9   0.4   9.3 11: 56 --* 13:099 15:045 93:003 07:308  1.85  14.84

REUN 97401M003  2 REUA 97401S001  1   -6.9   8.9  -5.2  3:335 *** 03:147 08:338 93:003 98:347  5.52   5.94
REUN 97401M003  2 REUB 97401S002  2   -1.9   6.2   0.9  3:335 -*- 03:147 08:338 02:013 14:362  5.52  12.96

MALD 22901S001  2 MALB 22901S002  1    5.0 -12.5  -6.7  5: 14 *** 00:150 04:361 05:198 14:362  4.58   9.45

KSTU 12349M002  4 KRAB 12349S001  2   -1.8   5.2   5.3  0:  1 -** 01:026 04:264 99:136 05:142  3.65   6.02

CHPI 41609M003  1 CACB 41609S001  1  -17.5   2.1 -31.7  4: 85 *-* 03:128 10:059 93:318 03:075  6.81   9.33
CHPI 41609M003  1 CADB 41609S002  1   -4.5  12.7 -70.9  4: 85 -** 03:128 10:059 04:102 08:216  6.81   4.31

AOML 49914S001  1 MIAB 49914S003  1    4.6   2.6  -0.9  5: 36 --- 97:324 03:221 05:043 14:362  5.72   9.87

THU3 43001M002  2 THUB 43001S005  2   22.8   3.5 -16.0  2:257 *-* 04:276 11:279 07:006 11:184  7.01   4.49
----------------------------------------------------------------------------------------------------------
SLR VLBI Tie Discrepancies
Id   DOMES     Soln Id  DOMES     Soln  East North    Up  Tie       -----Technique Epochs---------Spans-----
                                          mm    mm    mm  Epoch Flg Start  End    Start  End
----------------------------------------------------------------------------------------------------------
7605 10002M003  1 7845 10002S002  1   -1.5  -1.4  -3.8  9:238 --- 89:255 89:258 97:327 14:358  0.01  17.08

7601 10503M002  1 7806 10503S014  1   -3.9  -7.1  -5.4  0:299 -** 89:186 89:193 98:064 04:338  0.02   6.75

7243 12734S005  1 7541 12734M004  1    1.3   1.8  -0.3  4:300 --- 90:277 14:364 86:010 94:168 24.24   8.43
7243 12734S005  1 7941 12734S008  1    2.8   5.0   1.9  4:300 --- 90:277 14:364 01:184 14:361 24.24  13.48

7224 14201S004  1 8834 14201S018  1    3.7   7.1  16.7 12:153 -** 83:355 14:364 91:014 00:343 31.02   9.90

7227 21605S009  1 7837 21605S001  2    3.9   6.1  -7.5  3:332 -** 88:100 11:053 95:304 05:104 22.87   9.45
```

7232	30302S001	1	7501	30302M003	1	-0.8	3.3	6.7	3:214	--*	86:009	14:329	93:180	12:098	28.88	18.78
7232	30302S001	1	7501	30302M003	1	1.4	8.2	7.0	14: 58	-**	86:009	14:329	93:180	12:098	28.88	18.78
QUIN	40433M004	2	7109	40433M002	1	-4.6	12.6	32.0	85:247	-**	98:092	10:158	82:363	97:130	12.18	14.36
7613	40442S017	1	7080	40442M006	1	3.8	-0.6	11.6	93: 76	--*	92:013	14:338	88:043	14:359	22.89	26.87
7613	40442S017	1	7080	40442M006	1	-5.7	-2.4	-16.2	13: 54	*-*	92:013	14:338	88:043	14:359	22.89	26.87
7219	40499S001	1	7295	40499M002	1	-9.9	13.1	14.5	93: 4	***	84:004	92:234	88:090	95:110	8.63	7.05
7640	41719S001	1	7405	41719M001	1	-0.3	-1.3	0.6	3: 80	---	02:133	10:057	02:107	10:058	7.79	7.87
7640	41719S001	4	7405	41719M001	4	11.3	-17.6	-0.4	12:337	**-	11:045	14:150	11:072	14:084	3.29	3.03
7376	50107S012	1	7090	50107M001	1	4.7	3.6	36.1	10:201	--*	11:146	14:353	83:011	15:003	3.57	31.98

VLBI VLBI Tie Discrepancies

Id	DOMES	Soln	Id	DOMES	Soln	East mm	North mm	Up mm	Tie Epoch	Flg	-----Technique Epochs Start	End	Start	End	---------Spans-----	
7232	30302S001	1	7378	30302S009	1	-5.2	5.5	-0.1	14: 58	**-	86:009	14:329	12:285	14:357	28.88	2.20
7285	40127M001	1	7296	40127M004	1	0.0	-1.7	-10.2	1:285	--*	84:237	85:249	91:181	06:215	1.03	15.09
1311	40424S001	1	7298	40424S007	1	1.4	-0.3	2.1	2:319	---	84:189	94:074	93:159	14:353	9.69	21.53
7205	40440S002	1	7209	40440S003	1	-7.6	-4.1	7.9	96:278	*-*	79:215	92:182	81:133	14:247	12.91	33.31
7242	50116S002	1	7374	50116S007	1	3.8	3.1	0.4	9:330	---	89:269	14:234	10:280	14:353	24.90	4.20

DORIS DORIS Tie Discrepancies

Id	DOMES	Soln	Id	DOMES	Soln	East mm	North mm	Up mm	Tie Epoch	Flg	-----Technique Epochs Start	End	Start	End	---------Spans-----	
TLSA	10003S001	1	TLHA	10003S003	1	0.0	-7.4	-9.7	4: 34	-**	93:010	97:229	97:236	07:189	4.60	9.87
REYA	10202S001	1	REYB	10202S002	3	3.2	6.9	-3.2	4:248	-*-	93:003	98:242	00:177	04:249	5.65	4.20
REYA	10202S001	1	REZB	10202S003	1	5.6	5.4	-2.6	4:248	**-	93:003	98:242	04:256	05:079	5.65	0.52
SPIA	10317S002	1	SPIB	10317S004	1	-1.9	4.9	6.3	3:228	--*	93:003	99:080	99:213	03:229	6.21	4.04
SPIA	10317S002	1	SPJB	10317S005	1	-2.5	0.7	5.2	3:228	--*	93:003	99:080	03:228	14:362	6.21	11.37
META	10503S013	1	METB	10503S015	1	1.5	2.6	2.3	0:299	---	93:003	00:303	00:317	12:183	7.82	11.63
METB	10503S015	1	MEUB	10503S016	1	4.7	-0.7	0.5	12:184	---	00:317	12:183	12:183	14:362	11.63	2.49
SAKA	12329S001	4	SAKB	12329S002	1	0.1	0.3	2.2	4:231	---	04:025	04:235	04:241	05:324	0.57	1.23
KITA	12334S004	1	KITB	12334S005	1	12.7	2.2	7.1	1:115	*-*	93:003	96:147	96:147	01:119	3.39	4.92
KITA	12334S004	1	KIUB	12334S006	1	30.0	-0.6	3.2	1:115	*--	93:003	96:147	01:147	13:153	3.39	12.02
BADA	12338S001	1	BADB	12338S002	1	0.6	-1.8	-0.8	4:224	---	93:003	02:223	04:234	14:362	9.60	10.35
DIOA	12602S011	1	DIOB	12602S012	1	0.1	3.6	1.2	6:136	---	94:093	05:268	06:161	14:362	11.48	8.55
JIUB	21602S005	1	JIVB	21602S006	1	4.0	16.3	2.5	12:285	-*-	05:065	12:288	13:153	14:362	7.61	1.57

MANA	22006S001	1	MANB	22006S002	1	0.1	-1.9	-0.8	3: 54	---	93:045	03:019	03:089	04:193	9.93	1.28
HBKA	30302S202	1	HBKB	30302S006	1	1.5	8.5	2.9	3:214	-*-	93:003	97:145	00:226	06:267	4.39	6.11
HBKA	30302S202	1	HBLA	30302S005	1	-5.2	4.9	-12.7	3:214	*-*	93:003	97:145	97:159	00:226	4.39	3.18
ASDB	30602S004	1	ASEB	30602S005	1	1.0	-2.3	11.2	10:164	--*	99:101	09:095	10:220	14:362	9.98	4.39
TRIA	30604S001	2	TRIB	30604S002	1	2.8	-14.0	-15.2	2: 23	-**	99:199	01:147	02:048	04:235	1.86	2.51
TRIB	30604S002	3	TRJB	30604S003	1	-0.3	-2.1	1.0	12:164	---	09:235	10:024	13:055	14:362	0.42	1.84
HELA	30606S002	1	HELB	30606S003	1	12.7	15.8	-5.6	3: 80	***	93:003	97:103	98:116	00:037	4.27	1.78
HELA	30606S002	1	HEMB	30606S004	1	11.4	20.6	-3.3	3: 80	**-	93:003	97:103	03:081	08:216	4.27	5.37
PDLB	31906S001	1	PDMB	31906S002	1	0.3	-1.6	-0.1	1: 79	---	99:010	01:231	01:287	07:280	2.61	5.98
LIBA	32809S002	1	LIBB	32809S003	1	-6.4	2.1	-8.9	99: 36	*-*	93:010	99:038	99:087	05:338	6.08	6.69
MAHB	39801S005	1	MAIB	39801S006	1	-3.9	3.1	25.2	12:168	--*	01:189	09:074	13:055	14:362	7.69	1.84
STJB	40101S002	1	STKB	40101S003	1	-3.7	5.2	-3.4	13:190	-*-	99:276	13:118	13:265	14:362	13.57	1.27
YELB	40127S008	1	YEMB	40127S009	1	-0.8	1.7	2.4	1:285	---	01:301	07:140	07:202	14:362	5.56	7.44
KOKA	40424S008	1	KOLB	40424S009	1	-3.2	0.6	-7.5	2:319	--*	93:003	02:321	02:342	14:362	9.87	12.05
MONB	40497S008	1	MOOB	40497S009	1	-0.7	0.6	0.6	5:335	---	05:344	07:350	07:357	10:038	2.02	2.13
RIOA	41507S003	1	RIOB	41507S004	2	4.5	9.9	-6.5	1: 15	-**	93:003	95:022	98:081	01:014	2.05	2.82
RIOA	41507S003	1	RIPB	41507S005	1	9.3	-7.9	7.3	1: 15	***	93:003	95:022	01:070	08:111	2.05	7.11
EASA	41703S008	1	EASB	41703S009	1	8.5	-11.4	18.4	1: 46	***	93:003	01:014	01:238	08:202	8.03	6.90
SAOB	41705S008	1	SANB	41705S009	1	-0.8	0.8	0.1	96:339	---	97:012	00:338	01:189	06:008	3.89	4.50
YARB	50107S010	1	YASB	50107S011	1	-7.0	-3.7	2.6	3:305	*--	99:311	03:334	03:334	14:362	4.06	11.08
MSOB	50119S002	1	MSPB	50119S004	1	-2.3	-2.6	-1.0	1:209	---	99:066	03:019	04:102	14:362	3.87	10.71
MORA	51001S001	1	MORB	51001S002	1	-5.3	5.3	5.7	2: 79	***	93:003	02:076	02:111	10:010	9.20	7.72
SYOB	66006S001	1	SYPB	66006S003	1	10.9	1.1	33.6	0: 1	*-*	93:115	98:116	99:101	08:195	5.00	9.26
ROTA	66007S001	1	ROTB	66007S002	1	-0.6	0.1	0.0	5: 54	---	93:003	97:047	05:085	07:189	4.12	2.28
ROTB	66007S002	1	ROUB	66007S003	1	-2.9	-1.0	6.8	11: 33	--*	05:085	07:189	07:315	11:038	2.28	3.24
ROTB	66007S002	1	ROVB	66007S004	1	-4.0	-5.4	29.2	11: 33	-**	05:085	07:189	11:100	14:341	2.28	3.66
KERB	91201S003	1	KESB	91201S004	1	10.6	5.3	12.1	7:101	***	94:324	01:084	01:119	04:039	6.34	2.78
KERB	91201S003	1	KETB	91201S005	1	11.4	16.9	13.5	7:101	***	94:324	01:084	07:112	14:348	6.34	7.65
CROB	91301S001	1	CRPB	91301S002	1	0.4	0.7	0.2	7: 96	---	04:045	07:098	07:090	09:088	3.15	1.99
AMSA	91401S001	1	AMTB	91401S003	1	5.5	8.6	7.0	3:326	***	93:010	96:007	01:112	05:254	2.99	4.39
AMTB	91401S003	1	AMUB	91401S004	1	1.7	-0.5	-3.9	7:108	---	01:112	05:254	07:147	09:102	4.39	1.88

ADEA	91501S001	1	ADEB	91501S002	1	0.6	7.4	3.3	2:104	-*-	93:003	98:088	04:081	08:041	5.23	3.89
ADEA	91501S001	1	ADEB	91501S002	1	0.6	7.7	1.4	8: 39	-*-	93:003	98:088	04:081	08:041	5.23	3.89
ADEA	91501S001	1	ADFB	91501S003	1	3.9	4.0	3.5	8: 39	---	93:003	98:088	08:055	10:248	5.23	2.53
PAPB	92201S007	1	PAQB	92201S008	1	-0.6	14.2	6.0	7:278	-**	95:218	98:102	98:270	07:280	2.68	9.03
PAPB	92201S007	1	PATB	92201S010	1	0.2	6.2	10.5	7:278	-**	95:218	98:102	07:301	14:362	2.68	7.17
RILB	92301S003	1	RIMB	92301S004	1	1.2	-0.7	0.2	11:218	---	09:088	11:100	11:233	14:362	2.03	3.35
NOUA	92701S001	1	NOUB	92701S002	1	-0.4	-7.3	3.2	5:236	-*-	93:010	00:191	02:083	02:286	7.50	0.56
NOUA	92701S001	1	NOWB	92701S003	1	-1.3	7.5	26.5	5:236	-**	93:010	00:191	05:247	11:121	7.50	5.66
FUTB	92902S001	1	FUUB	92902S003	1	18.9	-15.8	-8.7	12:139	***	01:028	08:356	12:253	14:285	7.90	2.09
KRUB	97301S004	1	KRWB	97301S006	1	-0.7	-20.5	13.8	11: 56	-**	93:003	07:308	11:142	14:362	14.84	3.60
REUA	97401S001	1	REUB	97401S002	2	5.0	-2.7	6.1	3:335	--*	93:003	98:347	02:013	14:362	5.94	12.96
DJIA	39901S002	1	DJIB	39901S003	1	0.1	0.9	-0.6	6:178	---	93:010	98:333	06:204	14:362	5.88	8.43
DJIA	39901S002	1	DJIB	39901S003	1	0.2	0.8	-0.7	0:183	---	93:010	98:333	06:204	14:362	5.88	8.43
CACB	41609S001	1	CADB	41609S002	1	13.0	10.6	-39.2	4: 85	***	93:318	03:075	04:102	08:216	9.33	4.31
BELB	66018S001	1	BEMB	66018S002	1	-0.5	0.3	-0.7	5: 42	---	04:066	04:130	05:127	14:362	0.18	9.64

Appendix 2 ITRF2014 JGR paper

AGU PUBLICATIONS

JGR

Journal of Geophysical Research: Solid Earth

RESEARCH ARTICLE
10.1002/2016JB013098

Key Points:
- ITRF2014 benefits from accurate modeling of station annual and semiannual displacements
- ITRF2014 benefits from accurate modeling of postseismic deformations for sites affected by major earthquakes
- Leading to the determination of accurate and robust secular frame and site velocities

Correspondence to:
Z. Altamimi,
zuheir.altamimi@ign.fr

Citation:
Altamimi, Z., P. Rebischung, L. Métivier, and C. Xavier (2016), ITRF2014: A new release of the International Terrestrial Reference Frame modeling nonlinear station motions, *J. Geophys. Res. Solid Earth*, *121*, 6109–6131, doi:10.1002/2016JB013098.

Received 15 APR 2016
Accepted 12 JUL 2016
Accepted article online 18 JUL 2016
Published online 4 AUG 2016

ITRF2014: A new release of the International Terrestrial Reference Frame modeling nonlinear station motions

Zuheir Altamimi[1], Paul Rebischung[1], Laurent Métivier[1], and Xavier Collilieux[2]

[1]IGN LAREG, Université Paris Diderot, Paris, France, [2]Institut National de l'Information Géographique et Forestière, Service de la géodésie et du nivellement, Saint-Mandé, France

Abstract For the first time in the International Terrestrial Reference Frame (ITRF) history, the ITRF2014 is generated with an enhanced modeling of nonlinear station motions, including seasonal (annual and semiannual) signals of station positions and postseismic deformation for sites that were subject to major earthquakes. Using the full observation history of the four space geodetic techniques (very long baseline interferometry (VLBI), satellite laser ranging (SLR), Global Navigation Satellite Systems (GNSS), and Doppler orbitography and radiopositioning integrated by satellite (DORIS)), the corresponding international services provided reprocessed time series (weekly from SLR and DORIS, daily from GNSS, and 24 h session-wise from VLBI) of station positions and daily Earth Orientation Parameters. ITRF2014 is demonstrated to be superior to past ITRF releases, as it precisely models the actual station trajectories leading to a more robust secular frame and site velocities. The ITRF2014 long-term origin coincides with the Earth system center of mass as sensed by SLR observations collected on the two LAGEOS satellites over the time span between 1993.0 and 2015.0. The estimated accuracy of the ITRF2014 origin, as reflected by the level of agreement with the ITRF2008 (both origins are defined by SLR), is at the level of less than 3 mm at epoch 2010.0 and less than 0.2 mm/yr in time evolution. The ITRF2014 scale is defined by the arithmetic average of the implicit scales of SLR and VLBI solutions as obtained by the stacking of their respective time series. The resulting scale and scale rate differences between the two solutions are 1.37 (±0.10) ppb at epoch 2010.0 and 0.02 (±0.02) ppb/yr. While the postseismic deformation models were estimated using GNSS/GPS data, the resulting parametric models at earthquake colocation sites were applied to the station position time series of the three other techniques, showing a very high level of consistency which enforces more the link between techniques within the ITRF2014 frame. The users should be aware that the postseismic deformation models are part of the ITRF2014 products, unlike the annual and semiannual signals, which were estimated internally with the only purpose of enhancing the velocity field estimation of the secular frame.

1. Introduction

Earth observation is fundamental to addressing scientific challenges pertaining to the quantification of changes that are affecting the Earth system. How is the Earth deforming due to, e.g., plate tectonics, coseismic and postseismic deformations, global geophysical fluid dynamics, or current ice melting? How to accurately determine point positions at the Earth surface that is constantly deforming? What is the rate of sea level rise, its spatiotemporal variability, and its ramification with climate change? Global geodesy is one of the key Earth science disciplines that not only measures changes of the Earth system in space and time but also is the only science that provides the indispensable standard against which the changes and their variability are quantified and properly referenced. In order to answer these scientific questions, fundamental to understanding the Earth dynamics, and also to precisely determine the orbits of the Earth-observing artificial satellites, it is critically important to ensure the continuous availability and updates of an accurate, long-term stable and truly global Terrestrial Reference Frame, such as the International Terrestrial Reference Frame (ITRF). The recent resolution adopted on 26 February 2015 by the General Assembly of the United Nations on the Global Geodetic Reference Frame (GGRF) for Sustainable Development (http://www.un.org/ga/search/view_doc.asp?symbol=A/69/L.53), recognizing the adoption of the ITRF by the scientific community, is a testimony of the critical importance of the reference frame for science and society.

Table 1. Summary of Submitted Solutions to ITRF[a]

TC	Data Span	Sampling	Solution Type	Constraints	EOPs
IVS	1980.0–2015.0	Daily	Normal equation	None	PM, PMr, LOD, UT1-UTC
ILRS	1983.0–1993.0	Fortnightly	Variance-covariance	Loose	PM, LOD
	1993.0–2015.0	Weekly	Variance-covariance	Loose	PM, LOD
IGS	1994.0–2015.1	Daily	Variance-covariance	Minimum	PM, PMr, LOD
IDS	1993.0–2015.0	Weekly	Variance-covariance	Minimum	PM

[a]PM: polar motion, PMr: polar motion rate, and LOD: length of day.

The space geodetic techniques that contribute to the ITRF construction are Doppler orbitography and radiopositioning integrated by satellite (DORIS), Global Navigation Satellite Systems (GNSS), satellite laser ranging (SLR), and very long baseline interferometry (VLBI). These techniques are organized as scientific services within the International Association of Geodesy (IAG) and known by the International Earth Rotation and Reference Systems Service (IERS) as Technique Centers (TCs): the International DORIS Service (IDS) [*Willis et al.*, 2010], the International GNSS Service, formerly the International GPS Service (IGS) [*Dow et al.*, 2009], the International Laser Ranging Service (ILRS) [*Pearlman et al.*, 2002], and the International VLBI Service (IVS) [*Schuh and Behrend*, 2012]. As none of the four space geodetic techniques is able to provide the full reference frame-defining parameters, the ITRF is demonstrated to be the most accurate reference frame available today, gathering the strengths of the four space geodesy techniques contributing to its construction and compensating for their weaknesses and systematic errors.

The ITRF2014 is an improved release compared to past realizations of the International Terrestrial Reference System (ITRS) [*Altamimi et al.*, 2002a, 2007, 2011], based on reprocessed solutions of the four space geodetic techniques, using data spanning their full observation histories up to the end of 2014. It provides precise quantifications of the coseismic and postseismic displacements and deformations caused by major earthquakes, in particular the devastating recent ones in Chile (2010) and Japan (2011). Its publication coincides not only with the United Nations General Assembly resolution on the GGRF but also with the thirtieth anniversary of the first combined Terrestrial Reference Frame (TRF) using space geodesy data [*Boucher and Altamimi*, 1985]. Since then, the ITRF solutions have improved in accuracy, and each new solution is demonstrated to be superior to past versions, thanks to continuously improved strategy of the ITRF combination and submitted solutions.

The ITRS Center of the IERS, hosted by IGN France, is responsible for the maintenance of the ITRS/ITRF and official ITRF solutions. Two other ITRS combination centers are also generating combined solutions using ITRF input data: Deutsches Geodätisches Forschungsinstitut (DGFI) an der Technischen Universität München (TUM) [*Seitz et al.*, 2012] and Jet Propulsion Laboratory (JPL) [*Wu et al.*, 2015].

2. ITRF2014 Input Data

The ITRF determination fundamentally depends not only on space geodesy solutions but also on the availability of terrestrial measurements, or local surveys, connecting the reference points of geodetic instruments at colocation sites. The following two sections describe the two ensembles of data used in the ITRF2014 construction.

2.1. Space Geodesy Solutions

Table 1 lists the four-technique combined time series submitted to the ITRF2014. It summarizes the data span, the sampling integration for station positions (daily for GNSS, session-wise for VLBI, weekly for DORIS, and fortnightly and weekly for SLR), the solution type (normal equations or variance-covariance), the constraints applied for the reference frame definition (free, loose, or minimum constraints), and the Earth Orientation Parameters (EOPs) provided in addition to station positions. Each per-technique time series is already a combination of the individual analysis center (AC) solutions of that technique. For more details regarding the type of reference frame constraints applied by the techniques, and the minimum constraints concept, in general, the reader may refer to *Dermanis* [2000, 2003], *Sillard and Boucher* [2001], *Altamimi et al.* [2002b, 2004], or to chapter 4 of the IERS Conventions [*Petit and Luzum*, 2010, chap. 4].

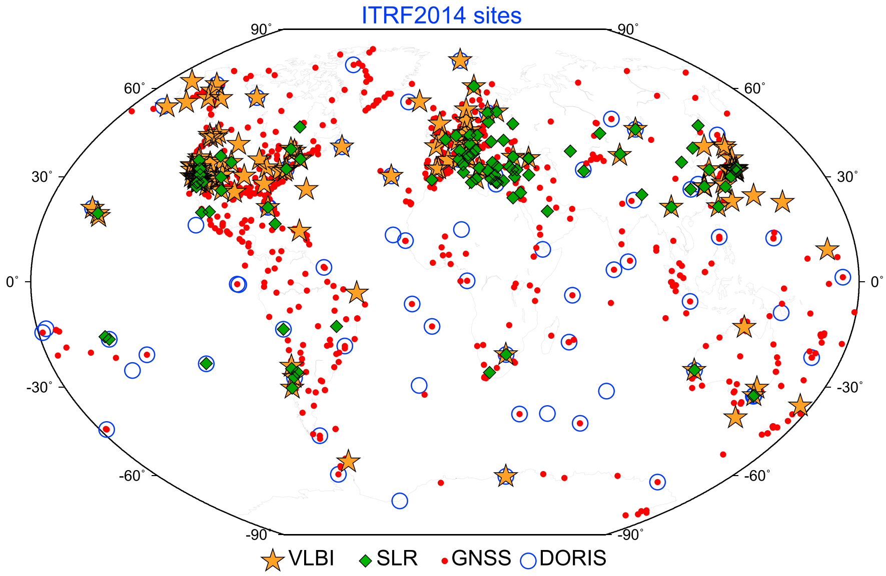

Figure 1. ITRF2014 network highlighting VLBI, SLR, and DORIS sites colocated with GNSS.

The submitted solutions cover the entire observation history of each one of the four techniques. The VLBI contribution involves 5789 session-wise solutions [*Bachmann et al.*, 2015], [*Nothnagel et al.*, 2015]; 407 sessions involving only two stations were discarded from the ITRF2014 processing since they were not designed for the TRF determination. The majority (86%) of the VLBI sessions includes a small number of stations, ranging between 3 and 9. Three hundred ninety-one sessions involve 10–19 stations, eight sessions with 20 stations, while two sessions exceptionally include 21 and 32 stations.

The ILRS solution comprises 244 fortnightly solutions, with polar motion and length of day (LOD) estimated every 3 days for the period 1983.0–1993.0, using LAGEOS I satellite data, and 1147 weekly solutions with daily polar motion and LOD estimates afterward, using data acquired on LAGEOS I and II and ETALON I and II satellites [*Luceri and Pavlis*, 2016].

The IGS-submitted time series comprise 7714 daily solutions, resulting from the second reprocessed campaign, and cover the time period 1994.0–2015.1 [*Rebischung et al.*, 2016]. Two IGS analysis centers have used available and exploitable GLObal NAvigation Satellite System (GLONASS) data in addition to GPS, namely, the Center for Orbit Determination in Europe (CODE) and the European Space Operations Center (ESOC). The starting dates of GLONASS observations are 2002 for CODE and 2009 for ESA when the constellation became almost complete [*Rebischung et al.*, 2016].

The DORIS contribution is a combined time series involving six ACs, using data from all available satellites with an onboard DORIS receiver, and comprises 1140 weekly solutions, spanning the period 1993.0–2015.0 [*Moreaux et al.*, 2016].

Figure 1 illustrates the full ITRF2014 network, comprising 1499 stations located in 975 sites, where about 10% of them are colocated with two, three, or four distinct space geodetic instruments.

2.2. ITRF2014 Local Ties in Colocation Sites

The ITRF combination fundamentally depends on the availability of colocation sites where (1) two or more geodetic instruments of different techniques are operated and (2) local surveys between instrument measuring points are available. Local surveys are usually conducted using terrestrial measurements (direction angles, distances, and spirit leveling) or the GPS technique. Least squares adjustments of local surveys are performed by national agencies operating ITRF colocation sites to provide differential coordinates (local ties) connecting the instrument reference points.

In addition to the local ties used in the ITRF2008 computation, a certain number of local ties used here are new, resulting either from new colocation sites or from new surveys. Thirty-six new surveys were conducted since the release of ITRF2008, and their determined local tie Solution Independent Exchange (SINEX) files, together with the old ones, were used in the ITRF2014 computation. In total, 139 local tie SINEX files were used in the ITRF2014 versus 104 for ITRF2008. Over the entire ITRF2014 observation history, we used local ties available for 91 colocation sites with two or more technique instruments which were or are currently operating.

The agencies that provided new local tie SINEX files are the following: Geoscience Australia, Istituto Nazionale di Astrofisica, Bologna, Italy, U.S. National Geodetic Survey, Onsala Space Observatory, Sweden, Geodetic Observatory Wettzell/Bundesamts für Kartographie und Geodäsie, Germany, and Geographical Survey Institute (GSI), Japan. All the DORIS colocation sites were readjusted by the IGN survey department in order to generate full SINEX files, including the most recent surveys operated at these sites. All the local tie SINEX files used in the ITRF2014 combination are available at http://itrf.ign.fr/local_surveys.php.

Similar to past ITRF solutions, the local ties used in the ITRF2014 combination are provided in SINEX (Solution Independent Exchange) format with known measurement epochs (with the exception of a few old ties), and 80% of them are available with full variance-covariance information.

Counting the number of colocations between VLBI, SLR, and DORIS, taken by pairs, we find 11 VLBI-SLR, 12 VLBI-DORIS, and 11 SLR-DORIS. These are very small numbers of colocations to allow a reliable combination of these three techniques alone. Therefore, the GNSS network is playing a major role in the ITRF combination, by linking together the three other techniques [*Altamimi and Collilieux*, 2009]. We count in total 212 tie vectors between GNSS and the three other technique reference points: 62 for VLBI, 50 for SLR, and 67 for DORIS. Additional 14 ties were also used between old and current DORIS beacon reference points in DORIS-only sites.

3. ITRF2014 Data Analysis

The procedure adopted for the ITRF formation involves two steps [*Altamimi et al.*, 2002a, 2007, 2011]: (1) stacking the individual time series to estimate a long-term solution per technique comprising station positions at a reference epoch, station velocities, and daily EOPs, and (2) combining the resulting long-term solutions of the four techniques together with the local ties at colocation sites.

3.1. ITRF2014 Time Series Analysis

As detailed in the following sections, the first step of the ITRF2014 analysis, i.e., analyzing and stacking the individual time series, involved for the first time in the context of the ITRF analysis two main innovations dealing with nonlinear station motions: modeling the periodic seasonal signals for stations with sufficient time span and postseismic deformation (PSD) for sites affected by major earthquakes. Modeling the station seasonal signals is accomplished by adding to the combination model the appropriate parameters (coefficients) of sinusoidal functions, while the PSDs were accounted for, before the stacking, by applying parametric models that were first fitted to IGS daily station position time series.

The full equations of the combination model, together with the periodic signals and PSDs, are detailed in the appendices.

The analysis of station position time series used in the first step of the ITRF construction allows capturing not only the linear motions but also all sorts of nonlinear motions: discontinuities, periodic signals, postseismic deformation, velocity changes due to current ice melting, and some other unidentified behaviors of station trajectories. The latter kind of nonlinear motion might be attributed to local effects (e.g., anthropogenic groundwater pumping) or in some cases to systematic errors in the data analysis.

An iterative outlier elimination process was applied in this first step of the stacking of the individual technique solutions, until no observations with normalized residuals larger than 3 remained.

During the stacking of the individual technique time series, nearby stations or multiple segments of the same station in case of discontinuities are constrained to have the same velocity using the following equation:

$$\dot{X}_i = \dot{X}_j \quad (\sigma_v) \tag{1}$$

where i and j are two close-by stations or two consecutive segments of a station with discontinuities. σ_v is the uncertainty constraint at which equation (1) is satisfied, which is chosen to be 10^{-6} m/yr. Such a tight constraint value has the advantage, in the context of time series stacking, to help identify possible velocity discontinuities for some stations or/and discrepant velocities for nearby stations. In case of such apparent velocity discontinuities, different velocities were estimated before and after the discontinuity events in case of clear apparent slope change. This also holds for some (not all) stations with postseismic deformation behavior.

In order to satisfy the ITRF concept of a linear (secular) frame, it is fundamental to accurately model all kinds of motion and retain the linear trends of the stations, as part of the ITRF parameters.

3.2. Periodic Signals

It is very common to observe periodic signals in the station position time series, which are the manifestation of not only geophysical phenomena, e.g., loading effects caused by the atmosphere, terrestrial water, and ocean circulation [*Dong et al.*, 2002], but also technique systematic errors, such as the draconitic periods for satellite techniques, as shown by *Ray et al.* [2008] for GPS.

It is not expected that the periodic signals present in the station position time series affect the ITRF-defining parameters, especially the origin and the scale [*Collilieux et al.*, 2010], although the velocities of stations with less than 2.5 years of observations might be impacted by these effects [*Blewitt and Lavalée*, 2002]. It is, however, expected that estimating the periodic signals improves the linear station velocity determination, especially for stations with large seasonal signals. Another important advantage of estimating seasonal signals is that it helps the detection of discontinuities in the time series and consequently improves the offset determination.

As described in Appendix B, when stacking time series of station positions, and since our combination model includes a seven-parameter similarity transformation between each input solution and the long-term combined solution, we need to specify how to separate seasonal variations of the transformation parameters from seasonal variations of the station positions. To that end, we chose the internal constraint approach for the translation and scale components, that is, to constrain to zero the periodic signals embedded in the time series of the corresponding transformation parameters. This approach is justified by the fact that it avoids the absorption of part of the station motions by the origin and scale time series. As regard to the rotation parameters, we chose the minimum constraint approach, i.e., imposing no net periodic rotation conditions on a set of well and homogeneously distributed reference stations.

We performed several stacking tests of the individual time series of the four techniques, estimating annual, semiannual signals, as well as a number of draconitic signals, up to the seventh harmonic of the GPS draconitic year (351.4 days). We found that estimating the draconitic signals, in addition to the annual and semiannual signals, has no significant impact on the station linear velocities, compared with the stacking that accounts for annual and semiannual signals only.

Using the IGS daily solutions, we compared the estimated linear site velocities obtained when the annual and semiannual signals are estimated to those obtained when no periodic signals are considered. We found that the horizontal velocity differences are almost all negligible for all stations and are less than 0.05 mm/yr, while the vertical velocity differences are larger and may reach 1 mm/yr as illustrated by Figure 2. The larger vertical velocity differences are for sites with large seasonal signals, with data gaps or with large number of discontinuities. The reduction of the velocity formal errors of about 10% when estimating the seasonal signals could be regarded as an improvement of the velocity determination.

We also performed stacking tests where the station positions of the individual daily or weekly solutions were corrected by a nontidal atmospheric loading (NTAL) model provided by Tonie van Dam (personal communication, 2015), according to the model of the National Center for Environmental Prediction surface pressure. The data are provided on a $2.5 \times 2.5°$ global grid and sampled at 6-hourly rate. A mean of 20 year was removed, and periodic signals less than 26 h were filtered from the station time series to remove the diurnal and semidiurnal atmospheric tides. We interpolated the model to compute the NTAL effect at the central epoch of the daily or weekly observations. Only NTAL of the unmodeled loading effects is evaluated here, because (1) we initially proposed in the ITRF2014 call for participation to apply NTAL model corrections at the stacking step of the ITRF2014 computation and (2) we want to study the performance of the NTAL application versus estimating the annual and semiannual signals. Table 2 lists the averages of the weighted root-mean-square (WRMS) scatters, computed over the time series of daily or weekly station position residuals, for three different stacking tests: standard stacking (STD), stacking with NTAL applied, and stacking where the annual and semiannual frequencies (FREQ2) are estimated with no NTAL model corrections applied. From the WRMS values presented in Table 2, we can see that for all four techniques, the FREQ2 test is

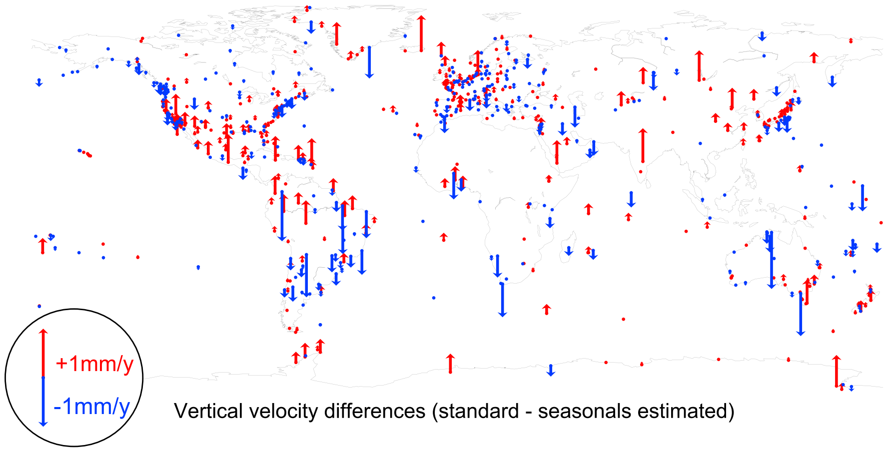

Figure 2. Differences between IGS site velocities obtained from a standard cumulative solution and a solution where annual and semiannual signals are estimated.

performing better than the two other tests, especially in the horizontal components, suggesting that estimating annual and semiannual signals is superior to applying NTAL model. We also computed individual WRMS values for each station resulting from the three stacking tests. In order to compare the performance of the FREQ2 versus NTAL approaches, we plotted in Figure 3 the station WRMS differences for all IGS stations between the NTAL and FREQ2 solutions or (NTAL−FREQ2) values. Positive values as depicted by Figure 3 mean that the WRMS of the FREQ2 solution are smaller than those of the NTAL solution. The percentages of positive values (i.e., better performance for FREQ2 solution) are 84%, 75%, and 59%, in the north, east, and up components, respectively. Similar percentage values are also obtained for the three other techniques. We believe that the better NTAL model performance for 41% of the GNSS/GPS stations in the vertical component is most likely driven by the fact that the NTAL model is able to capture short-period variations which are not accounted for by the annual and semiannual signals. However, although WRMS might not be the only

Table 2. WRMS Averages of Postfit Residuals, in mm, as Result of Three Stacking Tests: Standard Stacking (STD), Stacking With NTAL Applied, and Stacking Where the Annual and Semiannual Frequencies (FREQ2) Are Estimated With No NTAL Model Corrections Applied

Solution	East	North	Up
	IVS/VLBI, Session-Wise Sampling		
STD	3.79	3.97	11.00
NTAL	3.75	3.93	10.81
FREQ2	3.74	3.91	10.81
	ILRS/SLR, Weekly Sampling		
STD	8.91	10.91	8.18
NTAL	8.90	10.76	8.14
FREQ2	8.83	10.54	8.03
	IDS/DORIS, Weekly Sampling		
STD	13.34	10.21	11.84
NTAL	13.32	10.18	11.89
FREQ2	13.17	9.90	11.49
	IGS/GNSS, Daily Sampling		
STD	1.90	1.89	5.61
NTAL	1.85	1.84	5.07
FREQ2	1.74	1.71	5.04

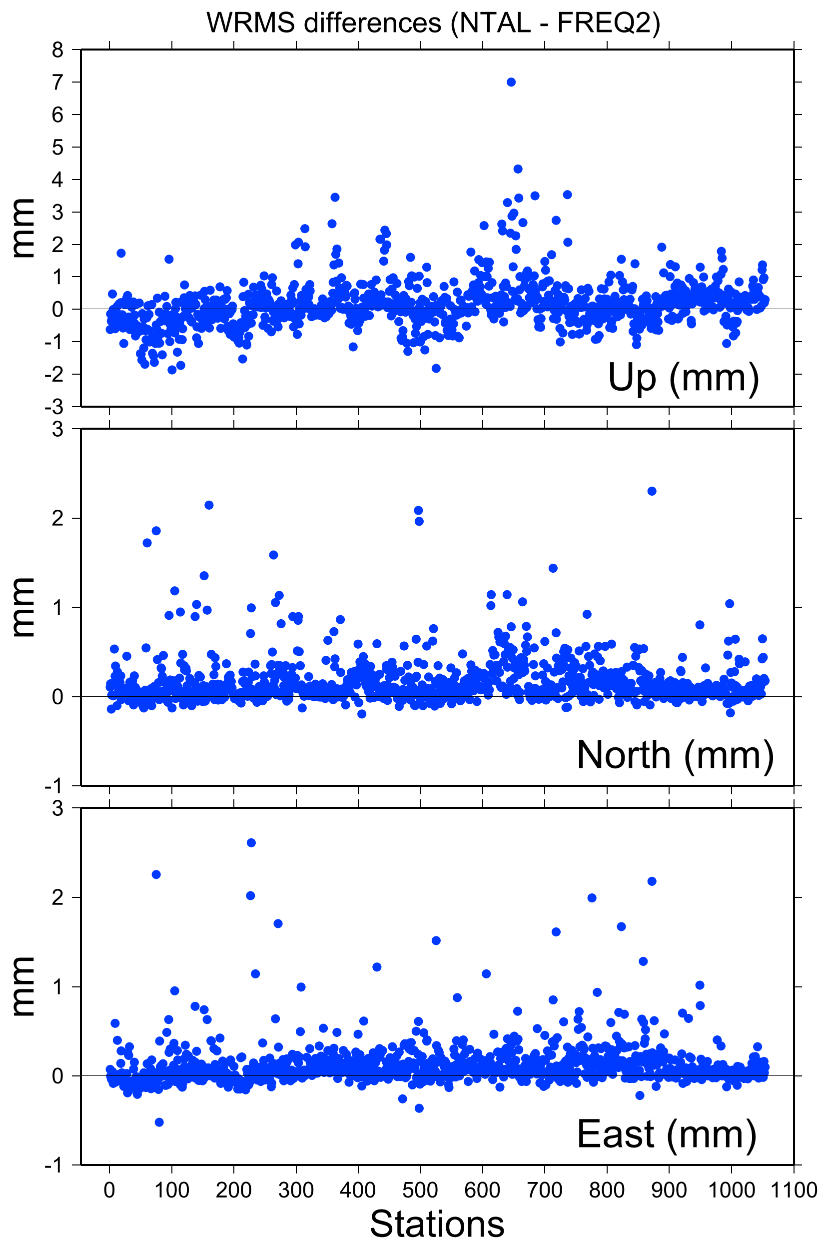

Figure 3. WRMS differences per GNSS station between a solution where nontidal atmospheric loading (NTAL) model was applied before stacking the time series and a solution where annual and semiannual signals were estimated during the stacking without the application of any NTAL corrections.

appropriate discriminator between the two approaches, as could be deduced from Figure 3, the performance of FREQ2 may reach up to 2.5 and 7 mm for some stations in the horizontal and up components, respectively, while the NTAL performance is well below 1 and 2 mm. We also noticed (not shown here) that the remaining station residuals after applying the NTAL corrections still exhibit periodic signals, mainly at the annual and semiannual frequencies, which are most likely reflecting other loading effects, such as ocean circulation and hydrology, or other remaining systematic errors.

For the ITRF2014 solution, based on the results described above, we decided to estimate annual and semiannual signals for stations with sufficient time span (longer than 2 years) for all four techniques and not to apply any external loading model corrections. While more investigations still need to be done, we might consider for future ITRF solutions to operate both loading model corrections and estimate annual and semiannual signals. However, we note that the approach using periodic functions helps to minimize any bias in the station position estimates, whereas this is not necessarily assured when applying NTAL model.

3.3. Handling of Discontinuities

GNSS station position time series are known to contain discontinuities of various origins, whose correct identification is critical for reliable estimation of the station velocities [*Williams*, 2003]. At present, manual methods for detecting discontinuities in GNSS time series tend to give better results than automated methods [*Gazeaux et al.*, 2013]. In order to identify the discontinuities present in the IGS-submitted time series, we therefore inspected them visually. To each of the time series, we iteratively fitted a model composed of a step function, a constant velocity, annual and semiannual signals, and, when needed, functions describing postseismic deformation behaviors (see the following section), until no discontinuity could be seen in the residual time series. To help in identifying discontinuities and relating them to known events, we made use of two external information sources. On one hand, we collected information about equipment changes from station log files gathered from different sources [*Rebischung et al.*, 2016]. On the other hand, we built a catalog of predicted coseismic offsets following the approach of *Métivier et al.* [2014]. For each earthquake registered in the Global Centroid Moment Tensor Project [*Dziewonski et al.*, 1981; *Ekström et al.*, 2012] during the period 1980–2015, we calculated the coseismic ground deformation at all the ITRF2014 station positions using Okada's algorithm [*Okada*, 1992] and assuming a combination of published earthquake self-similar scaling laws [*Scholz*, 1990; *Mai and Beroza*, 2000; *Yen and Ma*, 2011]. The calculations were made for more than 40,000 earthquakes with magnitude larger than 4, and all computed coseismic displacements larger than 1 mm were flagged as possible causes of discontinuities. In specific cases, a constant velocity was not enough to adequately describe the whole station position time series and velocity discontinuities were introduced in addition to position discontinuities. Most introduced velocity discontinuities describe instantaneous rate changes (mostly due to earthquakes) and are therefore associated with well-determined dates. But about one third (69 out of 187) of the velocity discontinuities were introduced to describe continuous rate changes in the series due to, e.g., slow-slip events or elastic response to current ice melting. In those cases, the dates of the velocity discontinuities were chosen so as to minimize the WRMS of the station residual time series. In the 1054 GNSS station position time series used in the ITRF2014 computation, a total of 1928 position-only or position+velocity discontinuities were identified. Nine hundred forty-two could be related to equipment changes, 567 to earthquakes, 69 were introduced to described continuous rate changes, while the remaining 350 have unknown causes.

For DORIS, SLR and VLBI, we used the same discontinuity epochs as for GNSS at earthquake colocation sites in order to ensure the consistency between the four techniques. The number of discontinuities due to earthquakes are 26 (out of 62), 20 (out of 41), and 40 (out of 49), for DORIS, SLR, and VLBI, respectively. For noncolocation sites, discontinuities were identified by visual inspection of the station position detrended residuals, as results from the individual stacking of the time series where seasonal signals were estimated.

3.4. Postseismic Deformation

After the release of ITRF2008 in 2010, it became more and more obvious that stations impacted by major earthquakes, and in particular the devastating ones in Sumatra (2004), Chile (2010), and Japan (2011), have nonlinear trajectories after these tragic events. Modeling the postseismic deformation (PSD) by piecewise linear functions as in the past ITRF versions is no longer an appropriate approach, at least because the estimated linear velocities of the segmented station time series are imprecise and do not adequately describe the real station postseismic trajectories.

Modeling the PSD for ITRF2014 sites could of course be done using possible available models constructed for each major earthquake individually [*Freed et al.*, 2006; *Pollitz*, 1997, 2014; *Trubienko et al.*, 2013]. However, not all earthquakes impacting the ITRF2014 sites have corresponding published models nor would it be manageable for us to evaluate and test the performance of available models against ITRF2014 input data.

For the ITRF2014 and in order to account for the PSDs of stations subject to major earthquakes, we adopted a more pragmatic approach by fitting parametric models to the ITRF2014 input time series of station positions. The four retained parametric models are (1) (Log)arithmic, (2) (Exp)onential, (3) Log+Exp, and (4) Exp+Exp. It is known that the PSDs have different structures, such as "transient after slip creep" behavior [*Marone et al.*, 1991; *Perfettini and Avouac*, 2004; *Savage et al.*, 2005] tending to follow a logarithmic function or of "viscoelastic relaxation" type [*Savage and Prescott*, 1978; *Pollitz*, 1997] that is better described by an exponential decay.

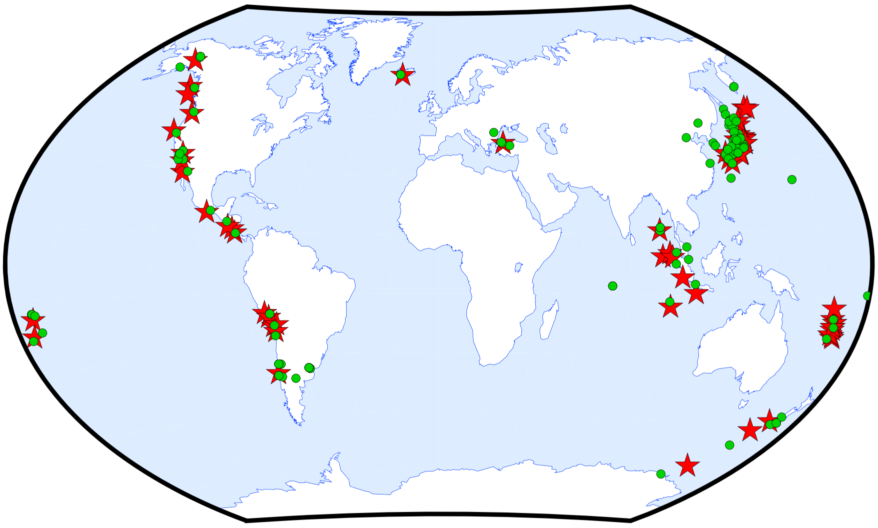

Figure 4. Distribution of earthquake epicenters (red) and ITRF2014 sites (green) impacted by postseismic deformation.

Logarithmic models were used by *Bevis and Brown* [2014] to describe the trajectory of earthquake sites using GPS time series, while *Freed et al.* [2010] used a combination of a logarithmic variation and an exponential decay.

We used the IGS GNSS contributed daily time series to fit parametric models for stations where PSD was judged visually significant, including a few stations impacted by major earthquakes that occurred prior to the start of their observations. The PSD models were fitted separately in each east, north, and up component, simultaneously with piecewise linear functions, annual, and semiannual signals. In case of a series with a unique earthquake causing PSD, 10 different models were first tried: None (0), Log (1), Exp (2), Log+Exp (3), and Exp+Exp (4), each combined with either a position-only or a position+velocity coseismic discontinuity. Among the tested models, those for which the relaxation time of at least one logarithmic or exponential function did not converge were discarded, as well as those leading to at least one insignificant estimated parameter (i.e., smaller than its formal error). Among the remaining models, we finally selected the model with the lowest Bayes Information Criterion [*Schwarz*, 1978], [*Kass and Raftery*, 1995]. For series with $n > 1$ earthquakes causing PSD, all possible 10^n model combinations were similarly tried and the best model combination was selected based on the same criteria.

Figure 4 illustrates in red the location of 59 earthquake epicenters that caused significant PSD at ITRF2014 sites and in green the impacted 123 stations located at 117 sites. We then applied the corrections predicted by the GNSS fitted models to the nearby stations of the three other techniques at earthquake colocation sites, before stacking their respective time series. In order to illustrate the performance of the PSD parametric models, Figure 5 displays the position time series of GNSS/GPS and the colocated VLBI stations at Tsukuba (Japan): in blue the raw data, in green the piecewise linear trajectories given by the ITRF2014 coordinates, and in red the trajectories obtained when adding the parametric PSD model. In that figure, one can see the remarkable fit of the PSD model, not only to the GNSS but also to the VLBI data.

While the ITRF2014 solution provides the usual/classical estimates: station positions at epoch 2010.0, station velocities, and EOPs, the PSD models are also part of the ITRF2014 products. The users should then be aware that they must compute the model corrections, using the equations supplied in Appendix C, to be then added to the ITRF2014 coordinates if the needed position epoch occurs during the postseismic relaxation period. Failing to do so would introduce position errors at the decimeter level for many stations impacted by PSDs. More information and some useful subroutines in Fortran are provided at the ITRF2014 website: http://itrf.ign.fr/ITRF_solutions/2014/.

3.5. ITRF2014 Multitechnique Combination

Once the first step is finalized and long-term frames of the four technique solutions are established, the second step of the ITRF2014 construction is operated. It consists of combining the derived four long-term solutions

10.1002/2016JB013098

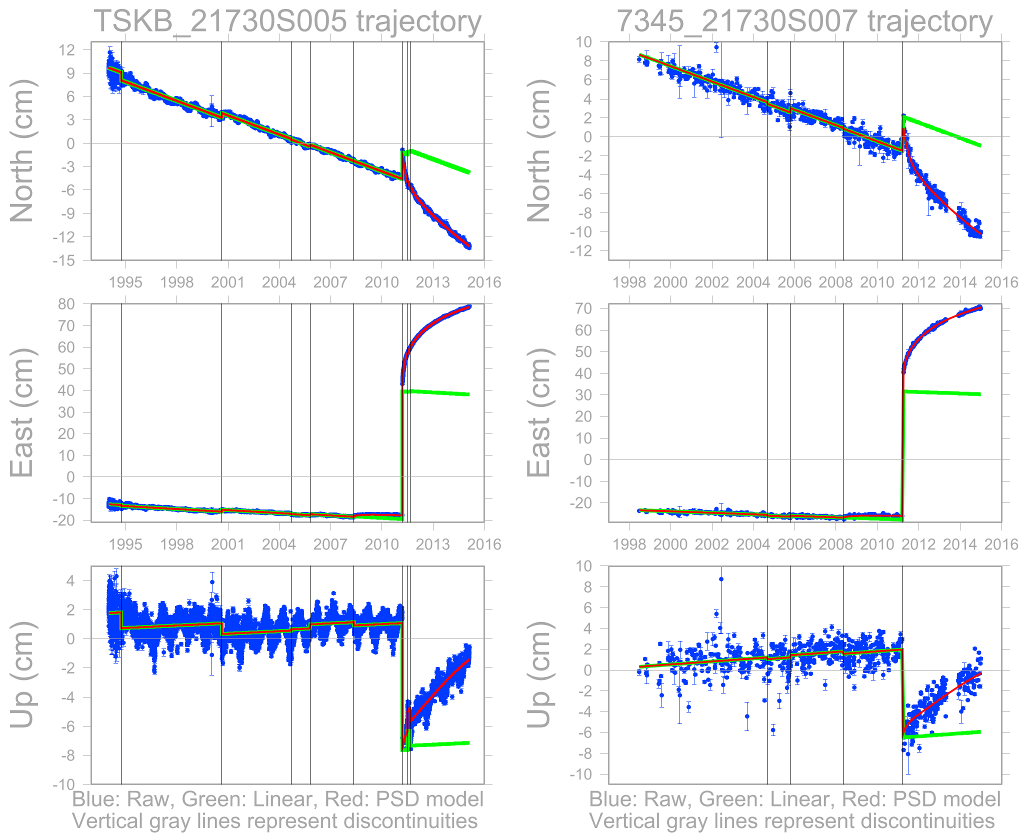

Figure 5. Trajectory of Tsukuba (Japan) site. (left column) GPS and (right column) VLBI. In blue raw data, in green the piecewise linear trajectories given by the ITRF2014 coordinates, and in red the trajectories obtained when adding the parametric PSD model.

together with local ties at colocation sites, involving station positions, velocities, and EOPs. At colocation sites, the seasonal signals of the different technique solutions estimated during the stacking phase were not combined in this second and final step of the ITRF2014 computation. The main reason for this choice is that we noticed large discrepancies for the annual and semiannual terms between techniques and therefore their combination would be difficult to interpret. However, we plan to study these terms separately in future work.

A certain number of test combinations were performed, by varying the weighting of the four technique solutions as well as the local ties. It is worth repeating here what we have discussed in the ITRF2008 paper [*Altamimi et al.*, 2011], which is, it is very difficult to adequately use a mathematically or statistically prescribed method of variance component estimation as the degree of freedom or Helmert method [*Bähr et al.*, 2007]. The main reason is that we have observations and constraints at colocation sites of different types: global space geodesy solutions, local ties (which are local by nature), and velocity equality constraints (cf. equation (1)). In addition, there are significant tie and velocity discrepancies between technique solutions at a number of colocation sites that necessitate an iterative combination and empirical weighting process.

For the ITRF2014, we adopted the following consecutive steps for the relative weighting of the space geodetic technique solutions, the local ties, as well as for the uncertainties of the velocity constraints (σ_v of equation (1)):

1. The long-term solutions of the four techniques were first properly weighted by the a posteriori variance factors obtained from the individual stacking of their respective time series, whose square roots are 2.30, 4.80, 5.02, and 2.62 for GNSS/GPS, VLBI, SLR, and DORIS, respectively.
2. An iterative combination process of the technique velocity fields was performed, as detailed in the following section.

3. Adopting the weighting found in steps 1 and 2, the local tie SINEX files were added with their reevaluated variances, as described in section 3.5.2, and an iterative combination process was performed where discrepant ties were downweighted. During this step, we also ensured that the a posteriori individual variance factors of the four technique solutions should not exceed unity by more than 10%. In order to satisfy this last condition, we found, empirically, that it was necessary to rescale the variance factor of the DORIS long-term solution by a factor of 3.5, while the variance factors of the three other technique solutions were unchanged.
4. The final ITRF2014 adjustment was performed by adding the EOP parameters into the combination. At this final stage, we iterated the combination as necessary and at each iteration rejected any individual input EOP parameter if its normalized residual exceeded a threshold of 3. We also noticed here that when adding the polar motion estimates of the ILRS solution into the combination, it produces a small frame distortion, i.e., increases the position residuals, up to 4 mm with large normalized residuals exceeding the threshold of 3 for a few stations. This behavior needs further investigation in future work and is probably due to a network effect or station positions and polar motion mismatch. In the meantime, in order to avoid that small distortion in the SLR frame, we downweighted the ILRS polar motion estimates by a factor of 2. Doing so stabilized the SLR frame within the overall ITRF2014 combination, and the small distortion disappeared.

3.5.1. Equating Station Velocities at Colocation Sites

An initial combination of the four technique velocity fields was performed (downweighting station positions and local ties) in order to evaluate the level of the velocity agreement between techniques at colocation sites and consequently adopt the appropriate σ_v for the velocity constraint (equation (1)) between colocated reference points. Velocity constraints were added, using equation (1), between a chosen GNSS marker and reference points of the colocated instruments of the three other techniques that are available at these sites. In sites where multiple points of the same technique exist, only one pair of GNSS and other technique points were constrained in velocities, considering that almost all (with a few exceptions) of these multiple points were already constrained to the same velocity during the process of their stacking. The main criterion adopted for the selection of pairs of points (or segments in case of discontinuities) for the velocity constraints was to choose the longest and most stable time series by inspecting their respective detrended residuals. Note that 0.1 mm/yr per component was chosen as an initial value of the σ_v for the velocity constraints, over each component, between GNSS and SLR and VLBI colocated points, while 1 mm/yr was selected for the GNSS and DORIS points. This combination of velocity fields was iterated as necessary, and at each iteration the σ_v of equation (1) was increased for sites where the normalized velocity residual of any of the three components exceeded the threshold of 3. We noticed that selecting smaller initial values for σ_v would lead to an increase in its value for a significant number of colocated sites. Consequently, these initial values represent, for the best sites, the level of the velocity agreement between GNSS and the three other techniques.

3.5.2. Handling of Local Ties

It is worth recalling here that as always performed in previous ITRF combinations, the local ties are used as observations, as described in *Altamimi et al.* [2002b], with a proper weighting for each individual colocation site and local tie SINEX file. In the ITRF2014 combination, we introduced two scaling variance factors for the weighting of local ties: one for the horizontal and one for the vertical component. The justification of this choice is based on the fact that (1) local surveys are often operated using different and independent methods for the horizontal (mainly distance and direction measurements), and the vertical (usually by spirit leveling measurements) components, and (2) the terrestrial vertical measurements are more precise than not only the horizontal but also the vertical estimates of space geodesy.

The initial horizontal and vertical scaling variance factors are computed, for each individual local tie SINEX file, by reevaluating their variances expressed in the local frame, with the condition that the uncertainty per tie vector component (east, north, or up) should not be below 3 mm. The reasons for this condition are that (1) we believe that a local tie between physically inaccessible instrumental measurement reference points is unlikely to be precise to better than 3 mm and (2) the level of agreement between local ties and space geodesy estimates is by far larger than 3 mm for most of the colocation sites.

As for most of the colocation sites, there are discontinuities in the time series of station positions, due not only to earthquakes but also to equipment changes, especially for GNSS. We had to adopt a rationale for selecting the points (or segments) to be tied together. Assigning the tie to the segments spanning the epoch of the survey is not always appropriate, since (1) we have no means to know the real “true” station position among the different discontinuity segments and (2) for many cases we found that the epoch of the survey

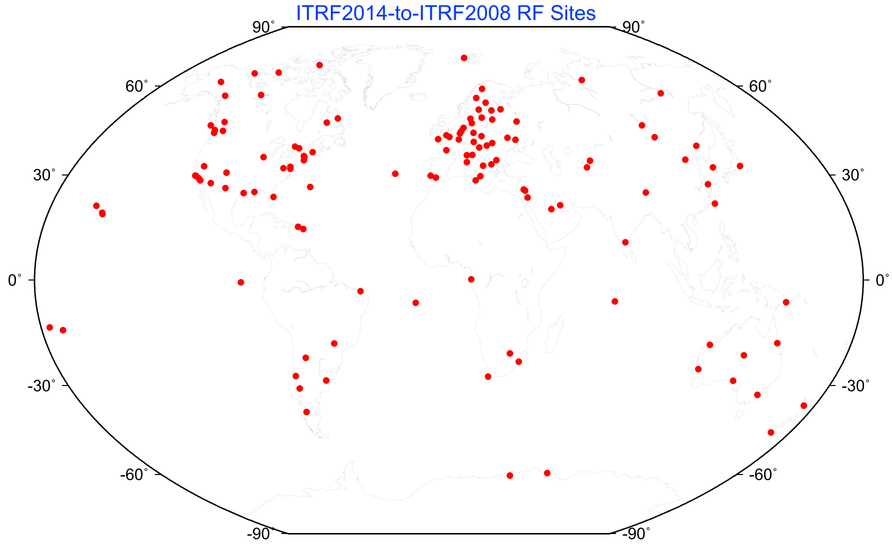

Figure 6. Location of the reference frame sites used in the estimation of the 14 transformation parameters between ITRF2014 and ITRF2008 and their orientation alignment.

coincides with segments with very short time spans. Therefore, we decided to assign the tie to the longest and most stable segments, by inspecting (as for the velocity ties) the detrended time series of the station position residuals. This choice holds for the 36 colocation sites where multiple ties (resulting from surveys conducted at different epochs) are available.

Using all available local ties, we empirically and iteratively downweighted the discrepant ties during the combination process in such a way that the normalized residual does not exceed a threshold of 3 for any of the three components. We choose to downweight the local ties rather than space geodesy solutions in order to avoid contaminating the combined frame-defining parameters by local tie and space geodesy discrepancies and at the same time to preserve the consistency between individual technique solutions and ITRF2014. Counting the percentages of tie discrepancies smaller than 5 mm between terrestrial tie vectors and space geodesy estimates, for stations with reasonable time span (>3 years) of observations, we found 42%, 29%, and 23% for GNSS-VLBI, GNSS-SLR, and GNSS-DORIS, respectively. For completeness, the full list of tie discrepancies is available at the ITRF2014 website.

3.5.3. ITRF2014 Frame Specifications

At this second step, the ITRF2014 is specified by the following frame parameters:

1. *Origin*. The ITRF2014 origin is defined in such a way that there are zero translation parameters at epoch 2010.0 and zero translation rates with respect to the mean origin of the ILRS SLR time series.
2. *Scale*. The scale of the ITRF2014 is defined in such a way that there is zero scale factor at epoch 2010.0 and zero scale rate with respect to the average of the implicit scales and scale rates of VLBI and SLR time series.
3. *Orientation*. The ITRF2014 orientation is defined in such a way that there are zero rotation parameters at epoch 2010.0 and zero rotation rates between ITRF2014 and ITRF2008. These two conditions were applied over a set of 127 reference stations located at 125 sites as illustrated by Figure 6.

4. ITRF2014 Results

4.1. ITRF2014 Origin and Geocenter Motion

As for previous ITRF solutions, the origin of ITRF2014 is defined solely by ILRS SLR data, i.e., satisfying the condition of zero translation and zero translation rate between ITRF2014 and the SLR cumulative solution. The long-term intrinsic origin of the latter is preserved via the usage of internal constraints [*Altamimi et al.*, 2007], over the time span 1993.0–2015.0. Figure 7 illustrates the full time series of the ILRS SLR origin components with respect to ITRF2014. However, when generating the final ILRS SLR cumulative solution used in the ITRF2014 computation, the annual and semiannual signals discernable in Figure 7 were constrained to zero

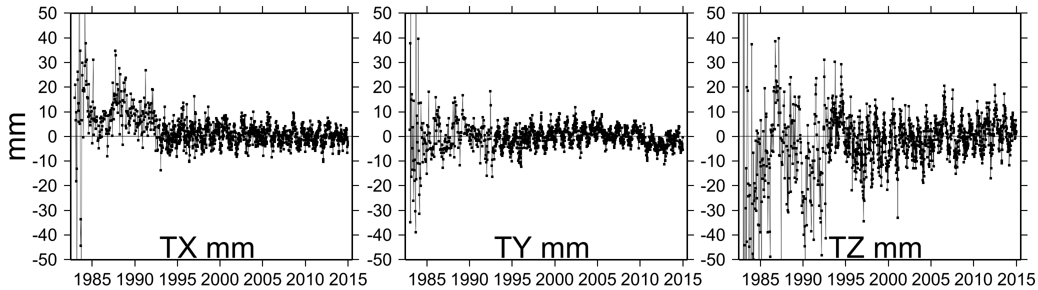

Figure 7. Time series of SLR geocenter components with respect to ITRF2014, in mm.

(over the 1993.0–2015.0 time span) via the usage of internal constraints, as defined by equation (B4). We verified that the small offset in the Y component around 2010 that can be seen in Figure 7 biases the long-term ITRF2014 origin along that component by a negligible amount of 0.1 mm/yr.

The performance and accuracy of the ITRF2014 origin could be evaluated by comparison to the ITRF2008 results. The comparison between the two frames showed small translation components at epoch 2010.0, namely, 1.6, 1.9, and 2.4 mm, along the three axes X, Y, Z., respectively. The translation rates are statistically zero over the three components. These results are an indication of the level of the ITRF origin stability achievable today using SLR data, dominated by LAGEOS I and II observations [*Luceri and Pavlis*, 2016].

Although there exist different definitions of the geocenter motion in the literature, it is defined here as the motion of the Center of Mass (CM) of the total Earth system with respect to the center of figure (CF) of the solid Earth surface, in response to various geophysical fluid displacements within the Earth system, such as the atmosphere, oceans, terrestrial hydrology, and ice sheets [*Wu et al.*, 2012]. While the rate of a possible secular component of the geocenter motion is believed to be less than 1 mm/yr [*Métivier et al.*, 2010, 2011], the amplitude of the annual signal is significant and may reach up to 6 mm along the Z axis.

While the ITRF2014 origin follows the average CM, realized by SLR data, only linearly with time, some applications such as satellite precise orbit determination require station coordinates to be referred to the

Table 3. Annual Amplitude (A) and Phase (ϕ) Fitted to the Time Series of the Translation Components and Scale Factors Estimated During the Staking of the Individual Technique Solutions[a]

	T_X		T_Y		T_Z		Scale	
	A	ϕ	A	ϕ	A	ϕ	A	ϕ
TC	(mm)	(deg)	(mm)	(deg)	(mm)	(deg)	(mm)	(deg)
				ITRF2014				
IVS	-	-	-	-	-	-	1.8	245
±							0.1	3
ILRS	2.6	46	2.9	320	5.7	28	0.7	258
±	0.1	3	0.1	2	0.2	2	0.1	8
IDS	2.6	158	3.5	308	0.5	151	0.4	204
±	0.1	3	0.2	2	0.7	71	0.1	13
				ITRF2008 [*Altamimi et al.*, 2011][b]				
IVS	-	-	-	-	-	-	2.2	241
±							0.1	3
ILRS	2.6	42	3.1	315	5.5	22	0.6	255
±	0.1	3	0.1	2	0.3	10	0.1	10
IDS	3.9	147	4.6	340	4.4	295	0.3	206
±	0.2	3	0.3	3	1.1	14	0.1	27

[a] Amplitude and phase are defined by $A\cos(2\pi \cdot t - \phi)$ with t in decimal year.
[b] 180° is added to the phase values of the translation components in order to be consistent with the geocenter motion definition of the IERS Conventions.

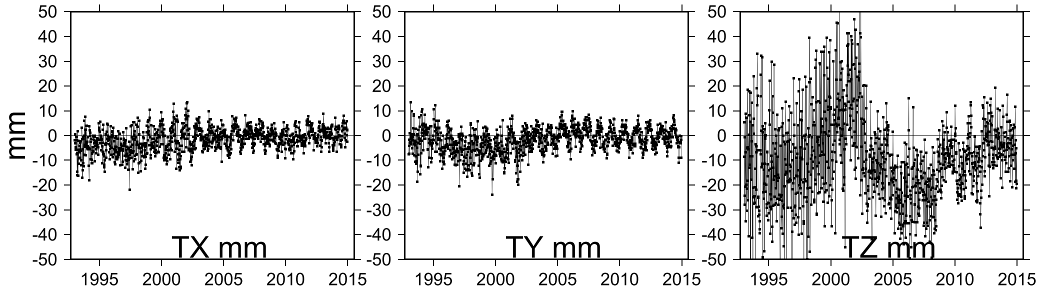

Figure 8. Time series of DORIS geocenter components with respect to ITRF2014, in mm.

instantaneous CM. In order to satisfy these applications, we recommend the usage of an annual geocenter motion model derived from the same SLR data that define the ITRF2014 long-term origin that is to apply to the ITRF2014 station coordinates a correction, δX_{CM}, given by

$$\delta X_{CM} = A\cos(2\pi \cdot t - \phi) \tag{2}$$

so that

$$X_{CM} = X_{ITRF2014} - \delta X_{CM} \tag{3}$$

where the amplitude A and phase ϕ are provided in Table 3 and t is the decimal year. Note that equation (3) is fully consistent with the IERS Conventions [*Petit and Luzum*, 2010, chap. 4]. Moreover, because estimating the scale when stacking the SLR time series may impact the parameters of the annual geocenter motion model [*Collilieux et al.*, 2011], we performed a stacking without estimating the scale parameter. The resulting amplitudes and phases along the three components are similar to, and within the uncertainties of the results listed in Table 3, at the level of 0.3 mm.

For comparison, we reproduce in Table 3 the ITRF2008 results published in *Altamimi et al.* [2011], by adding 180° to the phase values in order to be consistent with the geocenter motion definition of the IERS Conventions. Comparing the annual amplitudes and phases of the SLR translation components with those of ITRF2008, we noticed very similar estimates; i.e., the differences are less than the 3 sigma level for all the values listed in Table 3. The good agreement between ITRF2014 and ITRF2008 modeled geocenter motion, which is at the level of or better than 0.5 mm, is an indication of the intrinsic good performance of the SLR data in sensing the geocenter motion.

The time series of the DORIS geocenter components are plotted in Figure 8 where the annual and semiannual terms are not removed so that SLR (cf. Figure 7) and DORIS results can be compared. It is easy to see from Figures 7 and 8 that there is some similarity for X and Y components between the two techniques, SLR and DORIS, respectively. As listed in Table 3, the geocenter agreement in X and Y components between SLR and DORIS is at the level of 0.6 mm in amplitude, while larger phase discrepancy of 112° is found for the X geocenter component. However, the DORIS Z geocenter is much more scattered than that of SLR and is probably still suffering from some mismodeling issues, such as solar radiation pressure [*Gobinddass et al.*, 2009]. Moreover, from Table 3, we can observe that the amplitude of the DORIS Z geocenter component is discrepant by about 5 mm, compared to SLR estimate, and by about 4 mm compared to ITRF2008 DORIS results.

4.2. ITRF2014 Scale

We followed the same strategy as for ITRF2008 to specify the ITRF2014 scale, that is, to have zero scale and scale rate between ITRF2014 and the arithmetic average of the intrinsic scales of SLR and VLBI solutions. This choice is justified by the fact that we do not have any means to discriminate between the two technique solutions and therefore their simple average is a fair choice that minimizes the scale impact for these two techniques when using the ITRF2014 products. Figure 9 (left) displays the full time series of the scale factors of VLBI, SLR, and DORIS solutions with respect to ITRF2014. However, during the first step of the ITRF2014 computation, i.e., stacking of the individual times series, we made a selection of the weekly SLR and DORIS and daily (session-wise) VLBI solutions to define their respective long-term scales, using the internal constraints approach as described in *Altamimi et al.* [2007]. The justification of this filtering, for the scale definition, is to retain the most precise scale determinations of the three solutions. Therefore, in order to define the respective long-term scales of the three technique cumulative solutions, we excluded the ILRS time series before 1993.0,

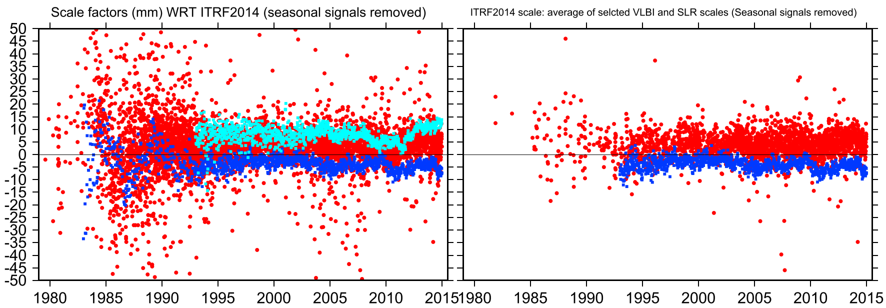

Figure 9. Full time series of (left) scale factors with respect to ITRF2014 and (right) selected SLR and VLBI scale factors whose average defines the ITRF2014 scale, in mm, annual and semiannual signals removed: daily VLBI (red) and weekly SLR and DORIS (blue and light blue), respectively.

the IVS sessions with less than five stations and sessions with regional coverage, and the DORIS data after 2012 because of the offset and drift change after that epoch which can be observed in Figure 9 (left). Figure 9 (right) illustrates the selected VLBI and SLR scale factors whose average defines the ITRF2014 scale. Similar to the *Y* component, the small SLR scale offset around 2010 has negligible impact on the long-term SLR scale of 0.1 mm/yr.

Several combinations of the long-term solutions of the four techniques were tested by varying the local tie weighting and number, such as using those tie vectors with discrepancies with space geodesy solutions smaller than 5 mm. The different combination tests yielded scale factors between SLR and VLBI solutions ranging between 1.4 and 1.7 ppb. We found that the most precise estimation (smallest uncertainty) of the scale factor between the two technique solutions is the one that makes use of all possible and available local tie SINEX files, properly weighted as described in section 3.5.2. The result of the final ITRF2014 combination showed then a scale factor between VLBI and SLR solutions of 1.37 ($\pm$0.10) ppb at epoch 2010.0 and a scale rate of 0.02 ($\pm$0.02) ppb/yr. The ITRF2014 results regarding the level of the scale agreement between SLR and VLBI confirm the ITRF2008 finding and are an indication of the persistent scale offset between the two technique solutions. These results suggest that there is still an urgent need for investigation on the causes of the scale discrepancy, e.g., range biases in case of SLR [*Appleby et al.*, 2016] and possible effects due to VLBI antenna gravity deformations [*Sarti et al.* 2009, 2010].

The scale offset of the DORIS solution with respect to ITRF2014 is 1.16 ppb at epoch 2010.0, and the scale rate is −0.02 ppb/yr. Note that the DORIS scale offset has increased by about 0.5 ppb, compared with ITRF2008 results, which is mainly due to the application of the DORIS ground antenna phase laws by the IDS analysis centers who contributed to the IDS combined solution submitted to the ITRF2014 [*Moreaux et al.*, 2016].

Using the filtered time series of VLBI, SLR, and DORIS scale factors, we computed the annual amplitudes and phases listed in Table 3. Note that the values listed in Table 3 result from the stacking where the periodic signals were not estimated. As can be seen in that table, the ITRF2014 results confirm those of ITRF2008 for the scale amplitudes and phases of the three techniques, at the level of (or better than) 3 sigma. Note, however, that while the VLBI phase is almost similar to SLR one, its amplitude is at least 2 times larger than SLR estimate. This large-amplitude difference can be related, partly, to some mismodeling of the VLBI antenna thermal deformation and partly to the difference of the network shapes of the two techniques. Indeed, the annual scale variation can be interpreted as the mean vertical motion of the implied network of stations [*Collilieux et al.*, 2010], which is different from one technique to another.

4.3. ITRF2014 Earth Orientation Parameters

As for the past ITRF2005 and ITRF2008 solutions, the ITRF2014 rigorous combination provides consistent and fully frame-compatible EOPs: polar motion (PM) components and their daily rates (PM rate), as well as universal time (UT1-UTC) and length of day (LOD). ITRF2014 PM components are the result of the combination of the four technique solutions, PM rate values are determined by combining GNSS and VLBI time series, while UT1-UTC and LOD are determined using VLBI data, uniquely, in order to avoid possible biased estimates from satellite techniques [*Ray*, 1996, 2009].

Figure 10 displays the PM postfit residuals in *x* and *y* components, illustrating the level of agreement between the four techniques, where one can see that GNSS PM series dominate the other technique estimates. The

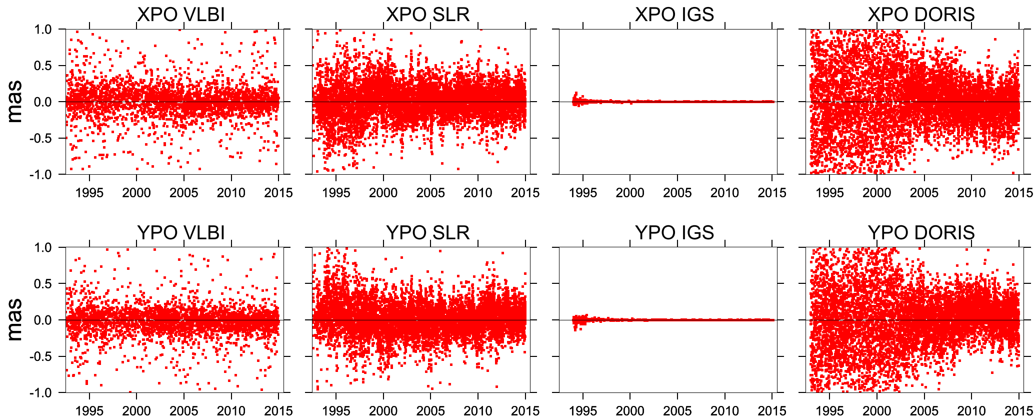

Figure 10. ITRF2014 postfit residuals of polar motion in milliarcseconds.

reader should, however, note that in the ITRF combination, common PM parameters help in tying the four technique solutions, via their relations with the two frame rotation parameters around the *X* and *Y* axes. It should also be noted that estimating station seasonal signals induces a small seasonal signal in the EOP time series. Indeed, using the IGS time series, we compared polar motion estimates resulting from two cumulative solutions, with and without estimating the seasonal signals. The difference between the two polar motion sets is a small sinusoidal curve with amplitude less than 5 μas, far less than the formal errors.

4.4. Transformation Parameters Between ITRF2014 and ITRF2008

In order to ensure the link between ITRF2014 and past ITRF solutions, for many geodetic applications, it is essential to provide to the users the 14 transformation parameters with respect to ITRF2008 and consequently to past ITRF solutions.

The same 127 stations displayed in Figure 6 that were used to ensure the alignment of the ITRF2014 orientation and rate parameters to the ITRF2008 were also used to estimate the transformation parameters between the two frames. The main criterion for the selection of these 127 stations were (1) to have the best possible site distribution; (2) to involve as many as possible VLBI, SLR, GNSS, and DORIS stations; and (3) to have the best agreement between the two frames in terms of postfit residuals of the 14-parameter transformation. Regarding this third criteria, the WRMS values of the 14-parameter similarity transformation fit are 1.8, 1.6, and 2.4 mm in position (at epoch 2010.0) and 0.2, 0.2, 0.3 mm/yr in velocity, in east, north, and vertical components, respectively. Table 4 lists the transformation parameters from ITRF2014 to ITRF2008, to be used with the transformation formula given by equation (4).

$$
\begin{cases}
\begin{pmatrix} x \\ y \\ z \end{pmatrix}_{i08} = \begin{pmatrix} x \\ y \\ z \end{pmatrix}_{i14} + T + D \begin{pmatrix} x \\ y \\ z \end{pmatrix}_{i14} + R \begin{pmatrix} x \\ y \\ z \end{pmatrix}_{i14} \\
\begin{pmatrix} \dot{x} \\ \dot{y} \\ \dot{z} \end{pmatrix}_{i08} = \begin{pmatrix} \dot{x} \\ \dot{y} \\ \dot{z} \end{pmatrix}_{i14} + \dot{T} + \dot{D} \begin{pmatrix} x \\ y \\ z \end{pmatrix}_{i14} + \dot{R} \begin{pmatrix} x \\ y \\ z \end{pmatrix}_{i14}
\end{cases} \tag{4}
$$

Table 4. Transformation Parameters at Epoch 2010.0 and Their Rates From ITRF2014 to ITRF2008, to Be Used With Equation (4)

	T_x (mm)	T_y (mm)	T_z (mm)	D (ppb)	R_x (mas)	R_y (mas)	R_z (mas)
	$\dot{T}_x$ (mm/yr)	$\dot{T}_y$ (mm/yr)	$\dot{T}_z$ (mm/yr)	$\dot{D}$ (ppb/yr)	$\dot{R}_x$ (mas/yr)	$\dot{R}_y$ (mas/yr)	$\dot{R}_z$ (mas/yr)
	1.6	1.9	2.4	−0.02	0.00	0.00	0.00
±	0.2	0.1	0.1	0.02	0.06	0.06	0.06
	0.0	0.0	−0.1	0.03	0.00	0.00	0.00
±	0.2	0.1	0.1	0.02	0.06	0.06	0.06

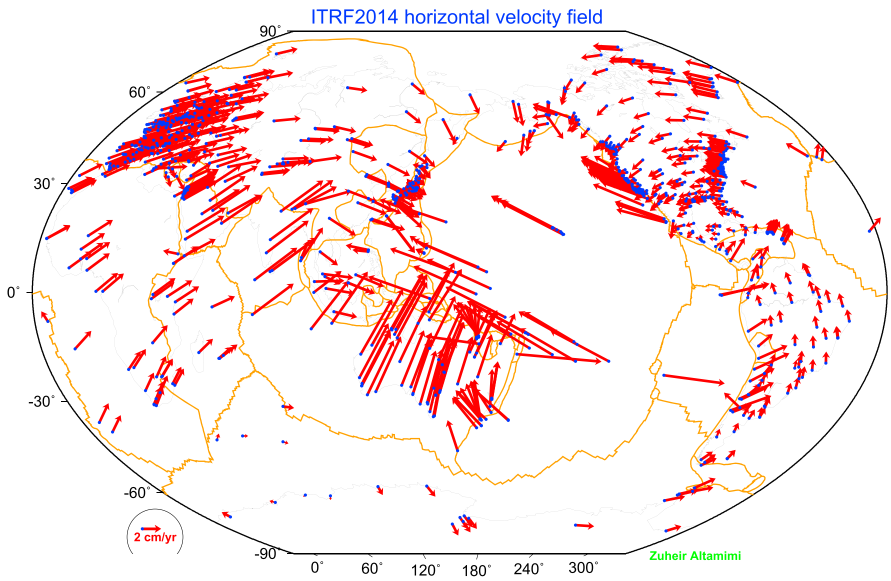

Figure 11. ITRF2014 horizontal site velocities with formal error less than 0.2 mm/yr. Major plate boundaries are shown according to *Bird* [2003].

where *i*08 designates ITRF2008 and *i*14 ITRF2014, T is the translation vector, $T = (T_x, T_y, T_z)^T$, D is the scale factor, and R is the matrix containing the rotation angles, given by

$$R = \begin{pmatrix} 0 & -R_z & R_y \\ R_z & 0 & -R_x \\ -R_y & R_x & 0 \end{pmatrix}$$

The dotted parameters designate their time derivatives. The values of the 14 parameters are those listed in Table 4. Note that the inverse transformation from ITRF2008 to ITRF2014 follows by interchanging (*i*14) with (*i*08) and changing the sign of the transformation parameters.

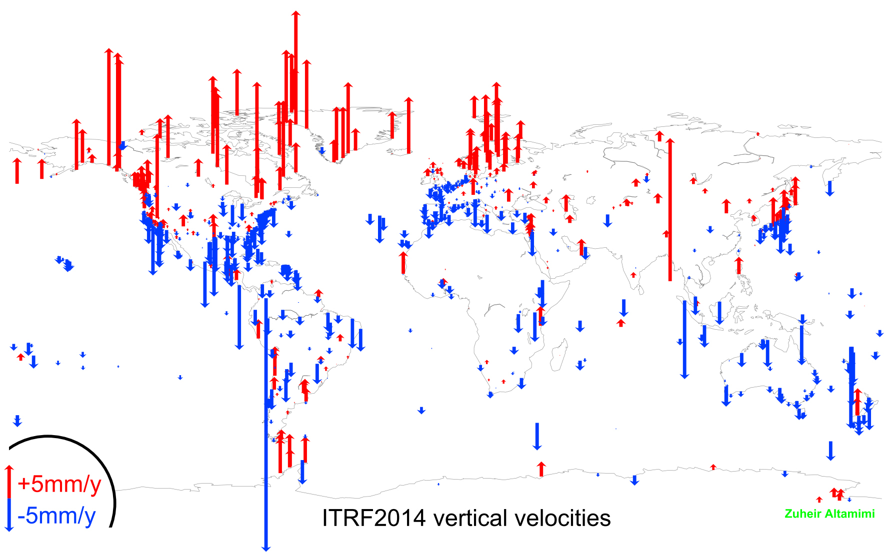

Figure 12. ITRF2014 vertical site velocities with formal error less than 0.2 mm/yr.

4.5. ITRF2014 Velocities

Figures 11 and 12 show the ITRF2014 horizontal and vertical velocity fields for sites with formal error less than 0.2 mm/yr. As the ITRF2014 includes more sites (especially GNSS sites) than ITRF2008, it is anticipated that a more robust plate motion model can be derived, compared to ITRF2008 one [*Altamimi et al.*, 2012], involving more sites on stable parts of the tectonic plates. A dedicated study is underway at the time of writing to develop a plate motion model consistent with ITRF2014.

The ITRF2014 vertical velocities illustrated by Figure 12 show clear regional patterns, especially in North America, Greenland, and Fennoscandia, reflecting the uplift caused by not only Glacial Isostatic Adjustment but also recent or current ice melting. The geophysical interpretation of the ITRF2014 vertical velocities is under investigation, as was the case for ITRF2008 [*Métivier et al.*, 2012] and will be the subject of a dedicated publication.

5. Conclusion

Precisely estimating seasonal signals present in the time series of station positions and modeling postseismic deformation for sites subject to major earthquakes are the main innovations implemented in the ITRF2014 construction.

Although the periodic signals were not expected to influence the ITRF2014 frame-defining parameters (which was numerically verified), estimating the annual and semiannual signals has negligible impact (less than 0.05 mm/yr) on horizontal station velocities, while up to 1 mm/yr vertical velocity changes are observed for some stations that are subject to large seasonal signals or a large number of discontinuities or data gaps in their time series. Estimating the seasonal frequencies performs better (in terms of WRMS reduction) than applying a nontidal atmospheric loading model, for about 80% and 60% of the GNSS stations in the horizontal and vertical components, respectively. Although more investigation still needs to be done, we might consider in future ITRF solutions applying a loading model and at the same time solving for seasonal signals.

Modeling the postseismic deformation for sites impacted by major earthquakes has the potential to accurately describe their actual trajectories and also to adequately infer the linear part of their motions. We showed that the fitted parametric models using IGS GNSS data match the station position time series of the other three techniques at colocation sites, thus enforcing their link and consistency within the ITRF2014 frame.

The ITRF2014 long-term origin is found to be close to that of ITRF2008 at the level of less than 3 mm over the time span of SLR observations (1993.0 onward), reflecting the intrinsic origin accuracy estimated by SLR data. For some applications, e.g., satellite precise orbit determination, where a geocenter motion model is needed to refer ITRF2014 coordinates to the instantaneous Earth Center of Mass (CM), we recommend the usage of the annual geocenter motion model published in this paper that is consistent with the ITRF2008-derived model at the level of 0.5 mm; see Table 3.

The ITRF2014 extensive data analysis, with various test combinations, confirms the persistent scale offset between SLR and VLBI solutions at the level of 1.4 ppb (≈8.7 mm at the equator). The ITRF2014 long-term scale being in the middle of the intrinsic scales of SLR and VLBI minimizes its impact on the results of these two techniques when using ITRF2014 products.

As was already shown with the past ITRF2008 results [*Altamimi et al.*, 2011], there are still significant discrepancies between space geodesy solutions and terrestrial local ties, since more than 50% of the available SLR and VLBI tie vectors to GNSS exhibit residuals larger than 5 mm, and about 30% have residuals larger than 10 mm. We believe that most of these discrepancies are related to technique systematic errors rather than to local ties. While there is still room for improving the technique analysis strategies and results, this should be coupled with improving the ground geodetic infrastructure, toward next generation of SLR and VLBI technologies, with better coverage between the Northern and Southern Hemispheres. VLBI in particular needs to evolve toward more frequent global observational session schedules, with increased number and well-distributed stations.

Maintaining and improving the geodetic infrastructure is the prerequisite for the long-term sustainability of the ITRF, as recognized by the United Nations General Assembly resolution on the global geodetic reference frame for sustainable development.

Appendix A: Combination Model

The main two equations of the combination model implemented in CATREF Software are given below. They involve a 14-parameter similarity transformation, station positions, and velocities, and EOPs and are written as

$$\begin{cases} X_s^i = X_c^i + \left(t_s^i - t_0\right) \dot{X}_c^i \\ \quad + T_k + D_k X_c^i + R_k X_c^i \\ \quad + \left(t_s^i - t_k\right) \left[\dot{T}_k + \dot{D}_k X_c^i + \dot{R}_k X_c^i\right] \\ \dot{X}_s^i = \dot{X}_c^i + \dot{T}_k + \dot{D}_k X_c^i + \dot{R}_k X_c^i \end{cases} \tag{A1}$$

$$\begin{cases} x_s^p &= x_c^p + R_{yk} \\ y_s^p &= y_c^p + R_{xk} \\ \mathrm{UT}_s &= \mathrm{UT}_c - \frac{1}{f} R_{zk} \\ \dot{x}_s^p &= \dot{x}_c^p \\ \dot{y}_s^p &= \dot{y}_c^p \\ \mathrm{LOD}_s &= \mathrm{LOD}_c \end{cases} \tag{A2}$$

where for each point i, X_s^i (at epoch t_s^i) and $\dot{X}_s^i$ are positions and velocities of technique solution s and X_c^i (at epoch t_0) and $\dot{X}_c^i$ are those of the combined solution c. For each individual frame k, as implicitly defined by solution s, D_k is the scale factor, T_k is the translation vector, and R_k is the rotation matrix. The dotted parameters designate their derivatives with respect to time. The translation vector T_k is composed of three origin components, namely, T_x, T_y, T_z, and the rotation matrix of three small rotation parameters, R_x, R_y, and R_z, following the three axes, respectively, X, Y, and Z. t_k is a conventionally selected epoch of the seven transformation parameters. In addition to equation (A1) involving station positions (and velocities), the EOPs are added by equation (A2), making use of pole coordinates x_s^p, y_s^p and universal time UT_s as well as their daily rates $\dot{x}_s^p$, $\dot{y}_s^p$ and LOD_s, where $f = 1.002737909350795$ is the conversion factor from UT into sidereal time. The link between the combined frame and the EOPs is ensured via the three rotation parameters appearing in the first three lines of equation (A2).

Note that equation (A1) uses the linearized form of the general similarity transformation formula, neglecting second- and higher-order terms [*Petit and Luzum*, 2010, chap. 4; *Altamimi and Dermanis*, 2012].

In the first step of the ITRF construction, the first two lines of (A1) and the entire equation (A2) are used to estimate long-term solutions for each technique, by accumulating (rigorously stacking) the individual technique time series of station positions and EOPs. In the second step, the entire two equations are used to combine the long-term solutions obtained in step 1, together with local ties in colocation sites.

Appendix B: Equations for Periodic Signals

The general equation used for the estimation of the periodic signals embedded in the time series of station positions is written as

$$\Delta X_f = \sum_{i=1}^{n_f} a^i \cos(\omega_i t) + b^i \sin(\omega_i t) \tag{B1}$$

where ΔX_f is the total sum of the contributions of all the frequencies considered, n_f is the number of frequencies, $\omega_i = \frac{2\pi}{\tau_i}$, where τ_i is the period of the ith frequency, e.g., annual and semiannual.

Each frequency adds six parameters per station, i.e., $(a_x^i, a_y^i, a_z^i, b_x^i, b_y^i, b_z^i)^T$, in addition to the six position and velocity parameters.

In the case of stacking of time series of station positions, and since the combination model described in Appendix A includes the transformation parameters for each daily or weekly solution with respect to the combined/stacked frame, each frequency introduces seven singularities in the normal equation system, corresponding to the three origin, one scale and three rotation components.

Several mathematical options could be implemented to avoid the seven singularities, such as minimum or internal constraint approaches, in the same way they are usually used for the reference frame definition.

B1. Periodic Signals: Minimum Constraints

In the stacking case, the equations of the minimum constraints approach take the form

$$(A^TA)^{-1}A^T \begin{pmatrix} \delta a_x^i \\ \delta a_y^i \\ \delta a_z^i \end{pmatrix} = (A^TA)^{-1}A^T \begin{pmatrix} a_{xR}^i - a_x^i \\ a_{yR}^i - a_y^i \\ a_{zR}^i - a_z^i \end{pmatrix} \quad \text{(B2)}$$

$$(A^TA)^{-1}A^T \begin{pmatrix} \delta b_x^i \\ \delta b_y^i \\ \delta b_z^i \end{pmatrix} = (A^TA)^{-1}A^T \begin{pmatrix} b_{xR}^i - b_x^i \\ b_{yR}^i - b_y^i \\ b_{zR}^i - b_z^i \end{pmatrix} \quad \text{(B3)}$$

where A is the well-known design matrix of partial derivatives of the seven transformation parameters and $(a_{xR}^i, a_{yR}^i, a_{zR}^i, b_{xR}^i, b_{yR}^i, b_{zR}^i)^T$ are the reference values for each frequency i that could be taken from an external loading model or as zeros over a set of homogeneously and well-distributed network of stations.

B2. Periodic Signals: Internal Constraints

The inclusion of the transformation parameters in the combination model offers the possibility to use the internal constraint approach as developed in *Altamimi et al.* [2007]. In the stacking case, one possibility is to constrain to zero, internally, the periodic signals embedded in the time series of a given transformation parameter $[P(t_1), \dots P(t_K)]$. In such a case the internal constraint equation takes the form

$$(B^TB)^{-1}B^T[P(t_1), \dots, P(t_K)]^T = 0 \quad \text{(B4)}$$

where K is the number of the individual daily or weekly solutions and B is the matrix of partial derivatives given by

$$B = \begin{pmatrix} \cos(\omega_i t_1) & \sin(\omega_i t_1) \\ \vdots & \vdots \\ \cos(\omega_i t_K) & \sin(\omega_i t_K) \end{pmatrix} \quad \text{(B5)}$$

Appendix C: Equations of Postseismic Deformation Models

After an earthquake, the position of a station during the postseismic trajectory, X_{PSD}, at an epoch t can be written as

$$X_{\mathrm{PSD}}(t) = X(t_0) + \dot{X}(t - t_0) + \delta X_{\mathrm{PSD}}(t) \quad \text{(C1)}$$

where $\dot{X}$ is the station linear velocity vector and $\delta X_{\mathrm{PSD}}(t)$ is the total sum of the postseismic deformation (PSD) corrections at epoch t. For each component $L \in \{E, N, U\}$, we note δL the total sum of PSD corrections expressed in the local frame at epoch t:

$$\delta L(t) = \sum_{i=1}^{n^l} A_i^l \log\left(1 + \frac{t - t_i^l}{\tau_i^l}\right) + \sum_{i=1}^{n^e} A_i^e \left(1 - e^{-\frac{t-t_i^e}{\tau_i^e}}\right) \quad \text{(C2)}$$

where

n^l: number of logarithmic terms of the parametric model;

n^e: number of exponential terms of the parametric model;

A_i^l: amplitude of the ith logarithmic term;

A_i^e: amplitude of the ith exponential term;

τ_i^l: relaxation time of the ith logarithmic term;

τ_i^e: relaxation time of the ith exponential term;

t_i^l: earthquake time (date) corresponding to ith logarithmic term;

t_i^e: earthquake time (date) corresponding to the ith exponential term.

The variance of $\delta L(t)$ is given by

$$\mathrm{var}(\delta L) = C.\mathrm{var}(\theta).C^T \tag{C3}$$

where θ is the vector of parameters of the postseismic deformation model:

$$\theta = \left[A_1^l, \tau_1^l, \ldots, A_{n^l}^l, \tau_{n^l}^l, A_1^e, \tau_1^e, \ldots, A_{n^e}^e, \tau_{n^e}^e\right]$$

Note that the values of var(θ) of the parametric models are provided to the users in SINEX format available at the ITRF2014 website.

The elements of the matrix $C = \frac{\partial \delta L}{\partial \theta}$ are computed by the following formulae:

$$\frac{\partial \delta L}{\partial A_i^l} = \log\left(1 + \frac{t - t_i^l}{\tau_i^l}\right) \tag{C4}$$

$$\frac{\partial \delta L}{\partial \tau_i^l} = -\frac{A_i^l\left(t - t_i^l\right)}{\left(\tau_i^l\right)^2\left(1 + \frac{t-t_i^l}{\tau_i^l}\right)} \tag{C5}$$

$$\frac{\partial \delta L}{\partial A_i^e} = 1 - \mathrm{e}^{-\frac{\left(t-t_i^e\right)}{\tau_i^e}} \tag{C6}$$

$$\frac{\partial \delta L}{\partial \tau_i^e} = -\frac{A_i^e\left(t - t_i^e\right)\mathrm{e}^{-\frac{\left(t-t_i^e\right)}{\tau_i^e}}}{\left(\tau_i^e\right)^2} \tag{C7}$$

Note that the PSD models are determined and provided to the users per component $L \in \{E, N, U\}$, independently, and so there are no cross terms (or correlations) between components. However, cross terms between amplitude and relaxation time for each LOG or/and EXP term should be taken into account in the variance calculation of equation (C3). As an example, if for a given station there are three earthquakes that were taken into account in the estimation of the PSD models of its component E, and it has one EXP for the first EQ, one EXP for the second EQ, and LOG+EXP for the third EQ, the one line matrix C for component E in equation (C3) will have eight terms.

Once the variances var(δE), var(δN), var(δU) are computed, the transformation into cartesian is obtained by

$$\mathrm{var}\begin{bmatrix}\delta X\\ \delta Y\\ \delta Z\end{bmatrix} = R.\begin{bmatrix}\mathrm{var}(\delta E) & 0 & 0\\ 0 & \mathrm{var}(\delta N) & 0\\ 0 & 0 & \mathrm{var}(\delta U)\end{bmatrix}.R^T \tag{C8}$$

where R is the transformation (Jacobian) matrix from topocentric to geocentric frame and where

$$\begin{bmatrix}\delta X\\ \delta Y\\ \delta Z\end{bmatrix} = R.\begin{bmatrix}\delta E\\ \delta N\\ \delta U\end{bmatrix} \tag{C9}$$

The components E,N,U expressed in the local frame refer to the GRS80 ellipsoid, as recommended by the IERS Conventions [*Petit and Luzum*, 2010, chap. 4].

Acknowledgments
The International Terrestrial Reference Frame (ITRF) is the result of a global collaboration of hundreds of institutions around the world: from the buildup of geodetic observatories, satellite missions, data collection, analysis and combination, to the ITRF generation, thanks to the investment of national mapping agencies, space agencies, universities, and research institutes. The ITRF activities are funded by the Institut National de l'Information Géographique et Forestière (IGN), France, and partly by the Centre National d'études Spatiales (CNES), under TOSCA grant. We are indebted to all Analysis and Combination Centers of the Technique Services of the four techniques which constantly provide data for ITRF solutions which would not exist without their valuable contributions. We thank Tonie van Dam for making available the nontidal atmospheric loading model evaluated in this paper. We acknowledge valuable comments and suggestions provided by the Editor and three anonymous reviewers which improved the content of this article. The input data used in the ITRF2014 computation are available at the NASA Crustal Dynamics Data Information System (CDDIS), http://cddis.nasa.gov/, or through the Technique Centers: http://ids-doris.org/, http://www.igs.org/, http://ilrs.gsfc.nasa.gov/, and http://ivscc.gsfc.nasa.gov/.

References

Altamimi, Z., and X. Collilieux (2009), IGS contribution to the ITRF, *J. Geod.*, *83*(3–4), 375–383, doi:10.1007/s00190-008-0294.
Altamimi, Z., and A. Dermanis (2012), The choice of reference system in ITRF formulation, in *7th Hotine-Marussi Symposium on Mathematical Geodesy, International Association of Geodesy*, vol. 137, pp. 329–334, Springer, Berlin, doi:10.1007/978-3-642-22078-4_49.
Altamimi, Z., P. Sillard, and C. Boucher (2002a), ITRF2000: A new release of the International Terrestrial Reference Frame for Earth science applications, *J. Geophys. Res.*, *107*(B10), 2214, doi:10.1029/2001JB000561.
Altamimi, Z., C. Boucher, and P. Sillard (2002b), New trends for the realization of the International Terrestrial Reference System, *Adv. Space Res.*, *30*(2), 175–184, doi:10.1016/S0273-1177(02)00282-X.
Altamimi, Z., P. Sillard, and C. Boucher (2004), ITRF2000: From theory to implementation, in *V Hotine-Marussi Symposium on Mathematical Geodesy, International Association of Geodesy*, vol. 127, edited by F. Sansò, pp. 157–163, Springer, Berlin, New York, doi:10.1007/978-3-662-10735-5_21.

Altamimi, Z., X. Collilieux, J. Legrand, B. Garayt, and C. Boucher (2007), ITRF2005: A New Release of the International Terrestrial Reference Frame based on time series of station positions and Earth Orientation Parameters, *J. Geophys. Res.*, *112*, B09401, doi:10.1029/2007JB004949.

Altamimi, Z., X. Collilieux, and L. Métivier (2011), ITRF2008: An improved solution of the International Terrestrial Reference Frame, *J. Geod.*, *85*(8), 457–473, doi:10.1007/s00190-011-0444-4.

Altamimi, Z., L. Métivier, and X. Collilieux (2012), ITRF2008 plate motion model, *J. Geophys. Res.*, *117*, B07402, doi:10.1029/2011JB008930.

Appleby, G., J. Rodriguez, and Z. Altamimi (2016), Assessment of the accuracy of global geodetic satellite laser ranging observations and estimated impact on ITRF scale: Estimation of systematic errors in LAGEOS observations 1993–2014, *J. Geod.*, 1–18, doi:10.1007/s00190-016-0929-2.

Bachmann, S., L. Messerschmitt, and D. Thaller (2015), IVS contribution to ITRF2014, in *IAG Commission 1 Symposium 2014: Reference Frames for Applications in Geosciences (REFAG2014)*, pp. 1–6, Springer, Berlin.

Bähr, H., Z. Altamimi, and B. Heck (2007), *Variance Component Estimation for Combination of Terrestrial Reference Frames*, Universität Karlsruhe Schriftenreihe des Studiengangs Geodäsie und Geoinformatik, ISBN: 978-3-86644-206-1.

Bevis, M., and A. Brown (2014), Trajectory models and reference frames for crustal motion geodesy, *J. Geod.*, *88*(3), 283–311, doi:10.1007/s00190-013-0685-5.

Bird, P. (2003), An updated digital model of plate boundaries, *Geochem. Geophys. Geosyst.*, *4*(3), 1027, doi:10.1029/2001GC000252.

Blewitt, G., and D. Lavalée (2002), Effect of annual signals on geodetic velocity, *J. Geophys. Res.*, *107*(B7), 2145, doi:10.1029/2001JB000570.

Boucher, C., and Z. Altamimi (1985), Towards an improved realization of the BIH terrestrial frame, in *Proceedings of the International Conference on Earth Rotation and Reference Frames, MERIT/COTES Rep.*, vol. 2, edited by I. I. Mueller, 551 pp., Ohio State Univ., Columbus, OH.

Collilieux, X., Z. Altamimi, D. Coulot, T. van Dam, and J. Ray (2010), Impact of loading effects on determination of the International Terrestrial Reference Frame, *Adv. Space Res.*, *45*, 144–154, doi:10.1016/j.asr.2009.08.024.

Collilieux, X., T. van Dam, J. Ray, D. Coulot, L. Métivier, and Z. Altamimi (2011), Strategies to mitigate aliasing of loading signals while estimating GPS frame parameters, *J. Geod.*, *86*, 1–14, doi:10.1007/s00190-011-0487-6.

Dermanis, A. (2000), Establishing Global Reference Frames. Nonlinear, Temporal, Geophysical and Stochastic Aspects, in *Gravity, Geoid and Geodynamics*, IAG Symposium, vol. 123, edited by M Sideris, pp. 35–42, Springer, Berlin.

Dermanis, A. (2003), The rank deficiency in estimation theory and the definition of reference systems, in *Hotine-Marussi Symposium on Mathematical Geodesy, IAG Symposia*, vol. 127, edited by F. Sans, pp. 145–156, Springer, Berlin.

Dong, D., P. Fang, Y. Bock, M. K. Cheng, and S. Miyazaki (2002), Anatomy of apparent seasonal variations from GPS-derived site position time series, *J. Geophys. Res.*, *107*(B4), 2075, doi:10.1029/2001JB000573.

Dow, J., R. E. Neilan, and C. Rizos (2009), The International GNSS Service in a changing landscape of Global Navigation Satellite Systems, *J. Geod.*, *83*(3–4), 191–198, doi:10.1007/s00190-008-0300-3.

Dziewonski, A. M., T.-A. Chou, and J. H. Woodhouse (1981), Determination of earthquake source parameters from waveform data for studies of global and regional seismicity, *J. Geophys. Res.*, *86*, 2825–2852, doi:10.1029/JB086iB04p02825.

Ekström, G., M. Nettles, and A. M. Dziewonski (2012), The global CMT project 2004–2010: Centroid-moment tensors for 13,017 earthquakes, *Phys. Earth Planet. Inter.*, *200–201*, 1–9, doi:10.1016/j.pepi.2012.04.002.

Freed, A. M., R. Bürgmann, E. Calais, J. Freymueller, and S. Hreinsdóttir (2006), Implications of deformation following the 2002 Denali, Alaska, earthquake for postseismic relaxation processes and lithospheric rheology, *J. Geophys. Res.*, *111*, B01401, doi:10.1029/2005JB003894.

Freed, A. M., T. Herring, and R. Bürgmann (2010), Steady-state laboratory flow laws alone fail to explain postseismic observations, *Earth and Planet. Sci. Lett.*, *300*(1), 1–10, doi:10.1016/j.epsl.2010.10.005.

Gazeaux, J., et al. (2013), Detecting offsets in GPS time series: First results from the detection of offsets in GPS experiment, *J. Geophys. Res. Solid Earth*, *118*, 2397–2407, doi:10.1002/jgrb.50152.

Gobinddass, M. L., P. Willis, O. de Viron, A. Sibthorpe, J. C. Ries, N. P. Zelensky, Y. Bar-Sever, M. Diament, and R. Ferland (2009), Systematic biases in DORIS-derived geocenter time series related to solar pressure mis-modeling, *J. Geod.*, *83*(9), 849–858, doi:10.1007/s00190-009-0303-8.

Kass, R. E., and A. E. Raftery (1995), Bayes factors, *J. Am. Stat. Assoc.*, *90*(430), 773–795.

Luceri, V., and E. Pavlis (2016), The ILRS contribution to ITRF2014. [Available at http://itrf.ign.fr/ITRF_solutions/2014/doc/ILRS-ITRF2014-description.pdf.]

Mai, M., and G. C. Beroza (2000), Source scaling properties from finite-fault-rupture models, *Bull. Seismol. Soc. Am.*, *90*(3), 604–615.

Marone, C. J., C. H. Scholtz, and R. Bilham (1991), On the mechanics of earthquake afterslip, *J. Geophys. Res.*, *96*(B5), 8441–8452, doi:10.1029/91JB00275.

Métivier, L., M. Greff-Lefftz, and Z. Altamimi (2010), On secular geocenter motion: The impact of climate changes, *Earth Planet. Sci. Lett.*, *3–4*, 360–366, doi:10.1016/j.epsl.2010.05.021.

Métivier, L., M. Greff-Lefftz, and Z. Altamimi (2011), Erratum to "On secular geocenter motion: The impact of climate changes" [Earth Planet. Sci. Lett. 296 (2010) 360–366], *Earth Planet. Sci. Lett.*, *306*(1–2), 136–136, doi:10.1016/j.epsl.2011.03.026.

Métivier, L., X. Collilieux, and Z. Altamimi (2012), ITRF2008 contribution to glacial isostatic adjustment and recent ice melting assessment, *Geophys. Res. Lett.*, *39*, L01309, doi:10.1029/2011GL049942.

Métivier, L., X. Collilieux, D. Lercier, Z. Altamimi, and F. Beauducel (2014), Global coseismic deformations, GNSS time series analysis, and earthquake scaling laws, *J. Geophys. Res. Solid Earth*, *119*, 9095–9109, doi:10.1002/2014JB011280.

Moreaux, G., F. G. Lemoine, H. Capdeville, S. Kuzin, M. Otten, P. Stepanek, P. Willis, and P. Ferrage (2016), Contribution of the International DORIS Service to the 2014 realization of the International Terrestrial Reference Frame, *Adv. Space Res.*, doi:10.1016/j.asr.2015.12.021, in press.

Nothnagel, A., et al. (2015), *The IVS Data Input to ITRF2014. International VLBI Service for Geodesy and Astrometry*, GFZ Data Services, Helmoltz Centre, Potsdam, Germany.

Okada, Y. (1992), Internal deformation due to shear and tensile faults in a half-space, *Bull. Seismol. Soc. Am.*, *82*(2), 1018–1040.

Pearlman, M. R., J. J. Degnan, and J. M. Bosworth (2002), The International Laser Ranging Service, *Adv. Space Res.*, *30*(2), 135–143.

Perfettini, H., and J.-P. Avouac (2004), Postseismic relaxation driven by brittle creep: A possible mechanism to reconcile geodetic measurements and the decay rate of aftershocks, application to the Chi-Chi earthquake, Taiwan, *J. Geophys. Res.*, *109*, B02304, doi:10.1029/2003JB002488.

Petit, G., and B. Luzum (2010), IERS Conventions (2010), *IERS Tech. Note 36*, Verlag des Bundesamts für Kartographie und Geodäsie, 179 pp., Frankfurt am Main, Germany.

Pollitz, F. F. (1997), Gravitational viscoelastic postseismic relaxation on a layered spherical Earth, *J. Geophys. Res.*, *102*(B8), 17,921–17,941, doi:10.1029/97JB01277.

Pollitz, F. F. (2014), Post-earthquake relaxation using a spectral element method: 2.5-D case, *Geophys. J. Int.*, *198*(1), 308–326, doi:10.1093/gji/ggu114.

Ray, J., Z. Altamimi, X. Collilieux, and T. van Dam (2008), Anomalous harmonics in the spectra of GPS position estimates, *GPS Solut.*, *12*(1), 55–64, doi:10.1007/s10291-007-0067-7.

Ray, J. R. (1996), Measurements of length of day using the Global Positioning System, *J. Geophys. Res.*, *101*(B9), 20,141–20,149.

Ray, J. R. (2009), A Quasi-Optimal, Consistent Approach for Combination of UT1 and LOD, in *Geodetic Reference Frames, International Association of Geodesy Symposia*, vol. 134, edited by H. Drewes, pp. 239–243, Springer, Berlin, doi:10.1007/978-3-642-00860-3_37.

Rebischung, P., Z. Altamimi, J. Ray, and B. Garayt (2016), The IGS contribution to ITRF2014, *J. Geod.*, *90*(7), 611–630, doi:10.1007/s00190-016-0897-6.

Sarti, P., C. Abbondanza, and L. Vittuari (2009), Gravity-dependent signal path variation in a large VLBI telescope modelled with a combination of surveying methods, *J. Geod.*, *83*(11), 1115–1126, doi:10.1007/s00190-009-0331-4.

Sarti, P., C. Abbondanza, L. Petrov, and Negusini M. M. (2010), Height bias and scale effect induced by antenna gravity deformations in geodetic VLBI data analysis, *J. Geod.*, *85*(1), 1–8, doi:10.1007/s00190-010-0410-6.

Savage, J. C., and W. H. Prescott (1978), Asthenosphere readjustment and the earthquake cycle, *J. Geophys. Res.*, *83*(B7), 3369–3376.

Savage, J. C., J. L. Svarc, and S.-B. Yu (2005), Postseismic relaxation and transient creep, *J. Geophys. Res.*, *110*, B11402, doi:10.1029/2005JB003687.

Seitz, M., D. Angermann, M. Bloßfeld, H. Drewes, and M. Gerstl (2012), The 2008 DGFI realization of the ITRS: DTRF2008, *J. Geod.*, *86*, 1097–1123.

Schuh H., and D. Behrend (2012), VLBI: A fascinating technique for geodesy and astrometry, *J. Geodyn.*, *61*, 68–80, doi:10.1016/j.jog.2012.07.007.

Schwarz, G. (1978), Estimating the dimension of a model, *Ann. Stat.*, *6*, 461–464.

Sillard, P., and C. Boucher (2001), Review of algebraic constraints in terrestrial reference frame Datum definition, *J. Geod.*, *75*, 63–73.

Scholz, C. H. (1990), *The Mechanics of Earthquakes and Faulting*, Cambridge Univ. Press, Cambridge, U. K.

Trubienko, O., L. Fleitout, J. D. Garaud, and C. Vigny (2013), Interpretation of interseismic deformations and the seismic cycle associated with large subduction earthquakes, *Tectonophysics*, *589*, 126–141, doi:10.1016/j.tecto.2012.12.027.

Williams, S. D. P. (2003), Offsets in Global Positioning System time series, *J. Geophys. Res.*, *108*(B6), 2310, doi:10.1029/2002JB002156.

Willis, P., et al. (2010), The International DORIS Service: Toward maturity, *Adv. Space Res.*, *45*(12), 1408–1420, doi:10.1016/j.asr.2009.11.018.

Wu, X., J. Ray, and T. van Dam (2012), Geocenter motion and its geodetic and geophysical implications, *J. Geodyn.*, *58*, 44–61, doi:10.1016/j.jog.2012.01.007.

Wu, X., C. Abbondanza, Z. Altamimi, T. M. Chin, X. Collilieux, R. S. Gross, M. B. Heflin, Y. Jiang, and J. W. Parker (2015), KALREF—A Kalman filter and time series approach to the International Terrestrial Reference Frame realization, *J. Geophys. Res. Solid Earth*, *120*, 3775–3802, doi:10.1002/2014JB011622.

Yen, Y.-T., and K.-F. Ma (2011), Source-scaling relationship for M 4.6–8.9 earthquakes, specifically for earthquakes in the collision zone of Taiwan, *Bull. Seismol. Soc. Am.*, *101*(2), 464–481, doi:10.1785/0120100046.

Appendix 3 IDS contribution

The DORIS contribution to ITRF2014

Guilhem Moreaux (CLS)
Frank Lemoine (GSFC)

DORIS data span

The DORIS data used for the IDS contribution to ITRF2014 are listed in Table 1. The data used in the combination started in January 1993, mainly because the DORIS station network was not completely implemented until the launch of TOPEX/Poseidon,(August 1992), and because a second satellite was necessary to strengthen the quality of the geodetic solutions. Data from three generations of DORIS instrument were processed. The first generation (1G) receiver could track only one DORIS beacon at a time. The main improvements in the following generation of instruments included miniaturization of the receiver, and of interest for geodesy the number of ground beacons that could be tracked: The SPOT2, SPOT3 and SPOT4 DORIS receivers also could only track one beacon at a time; The second-generation DORIS receivers on JASON-1, SPOT5 and Envisat, could track two beacons; The Jason-2, Cryosat-2, HY-2A and Saral third-generation (DGXX) DORIS receiver can track up to seven beacons (*Auriol and Tourain, 2010*).

The IDS AWG recommended that Jason-1 be added in order to ensure that data from satellites at two different inclinations were incorporated into the solutions from November 2004 to July 2008, i.e. between the end of the TOPEX/Poseidon and the start of the Jason-2 mission. Previously for ITRF2008, over that time period only data from the polar-orbiting satellites of the DORIS constellation were considered (*Valette et al., 2010*). The addition of data from the alternate inclination (66°) compared to the near-polar orbits of the other DORIS satellites improved the ground station observation geometry. The Jason-1 ultra-stable oscillator (USO) was known to exhibit high sensitivity to passage through the South Atlantic Anomaly (SAA). Thus, the analysis centers were required to use the Jason-1 SAA-corrected data from *Lemoine and Capdeville* (*2006*).

Since ITRF2008, *Štěpánek et al*. (2014) pointed out that the USO on SPOT5 also experienced perturbations after passage through the SAA, albeit at a lower level than on Jason-1. Similarily to Jason-1, H. Capdeville and J.-M. Lemoine developed a SAA data correction model for SPOT5 (*Capdeville et al., 2016*). The approach is similar to the one already used in the first Jason-1 data corrective model, based on the frequency drift grid map and the modeling of the recovery and memory effects. All the ACs were asked to use the SPOT5 SAA-corrected data starting on 2005/12/27 (2005:261 - SPOT5 cycle 138).

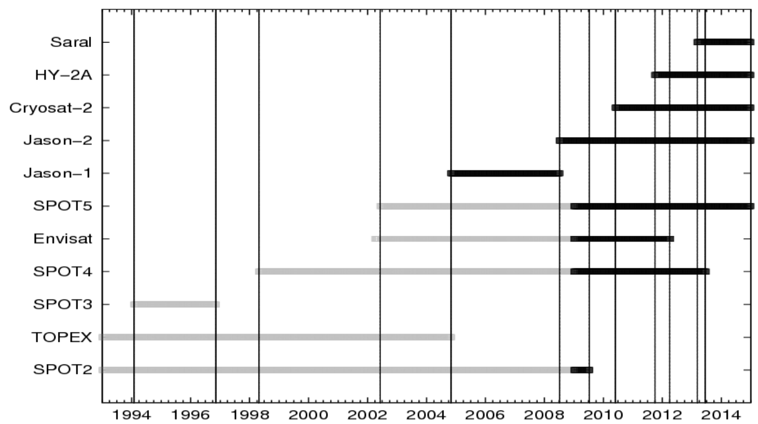

Figure 1 - Time evolution of the DORIS constellation for ITRF2014 (gray = ITRF2008 constellation – gray + black = ITRF2014 constellation). Vertical ines correspond to starting and ending dates of the DORIS missions. From Moreaux et al., 2016.

ACs contributions

Six IDS ACs contributed to the ITRF2014 DORIS combination. Among the standards for the analysis of the DORIS data and the satellite orbit dynamics model, all ACs used time-variable gravity models derived from the GRACE mission and most applied DORIS ground beacon phase center variation corrections. All SINEX deliveries were compliant with IERS call for participation to ITRF2014.

AC	AC solutions	Software	Sol. Id.	Type	Data span	EOPs
European Space Operations Center	**ESA**	NAPEOS	**wd10**	NEQ	1993.0-2014.5	Motion+rate +LOD
Geodetic Observatory Pecny	**GOP**	BERNESE	**wd43-46**	var-cov	1993.0-2015.0	Motion+rate
CNES/CLS	**GRG**	GINS/DYNAMO	**wd40**	var-cov	1993.0-2015.0	Motion
NASA Goddard Space Flight Center	**GSC**	GEODYN	**wd26**	NEQ	1993.0-2015.0	Motion
IGN/GPL	**IGN**	GYPSY/OASIS	**wd15**	var-cov	1993.0-2015.0	Motion
INASAN	**INA**	GYPSY/OASIS	**wd08**	var-cov	1993.0-2015.0	Motion

Table 1 - IDS Analysis Center submission summary using Normal Equations (NEQ) or variance–covariance output (COV).

SINEX Preprocessing analysis

The software used for the IDS combination was the IGN/LAREG CATREF package. As a validation step and before the weekly combination, each SINEX series was preprocessed with the following steps being applied:

(1) Verification of DORIS station identification (dome number, station mnemo),
(2) Rejection of stations over the whole time period (never used),
(3) Rejection of stations over specific periods (partially used),
(4) Verification/update of position discontinuities (but the solution number is set to 1 for the weekly combination),
(5) Inversion of the free singular normal equations for ESA and GSC.
(6) Projection using minimal constraints and rejection of perturbing stations,
(7) Comparison with ITRF2008 at the epoch of each weekly solution.
(8) Analysis and rejection of high residual stations.

Loosely constrained network solutions were projected over its proper space using minimal constraints. Some partial or complete rejections of stations from the SINEX were done resulting from analysis in the SSALTO DORIS ground processing segment or from analysts. After this validation step, all the SINEX files of a series were expressed in the same DORIS reference system and spurious points were removed. A cumulative position/velocity DORIS solution was calculated including recent DORIS data and used as a datum in the projection.

Combination strategy

Several iterations were necessary to provide the best IDS combination of the AC solutions. The combination process started with the individual series of solution files as output from the preprocessing step, i.e. with minimum constrained solutions. To strengthen the quality of the

combined weekly solutions, we only computed solutions for weeks where we had contributions from at least three ACs. In addition, each week, we only estimated positions of stations which had been estimated by at least three ACs. As applying DORIS antennae PCVs induced a scale offset, in order to not perturb the combined scale, since INA was the only AC not able to include DORIS PCVs in its ITRF2014 processing the INA solution was not allowed to contribute to the scale of the IDS solution. In addition we found that the SPOT2 satellite was identified as the source of spurious scale solutions in early 1994. As half of the ACs (GOP, GRG and GSC) did not include that mission in their multi-satellites solutions for the corresponding time period, to get a more accurate combined scale, we did not include ESA and IGN, in addition to INA, contributions at the scale level during this period of time. Analysis of all ACs scales showed an increase late 2011. Further investigations revealed that increase could be associated with either Jason-2, or Cryosat-2 or HY-2A. In addition, regarding to the scale increase, two groups of ACs could be identified (ESA/GRG/GSC vs. GOP/IGN/INA). The two groups were differentiated according to whether or not they computed the DORIS phase center corrections using their orbit determination software (ESA/GRG/GSC), or used phase center corrections provided by CNES in the DORIS data files (GOP/IGN/INA). Then, to minimize the scale increase of the combined solution, the IDS CC decided to not include the GOP, IGN and INA scale contributions to the combined scale starting in year 2011:275 (2011/10/02), as these three ACs presented large scale increases.
Analysis of differences of EOPs of the individual series with respect to the IERS C04 series (*Bizouard and Gambis,* 2009) showed that i) ESA series gave both larger differences and standard deviations and ii) GOP contribution presented spurious periodic signals with periods lower than 30 days, mainly in the X direction. Therefore, these two AC contributions were not included in the estimation of the combined pole. Table 4 of Moreaux et al. (2016) summarizes the contribution of each AC to the IDS 09 combined solution. For more information on the combination strategy, please refer to *Moreaux et al. (2016).*

The final IDS 09 combination included solutions for 160 DORIS stations on 71 different sites with 38 sites located in the northern hemisphere and 33 in the southern hemisphere (see Figure 2). For reference, the IDS network for ITRF2008 included 130 stations located at 66 sites with 34 (resp. 32) sites in the northern (resp. southern) hemisphere. The five new sites are: Betio, Cold Bay, Grasse, Socorro in the northern hemisphere and Rikitea in the southern hemisphere.

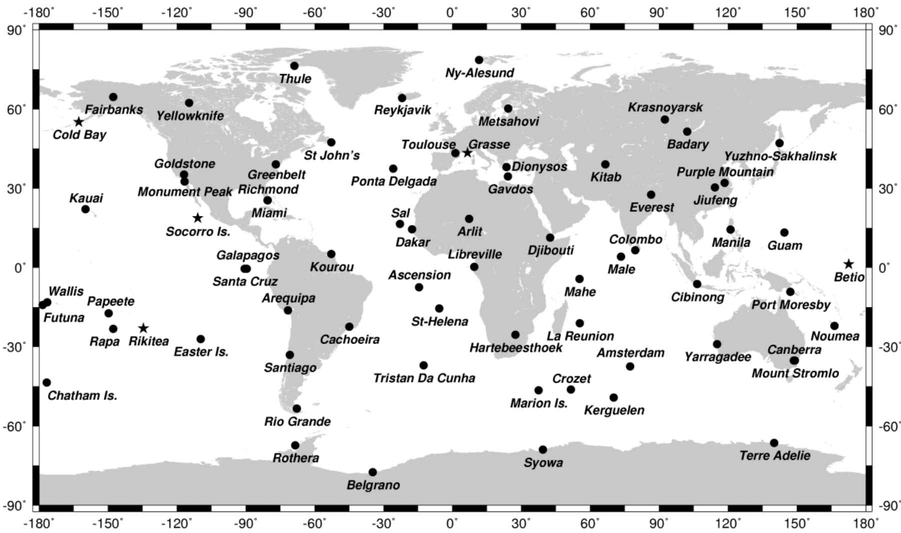

Figure 2 - Geographical distribution of the DORIS stations included in the IDS contribution to ITRF2014 (black stars indicate new sites with regards to ITRF2008). From Moreaux et al., 2016.

TRF parameters

The intrinsic TRF parameters of IDS-09 series are compared in Figure 3 to ITRF2008 for an external validation. From that figure we can observe that TX and TY remain most of the time within 20 mm while TZ presents higher variations (between -75 to +75 mm). We also see that from 1993.0 to 2008.5, the standard deviation of all the IDS 09 translations is lower than the IDS 03 ones. The most important reductions occur for the Z-component. These improvements may reflect a better solar radiation pressure modeling in the new series. Spectral analysis of the geocenter translations (see Table 6 of *Moreaux et al. 2016*) shows that TX and TY present annual signals of nearly 3 mm in amplitude, so a reduction of nearly 15% compared to IDS 03 thanks to use of time variable gravity fields in ITRF2014 processing. The spectral analysis also reveals that X and Y translations of the IDS 09 solution no longer contain any significant signal at 15 days. Meanwhile, the inclusion of Jason-1 and Jason-2 data introduced a 118-day signal in TY (draconitic period for these satellites) with amplitudes of nearly 1 mm. In addition, thanks to a longer time span, spectral analysis of TZ shows that, even if there is a decrease of around 25% in amplitude, IDS 09 is still dominated by an 11 year signal. That solar dependence of the TZ can also be observed from 2000 to 2002 with a TZ maximum which coincides with the peak of the solar cycle. Due to the inclusion of Jason-2, the TZ is more centered after July 2008.

Analysis of IDS 09 scale parameter with respect to ITRF2008 show stability until late 2011 (2011:275, i.e. 2011/10/02) and an increase up to 10 mm afterwards. Evaluation of single-satellite series for 2011-2014 with respect to ITRF2008 showed: i) HY-2A mission, which started in 2011:275, presented a high positive scale value; ii) the Jason-2 and Cryosat-2 scales were affected by an increase between 2012:092 (2012/04/01) and 2012:162 (2012/06/10). Unfortunately, so far, the reasons for both the Jason-2 and Cryosat-2 scale increases are still unknown and under investigation. Moreover, the origin of the high HY-2A scale values is unexplained. Then, if we restrict scale values from 1993 to mid-2011, the scale slope of IDS 09 is close to zero (0.029 mm/yr).

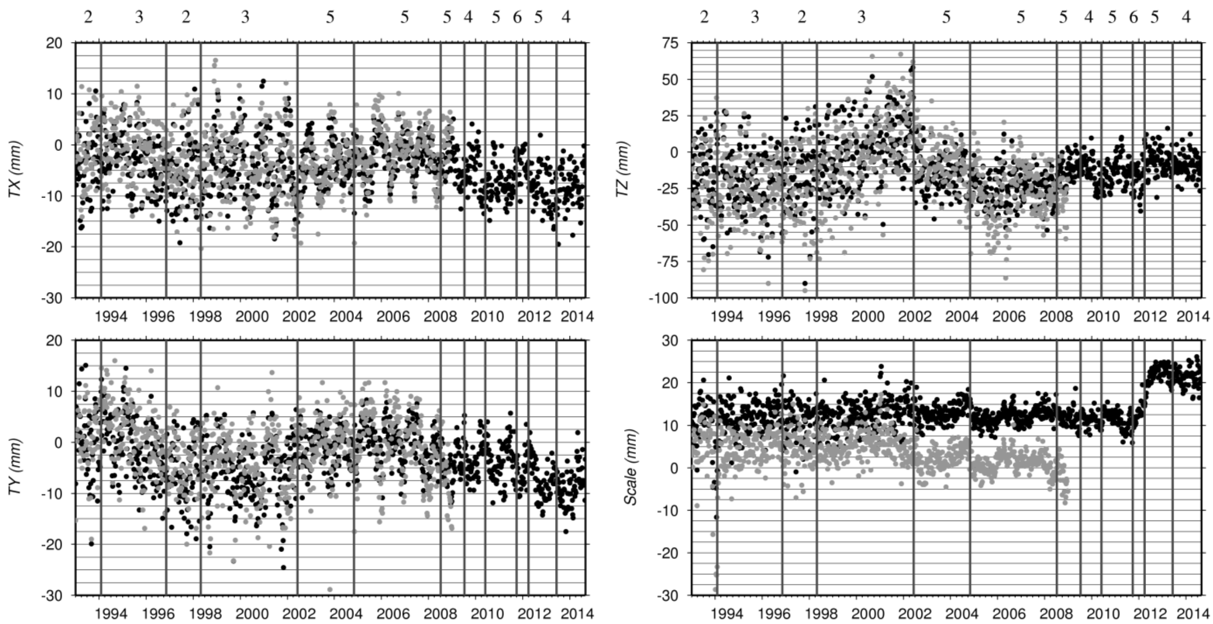

Figure 3 – IDS 09 (ITRF2014) and IDS 03 (ITRF2008) translation and scale parameters with respect to ITRF2008. Vertical lines correspond to DORIS satellite constellation changes and top numbers to satellites number. From Moreaux et al., 2016.

Residuals

From Figure 4, the North component is always the best determined, while the East is the worst one and whereas the Vertical is in the middle. This can be fully explained by the conjunction of two features of the DORIS technique: i) the Doppler technique provides observations that lack information in the direction perpendicular to the satellite track and, ii) except for TOPEX/Poseidon, Jason-1 and Jason-2, all the DORIS satellites have a near-polar orbit. In addition, we see that the WRMS of both IDS 03 and IDS 09 are correlated with the number of satellites. For instance, after April 2002, the WRMS in all the directions are below 15 mm with an improvement of around 30% and 50% for IDS 03 and IDS 09, respectively, as soon as more than three satellites are available. We also observe that IDS 09 performs less well than IDS 03 before April 2002, mainly in the East direction where the differences are at the order of 5 mm in mean value. However, from 1993 to 2002, if we use for the IDS 09 evaluation the weekly DORIS network of IDS 03, then the degradation is below 2 mm.

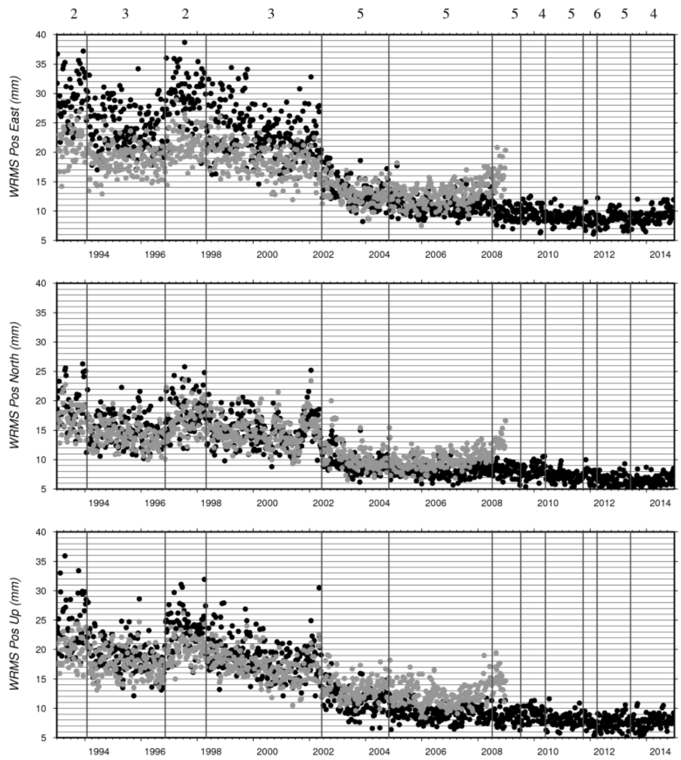

Figure 4 - IDS 03 (gray) and IDS 09 (black) weekly solutions WRMS of the station residuals wrt IDS-TRF2014. Vertical lines correspond to DORIS satellite constellation changes. From Moreaux et al., 2016.

Polar Motion

Figure 5 displays the difference of the IDS X and Y pole components with the IERS 08 C04 pole series (*Bizouard and Gambis, 2009*). As with the station positions residuals, the precision of the EOP significantly improves when the DORIS constellation has more than three satellites, i.e. after April 2002. Moreover, we also observe benefits of the satellite missions that include DGXX receivers, beginning with Jason-2 (July 2008) with a clear reduction of the standard deviations. Comparisons of IDS 09 and IDS 03 polar motion solutions show a substantial degradation of IDS 09 differences wrt. the IERS C04 series.

That degradation could be explained in one respect by the fact that IDS 09 EOPs are the combination of four ACs while IDS 03 used six ACs.

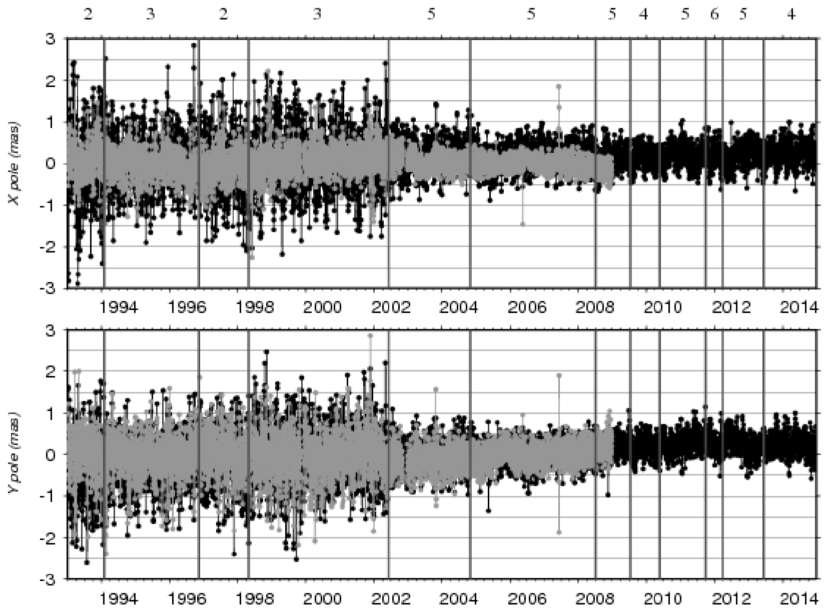

Figure 5 - IDS 03 (gray – IDS contribution to ITRF2008) and IDS 09 (black – IDS contribution to ITRF2014) polar motion compared to IERS 08 C04 series. Vertical lines correspond to DORIS satellite constellation changes. Courtesy from Moreaux et al. 2016.

For more information on the IDS-09 please contact
Guilhem Moreaux (CLS) at the IDS Combination Center (Email: Guilhem.Moreaux@cls.fr)
or Frank Lemoine (NASA) (Email: Frank.G.Lemoine@nasa.gov)
and refer to Moreaux et al. 2016.

References

Bizouard, C., Gambis, D. (2009) The combined solution C04 for Earth orientation parameters consistent with international terrestrial reference frame, 2005. In: Geodetic Reference Frames. In: Drewes, H. (Ed.), . IAG Symp, vol. 134. Springer-Verlag, Berlin, pp. 265–270. http://dx.doi.org/10.1007/978-3-642-00860-3_41.

Capdeville, H., Štěpánek, P., Lemoine, J.-M., et al. (2016) Update of the corrective model for Jason-1 DORIS data in relation to the South Atlantic Anomaly and a corrective model for Spot-5. Adv. Space Res., In review.

Lemoine, J.-M., Capdeville, H. (2006) A corrective model for Jason-1 DORIS Doppler data in relation to the South Atlantic anomaly. J. Geod. 80 (811), 507–523. http://dx.doi.org/10.1007/s00190-006-0068-2.

Moreaux, G., Lemoine, F.-G., Capdeville, et al. (2016) The International DORIS Service contribution to the 2014 realization of the International Terrestrial Reference Frame. Adv. Space Res., http://dx.doi.org/10.1016/j.asr.2015.12.021

Štěpánek, P., Dousa, J., Filler, V. (2014) SPOT-5 DORIS oscillator instability due to South Atlantic anomaly: mapping the effect and application of data corrective model. Adv. Space Res. 52 (7), 1355–1365. http://dx.doi.org/10.1016/j.asr.2013.07.010.

Valette, J.-J., Lemoine, F.G., Ferrage, P., et al. (2010) IDS contribution to ITRF2008, Adv. Space Res., 46(12), 1614-1632, http://dx.doi.org/10.1016/j.asr.2010.05.029

Appendix 4 IGS contribution

IGS Contribution to the ITRF2014

Paul Rebischung, IGN France

The IGS contribution to ITRF2014 is based on the products from the second IGS reprocessing campaign (repro2). A complete list of the models and conventions used in the repro2 data analyses can be found at http://acc.igs.org/reprocess2.html, where individual modeling aspects that have been changed since the repro1 campaign, are new, or have not been widely adopted previously have been highlighted using red font. The main updates since the repro1 campaign are:

- a switch from weekly to daily terrestrial frame integrations made to facilitate the study of station displacements,
- the analysis, by some ACs, of GLONASS data in addition to GPS data,
- the implementation of the IGb08/igs08.atx reference frame and calibration framework,
- the implementation, mostly, of the IERS 2010 Conventions, regarding in particular the conventional mean pole model, the geopotential model, tidal station displacements, tidal variations in the Earth's rotation, tropospheric and ionospheric propagation delays,
- the implementation, partly, of new attitude models for eclipsing satellites,
- the modeling of Earth radiation pressure and, mostly, of antenna thrust acting on GNSS satellites.

A total of 9 ACs contributed to the repro2 campaign and provided daily terrestrial frame(SINEX) solutions among other products. The AC repro2 SINEX time series were extended with consistent operational products up to GPS week 1831, when available, and daily combinations of the AC repro2 + operational SINEX solutions were performed over the period 1994-01-02 to 2015-02-14 (GPS weeks 730 to 1831), based on the following AC contributions:

- COD:
  - 0730_0 to 1772_6 : cf2 solutions included with weight
  - 1773_0 to 1831_6 : cof solutions included with weight
- EMR:
  - 0769_0 to 1785_6 : em2 solutions included with weight
  - 1786_0 to 1831_6 : emr solutions included with weight
- ESA:
  - 0782_0 to 1788_6 : es2 solutions included with weight
  - 1789_0 to 1831_6 : esa solutions included with weight
- GFZ:
  - 0730_0 to 1720_6 : gf2 solutions included for comparison only
  - 1721_0 to 1827_6 : gf2 solutions included with weight
  - 1828_0 to 1831_6 : gfz solutions included with weight
- GRG:
  - 0938_4 to 1825_3 : gr2 solutions included for comparison only
  - 1825_4 to 1831_6 : grg solutions included for comparison only
- GTZ:
  - 0730_0 to 1720_6 : gt2 solutions included with weight
- JPL:

  - 0730_0 to 1815_6 : jp2 solutions included with weight
  - 1816_0 to 1831_6 : jpl solutions included with weight
- MIT:
  - 0730_0 to 1803_6 : mi2 solutions included with weight
  - 1804_0 to 1831_6 : mit solutions included with weight
- ULR:
  - 0782_0 to 1773_1 : ul2 solutions included with weight
  - 1773_2 to 1825_2 : ul2 solutions included for comparison only

The resulting daily combined SINEX solutions, named "ig2", constitute the IGS contribution to ITRF2014.

The combination methodology comprises the following steps:

- Pre-processing of AC solutions:
  - Recovery, when necessary, of the unconstrained normal equation
  - Fixation of UT1-UTC and of the satellite phase center offsets
  - Application of ocean pole tide corrections, when necessary
  - Calibration of LOD estimates with respect to IERS Bulletin A
  - Explicitation of apparent geocenter coordinates
  - Pre-elimination of specific parameters (stations with abnormally large coordinate differences with the other ACs or with metadata errors; ULR's geocenter coordinates)
  - Inversion of the normal equation under NNR and NNT constraints
  - A priori scaling of the covariance matrix so that the median 3D station position formal error is set to 4 mm
- Iterative combinations:
  - The combined parameters include station positions, ERPs (pole coordinates, pole rates and LOD) and apparent geocenter coordinates.
  - Translation and rotation parameters are estimated between each AC solution and the combined solution.
  - After each iteration, unbiased WRMS of the station position residuals are computed for each AC and East/North/Up component. Stations with residuals larger than 5 times the unbiased WRMS in either East, North or Up are rejected from the corresponding AC solutions. It is however ensured that one station cannot be rejected from more than one AC solution during the same iteration.
  - Iterations are performed until no outlier is detected anymore.
- Final combination:
  - A posteriori variance factors are computed for each AC based on a variance component estimation method known as ”degree of freedom estimation”, and used to rescale the AC covariance matrices.
  - A final combination is performed.
  - The origin and orientation of the final combined solution are defined by NNT and NNR constraints with respect to a subset of selected IGb08 core stations.
  - The scale of the combined solution is a "natural" mean of the AC frame scales, hence conventionally defined by the igs08.atx satellite PCO values.

From WRMS values of the residuals of the daily repro2 combinations, the overall inter-AC level of agreement is assessed to be 1.5 mm for the horizontal components and 4 mm for the vertical component of station positions, 25-40 µas for pole coordinates, 140-200µas/d for pole rates, 8-20 µs/d for calibrated LOD estimates, 4 mm for the X and Y components of geocenter motion, 8 mm for its Z component and 0.5 mm for the terrestrial scale. On the long term, the origins (resp. scales) of the AC terrestrial frames show relative offsets and rates within ± 3 mm and ± 0.3 mm/yr (resp. ± 0.5 mm and ± 0.05 mm/yr).

The combination residuals also present AC-specific features, some of which are explained by known analysis specifics, while others remain under investigation.

The overall set of daily repro2 combined solutions comprises a total of 1845 different stations. However, only 58% (1073) of the 1845 stations indeed have position time series with more than 1000 points, and 17% (321) have series with more than 4000 points. Only 31% (578) of the 1845 stations are or have been part of the IGS network. Most of the remaining stations are part of either regional (EPN, SIRGAS...), national (CORS, ARGN...) or geophysically-oriented (PBO, SONEL...) permanent GNSS networks. The metadata blocks of the daily repro2 combined SINEX files thus rely on site logs gathered from different sources, or, when no site log could be found, on the metadata given in the AC SINEX files.

For more detail on the repro2 combination methodology and results, see: Rebischung P, Altamimi Z, Ray J, Garayt B (2016) The IGS contribution to ITRF2014. Journal of Geodesy, doi: 10.1007/s00190-016-0897-6.

Appendix 5 ILRS contribution

The ILRS contribution to ITRF2014

V. Luceri (e-GEOS S.p.A., ASI/CGS)
E. Pavlis (JCET/UMBC & NASA Goddard)

The ILRS contribution to ITRF2014 is a time series of weekly station coordinates and daily Earth Orientation Parameters (X-pole, Y-pole and excess Length-Of-Day (LOD)) estimated over 7-day arcs (15-day arcs for the period 1983-1992) aligned with calendar weeks (Sunday to Saturday), starting from January 1983. Each weekly solution is obtained through the combination of loosely constrained weekly solutions submitted by each of the official ILRS Analysis Centers. Both the individual and combined solutions have followed strict standards agreed upon within the ILRS Analysis Standing Committee to provide ITRS products of the highest possible quality.

Individual solutions

The individual solutions are computed by the official ILRS ACs (ASI, BKG, DGFI, ESA, GFZ, GRGS, JCET and NSGF) using the SLR data acquired from the global tracking network that observed the satellites LAGEOS, LAGEOS-2, Etalon-1 and Etalon-2. From 1983 to 1992 the dataset is made up of LAGEOS data only. This dataset is complemented with the LAGEOS-2 and ETALON satellites starting from 1993. The main difference in the data amount is due to the LAGEOS-2 data; the amount of the ETALON data is roughly one tenth the data of the two LAGEOS, and have a practically negligible impact on the results.

AC code	Analysis Center	SW	Time span
ASI	Agenzia Spaziale Italiana	Geodyn/Solve	1983-2014
BKG	Bundesamt für Kartographie und Geodäsie	Bernese	1993-2014
DGFI	Deutsches Geodätisches Forschungs Institut	DOGS	1983-2014
ESA	European Space Operation Center	Napeos	1983-2014
GFZ	GeoForschungsZentrum Potsdam	EPOSOC	1983-2014
GRGS	Groupe de Recherche de Géodésie Spatiale – Observatoire de la Cote d'Azur	GINS	1983-2014
JCET	Joint Center for Earth Systems Technology – NASA Goddard & UMBC	Geodyn/Solve	1983-2014
NSGF	NERC Space Geodesy Facility	SATAN	1983-2014

The SLR observations are retrieved from ILRS' CDDIS and/or EDC data archive facilities and analyzed to generate the individual EOP and station position solutions. The measurements are processed in intervals of 7 days (15 days in 1983-1992) to generate a loosely-constrained solution for station coordinates and EOP. The EOPs (X_p,Y_p and LOD) are all computed as daily averages since 1993 and as 3-day averages when only LAGEOS data are available. Daily UT parameters are also solved for, but they are of course considered as weakly-determined parameters by any satellite technique and are not included in the analysis product that is submitted to the combination centers. The station positions, with the midpoint of each 7-day (15-day for the period 1983-1992) interval as reference epoch, refer to the official station markers.
Analysis contributors are generally free to follow their own computation model and/or analysis strategy, but a number of constraints must be followed for consistency:

- The computational models follow the prevalent IERS Conventions as closely as possible (with documentation of any exceptions).
- Daily series of the Mean Pole (MP) coordinates and their rates based on the interpolated/extrapolated IERS MP series are adopted, instead of the fixed polynomial version in the IERS 2010 Conventions.

- As requested by the ITRF2013 Call for Participation, the non-tidal atmospheric loading effects are not modeled.
- The stations are included in the weekly analysis if the total number of observed LAGEOS plus LAGEOS 2 ranges is greater than 10. Data weighting is applied according to the analyst's preference. However, the ASC has agreed to down-weight "non-core" sites significantly.
- The center-of-mass correction for each satellite is applied following the site- and time-specific tables provided by Graham Appleby (Appleby et al. 2013) that take into account the various laser station technologies and mode of operation recorded in their site-logs over the years.
- Range corrections were modeled or estimated for a number of sites based either on engineering reports from these sites or long-term analysis of their systematic behavior. All of the applied corrections are documented in the ILRS Data Handling file available at http://ilrs.dgfi.tum.de/fileadmin/data_handling/ILRS_Data_Handling_File.snx.
- The weekly solutions are loosely constrained with an *a priori* standard deviation on station coordinates of ~1 meter and the equivalent of at least 1 m for EOPs.

Additional details on the individual AC analysis strategy can be found on the ILRS web page http://ilrs.gsfc.nasa.gov/science_analysis/analysis_centers.html and the comments included with each individual AC contribution.

ILRSA Combined time series

The official ILRS combined solution is produced by the Primary Combination Center, ASI/CGS, and named ILRSA; a backup combined solution (ILRSB) is computed at JCET/UMBC, the backup CC.
The ILRSA solution has been obtained by a direct combination of the loosely constrained solutions, taking advantage of the fact that loosely constrained solutions, although they possess an ill-defined datum, they still preserve the relative geometry of the station polyhedron figure.
The combination is based on the method described in "*Methodology for global geodetic time series estimation: A new tool for geodynamics*", [P. Davies and G. Blewitt, JGR, vol. 105, no. B5, 2000] and allows handling input solutions easily, with no inversion problems for the solution variance-covariance matrix, no need to know a priori values for the estimates and no need to estimate or remove relative rotations between the reference frames before combining the solutions.
Each contributing solution (and related variance-covariance matrix) is treated as an 'observation' whose misclosure with respect to the combined solution must be minimized in an iterative Weighted Least Squares approach. Each solution is stacked using its full covariance matrix rescaled by an estimated scale factor. A scaling of the covariance matrix of the *i*-th solution is required because the relative weights of the contributing solutions are arbitrary. Imposing $\chi^2=1$ for the combination residuals and requiring that each contribution to the total χ^2 is appropriately balanced, the relative scaling factors (σ_i) are estimated iteratively together with the combined solution. If R_i represents the solution residuals (with respect to the combined product), Σ_i the solution covariance matrix and N the number of solutions, the imposed conditions are:

$$R_1^T(\sigma_1\Sigma_1)^{-1}R_1 = \cdots = R_i^T(\sigma_i\Sigma_i)^{-1}R_i \cdots = R_N^T(\sigma_N\Sigma_N)^{-1}R_N \quad \text{and}$$
$$\chi^2 = R_1^T\Sigma_1^{-1}R_1 + \cdots + R_N^T\Sigma_N^{-1}R_N = 1$$

The first guess for the combination is obtained with $\sigma_i=1$ for each solution.

The scale factors for each contributing AC are reported in the Table below as mean value and standard deviation over the period 1993-2013 when the solutions are more stable with the complete 4 satellites configuration.

	ASI	BKG	DGFI	ESA	GFZ	GRGS	JCET	NSGF
Mean	4.3	4.9	11.6	3.9	7.6	4.7	5.4	10.6
Standard deviation	2.7	4.1	5.5	1.7	5.4	2.9	3.5	6.0

A rigorous editing (Brockmann, 1996) has been introduced to eliminate outliers with respect to the combined solution following a 5σ criterion for:

1. sites with less than 10 observations, erroneously present in the contributing solutions,
2. sites with too large uncertainties (> 1m) and
3. sites with large coordinate residuals with respect to the *a priori* SLRF2008 (>0.5m).

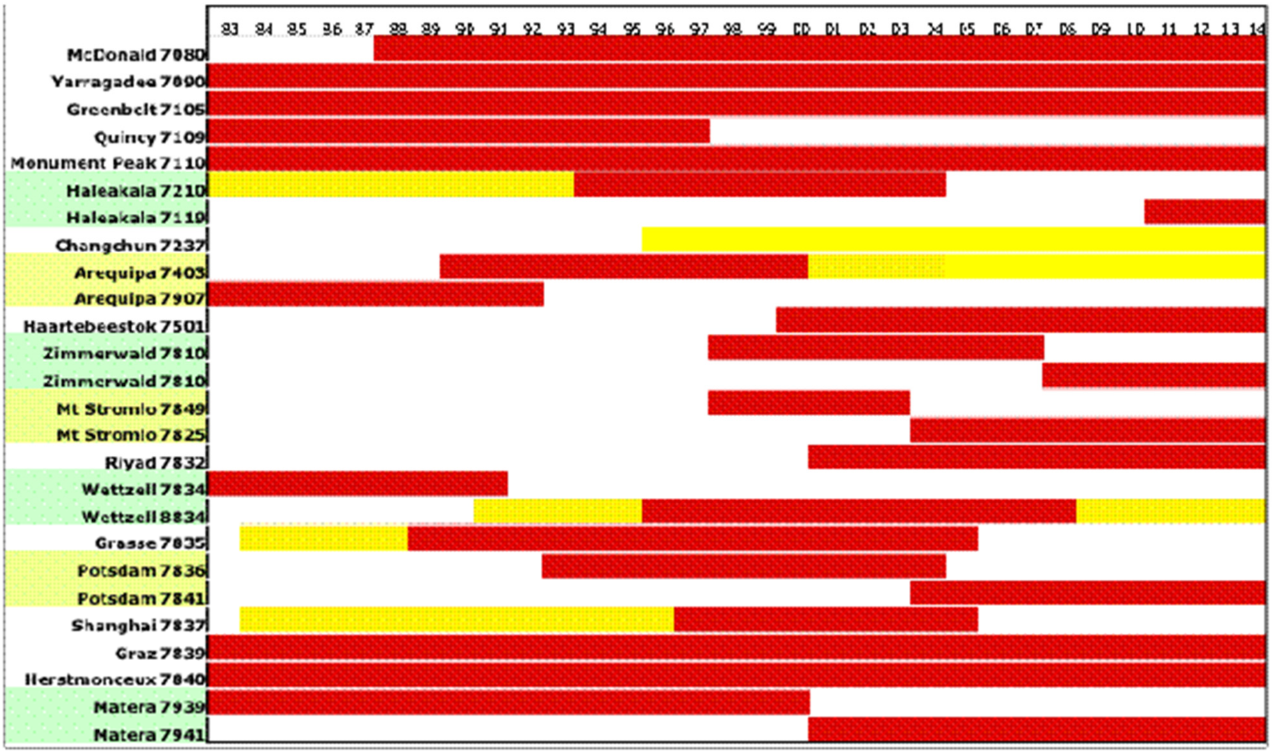

Figure 1: The adopted ILRS "core" sites that are used in aligning the individual AC solutions to the combined ILRS solutions over the time span of data used in developing ITRF2014.

The internal precision of the ILRSA solution is checked through the computation of the weighted root mean square (WRMS) over the time series of the coordinate residuals of each input solution with respect to the combination. Thus, a cumulative 3-dimensional value of the WRMS (3D WRMS) is computed for each solution using the coordinate residuals in all three components, of all the sites contributing to each solution (see table below). The coordinate residuals are computed after a rototranslation of each loose AC solution with respect to the combined solution using a set of core sites. The list of core sites has been officially defined, within the Analysis Standing Committee, considering the quality and stability of the entire set of network sites over several decades (Fig. 1).

3D WRMS of coordinate residuals wrt ILRSA

	1983-1992		1993-2014	
	mean	std	mean	std
ASI	14.0	9.1	4.7	2.4
BKG	---------	---------	5.2	2.9
DGFI	12.0	5.4	7.8	3.0
ESA	11.9	9.7	5.2	3.1
GFZ	19.3	9.9	7.1	2.9
GRGS	15.5	11.4	4.9	2.7
JCET	16.9	10.0	5.0	2.6
NSGF	14.6	5.4	7.7	3.5

The ILRSA solution has been compared to SLRF2008 in terms of 3D WRMS of the site coordinates residuals. The 3D WRMS is computed using both, the full network and using a subset of "core sites".

3D WRMS of the ILRSA coordinate residuals with respect to SLRF2008

Units in millimeters (mm)	1983-1992	1993-2013
All sites (mean)	15.4	7.7
Core sites (mean)	11.2	5.0

The ILRSA EOPs have been compared with the USNO final daily values. The comparison is performed in terms of WRMS of the residuals and the results agree in general with what is expected from the SLR technique and the current network capability: 167 μas for the X-component, 190 μas for the Y-component and 32 μts for LOD are the mean values in the 1993-2014 time span.

In addition to the official ILRSA combination series from the re-analysis products, the back-up Combination Center at JCET/UMBC delivered a back-up series designated ILRSB. The ILRSB series are developed in a slightly different formalism, using the de-constrained normal equations derived from the individual AC solutions and relative weighting of the input AC series determined through Variance Component Estimation. The two series however show excellent agreement in all reported parameters, with differences between the two being much smaller than their formal statistics. This is an additional internal check of the quality of the ILRS-delivered products.

Appendix 6 IVS contribution

IVS Contribution to the ITRF2014

Sabine Bachmann (BKG), John M. Gipson (NASA GSFC)

The official contribution of the International VLBI Service for Geodesy and Astrometry (IVS) to ITRF2014 consists of session-wise datum-free normal equations of altogether 5,796 daily 24h Very Long Baseline Interferometry (VLBI) network sessions from 1979.6 to 2015.0 including data of 158 different VLBI sites. It is the result of a combination of individual series of session-wise datum-free normal equations provided by nine analysis centers (ACs) of the IVS. All series are completely reprocessed following homogeneous analysis options according to the IERS Conventions 2010 and IVS Analysis Conventions. A correction for atmospheric pressure loading was not applied as it was approved by the IERS Directing Board. Parameters contained in the normal equation systems are station positions and EOPs. Zenith wet delays, atmosphere gradients and clock parameters were (pre-)reduced by the individual ACs. Source positions are not contained in the normal equations. The source positions of ICRF2 defining source are constrained to their a priori values, and ICRF2 special handling sources are treated as arc-parameter. All other sources could be either constrained to ICRF2 positions or treated as arc-parameters.

1) Analysis strategy:

As for the IVS contribution to ITRF2005 and ITRF2008, the combination is performed at the normal equation level. The strategy for the intra-technique combination mainly consists of three steps.

1) The session-wise datum-free normal equation systems of the individual ACs are transformed to an identical reference epoch and to an equal set of a priori values.

2) Weights for the normal equation systems of each AC are estimated for each single session within a variance component estimation procedure.

3) The weighted equation systems of each contributing AC are stacked to combined session-wise normal equation systems.

These session-wise combined normal equation systems form the IVS input to the ITRF2014.

2) ACs Contributions:

Nine ACs have contributed:

AC	Software	Time span	#sessions	#stations
BKG	Calc/Solve	1984.0 to 2015.0	4,682	91
CGS	Calc/Solve	1984.0 to 2015.0	4,681	131
GFZ	VieVS@GFZ	1979.6 to 2015.0	5,904	149
GSFC	Calc/Solve	1979.6 to 2015.0	4,592	153
IAA	QUASAR	1980.0 to 2015.0	4,470	111
OPAR	Calc/Solve	1979.6 to 2015.0	5,647	153
SHAO	Calc/Solve	1980.3 to 2015.0	5,422	147
USNO	Calc/Solve	1979.6 to 2015.0	4,688	142
VIE	VieVS	1979.6 to 2015.0	5,602	145

3) Combined Products:

AC	Software	Time span	#sessions	#stations
IVS	DOGS_CS	1979.6 to 2015.0	5,796	158

Consistency of the individual contributions to the IVS combination:

WRMS values computed from the single-session station position differences between the estimates of each individual contribution and the combined series for the north, east and height component.

AC - IVS comb.	North (mm)	East (mm)	Height (mm)
BKG	1.7	2.1	3.8
CGS	1.2	1.5	2.6
GFZ	2.3	2.9	3.8
GSFC	1.3	1.8	2.6
IAA	2.9	3.8	6.3
OPA	2.4	2.7	3.6
SHAO	1.1	1.4	2.4
USNO	2.1	1.6	2.6
VIE	2.2	2.7	3.7
average	1.9	2.3	3.5

Offset and rate of the scale parameter resulting from a Helmert transformation between the global individual solutions and the combined solution.

AC - IVS comb.	Scale Offset (ppb)	Scale Rate (ppb/yr)
BKG	0.05	0.00
CGS	0.04	-0.01
GFZ	-0.08	0.00
GSFC	-0.02	0.00
IAA	0.00	0.01
OPA	0.10	-0.01
SHAO	0.01	0.00
USNO	0.01	0.00
VIE	-0.05	0.00
average	0.01	0.0

WRMS values computed from the single-session EOP differences between the estimates of each individual contribution and the combined EOP series from 1984 to 2014 for polar motion, dUT1 and their first derivatives as well as nutation offsets.

AC - IVS comb.	X-pole (µas)	Y-pole (µas)	dUT1 (µs)	LOD (µs)	X-pole rate (µas/d)	Y-pole rate (µas/d)	dX (µas)	dY (µas)
BKG	71.0	72.0	5.0	6.0	177.0	175.0	51.0	53.0
CGS	46.0	40.0	4.0	5.0	117.0	110.0	34.0	34.0
GFZ	89.0	83.0	7.0	34.0	250.0	258.0	75.0	75.0
GFSC	45.0	41.0	5.0	4.0	107.0	106.0	31.0	32.0
IAA	106.0	105.0	7.0	13.0	269.0	278.0	75.0	75.0
OPA	80.0	68.0	10.0	6.0	179.0	174.0	139.0	137.0
SHAO	47.0	43.0	4.0	5.0	125.0	121.0	32.0	33.0
USNO	47.0	43.0	5.0	5.0	114.0	111.0	36.0	36.0
VIE	88.0	80.0	14.0	15.0	209.0	207.0	78.0	79.0
Average	68.8	63.9	6.7	10.3	171.9	171.1	61.2	61.6

For more detail on the VLBI combination strategy and results, see:

Bachmann S, Thaller D, Roggenbuck O, Lösler M, Messerschmitt L: IVS contribution to ITRF2014. Journal of Geodesy, 90: 631-654, doi: 10.1007/s00190-016-0899-4, 2016